

Superconducting Quantum Circuits, Qubits and Computing

G. Wendin and V.S. Shumeiko

*Department of Microtechnology and Nanoscience - MC2,
Chalmers University of Technology,
SE-41296 Gothenburg, Sweden*

(Dated: November 26, 2024)

This paper gives an introduction to the physics and principles of operation of quantized superconducting electrical circuits for quantum information processing.

Table of contents

I. Introduction	Variable inductive coupling
II. Nanotechnology, computers and qubits	Variable Josephson coupling
III. Basics of quantum computation	Variable phase coupling
(a) Conditions for quantum information processing	Variable capacitive coupling
(b) Qubits and entanglement	(h) Two qubits coupled via a resonator
(c) Operations and gates	X. Dynamics of multi-qubit systems
(d) Readout and state preparation	(a) General N-qubit formulation
IV. Dynamics of two-level systems	(b) Two qubits, Ising-type transverse zz coupling
(a) The two-level state	Biasing far away from the degeneracy point
(b) State evolution on the Bloch sphere	Biasing at the degeneracy point
(c) dc-pulses, sudden switching and precession	(c) Two qubits, transverse xx coupling
(d) Adiabatic switching	(d) Two qubits, yy coupling
(e) Harmonic perturbation and Rabi oscillation	(e) Effects of the environment: noise and decoherence
(g) Decoherence of qubit systems	XI. Experiments with single qubits and readout devices
V. Classical superconducting circuits	(a) Readout detectors
(a) Current biased Josephson junction	(b) Operation and measurement procedures
(b) rf-SQUID	(c) NIST current-biased Josephson junction qubit
(c) dc-SQUID	(d) Flux qubits
(d) Single Cooper pair Box	(e) Charge-phase qubit
VI. Quantum superconducting circuits	XII. Experiments with qubits coupled to quantum oscillators
VII. Basic qubits	(a) General discussion
(a) Josephson junction (JJ) qubit	(b) Delft persistent current flux qubit coupled to a quantum oscillator
(b) Charge qubits	(c) Yale charge-phase qubit coupled to a strip-line resonator
Single Cooper pair Box (SCB)	(d) Comparison of the Delft and Yale approaches
Single Cooper pair Transistor (SCT)	XIII. Experimental manipulation of coupled two-qubit systems
(d) Flux qubits	(a) Capacitively coupled charge qubits
rf-SQUID	(b) Inductively coupled charge qubits
3-junction SQUID - persistent current qubit (PCQ)	(c) Capacitively coupled JJ phase qubits
(e) Potential qubits	XIV. Quantum state engineering with multi-qubit JJ systems
VIII. Qubit read-out and measurement of quantum information	(a) Bell measurements
(a) Readout: why, when and how?	(b) Teleportation
(b) Direct qubit measurement	(c) Qubit buses and entanglement transfer
(c) Measurement of charge qubit with SET	(d) Qubit encoding and quantum error correction
(d) Measurement via coupled oscillator	XV. Conclusion and perspectives
(e) Threshold detection	Glossary
IX. Physical coupling schemes for two qubits	References
(a) General principles	
(b) Inductive coupling of flux qubits	
(c) Capacitive coupling of single JJ qubits	
(d) JJ coupling of charge qubits	
(f) Coupling via oscillators	
Coupling of charge qubits	
Phase coupling of SCT qubits	
(g) Variable-coupling schemes	

I. INTRODUCTION

The first demonstration of oscillation of a superconducting qubit by Nakamura et al. in 1999¹ can be said to represent the "tip of the iceberg": it rests on a huge volume of advanced research on Josephson junctions (JJ) and circuits developed during the last 25 years. Some of this work has concerned fundamental research on Josephson junctions and superconducting quantum interferometers (SQUIDs) aimed at understanding macroscopic quantum coherence (MQC)^{2,3,4,5}, providing the foundation of the persistent current flux qubit^{6,7,8}. However, there has also been intense research aimed at developing superconducting flux-based digital electronics and computers^{9,10,11}. Moreover, in the 1990's the single-Cooper-pair box/transistor (SCB, SCT)¹², was developed experimentally and used to demonstrate the quantization of Cooper pairs on a small superconducting island¹³, which is the foundation of the charge qubit^{1,14}.

Since then there has been a steady development^{15,16,17,18,19}, with observation of microwave-induced Rabi oscillation of the two-level populations in charge^{21,22,23}, and flux^{24,25,26,27} qubits and dc-pulse driven oscillation of charge qubits with rf-SET detection²⁸. An important step is the development of the charge-phase qubit, a hybrid version of the charge qubit consisting of an SCT in a superconducting loop^{21,22}, demonstrating Rabi oscillations with very long coherence time, of the order of 1 μ s, allowing a large set of basic and advanced ("NMR-like") one-qubit operations (gates) to be performed²³. In addition, coherent oscillations have been demonstrated in the "simplest" JJ qubits of them all, namely a single Josephson junction^{30,31,32,33}, or a two-JJ dc-SQUID³⁴, where the qubit is formed by the two lowest states in the periodic potential of the JJ itself.

Although a powerful JJ-based quantum computer with hundreds of qubits remains a distant goal, systems with 5-10 qubits will be built and tested by, say, 2010. Pairwise coupling of qubits for two-qubit gate operations is then an essential task, and a few experiments with coupled JJ-qubits with fixed capacitive or inductive couplings have been reported^{35,36,37,38,39,40}, in particular the first realization of a controlled-NOT gate with two coupled SCBs³⁶, used together with a one-qubit Hadamard gate to generate an entangled two-qubit state.

For scalability, and simple operation, the ability to control qubit couplings, e.g. switching them on and off, will be essential. So far, experiments on coupled JJ qubits have been performed without direct physical control of the qubit coupling, but there are many proposed schemes for two(multi)-qubit gates based on fixed or controllable physical qubit-qubit couplings or tunings of qubits and bus resonators.

All of the JJ-circuit devices introduced above are based on nanoscale science and technology and represent emerging technologies for quantum engineering and, at best, information processing. One may debate the impor-

tance of quantum computers on any time scale, but there is no doubt that the research will be a powerful driver of the development of solid-state quantum state engineering and quantum technology, e.g. performing measurements "at the edge of the impossible".

This article aims at describing the inner workings of superconducting Josephson junction (JJ) circuits, how these can form two-level systems acting as qubits, and how they can be coupled together to multi-qubit networks. Since the field of experimental qubit applications is only five years old, it is not even clear if the field represents an emerging technology for computers. Nevertheless, the JJ-technology is presently the only example of a working solid state qubit with long coherence time, with demonstrated two-qubit gate operation and readout, and with potential for scalability. This makes it worthwhile to describe this system in some detail.

It needs to be said, however, that much of the basic theory for coupled JJ-qubits was worked out well ahead of experiment^{14,41,42}, defining and elaborating basic operation and coupling schemes. We recommend the reader to take a good look at the excellent research and review paper by Makhlin et al.⁴² which describes the basic principles of a multi-JJ-qubit information processor, including essential schemes for qubit-qubit coupling. The ambition of the present article is to provide a both introductory and in-depth overview of essential Josephson junction quantum circuits, discuss basic issues of readout and measurement, and connect to the recent experimental progress with JJ-based qubits for quantum information processing (JJ-QIP).

II. NANOTECHNOLOGY, COMPUTERS AND QUBITS

The scaling down of microelectronics into the nanometer range will inevitably make quantum effects like tunneling and wave propagation important. This will eventually impede the functioning of classical transistor components, but will also open up new opportunities for multi-terminal components and logic circuits built on e.g. resonant tunneling, ballistic transport, single electronics, etc.

There are two main branches of fundamentally different computer architectures, namely logically irreversible and logically reversible. Ordinary computers are irreversible because they dissipate both energy and information. Even if CMOS circuits in principle only draw current when switching, this is nevertheless the source of intense local heat generation, threatening to burn up future processor chips. The energy dissipation can in principle be reduced by going to single-electron devices, superconducting electronics and quantum devices, but this does not alter the fact that the information processing is logically irreversible. In the simplest case of an AND gate, two incoming bit lines only result in a single bit output, which means that one bit is in practice erased

(initialized to zero) and the heat irreversibly dissipated to the environment. The use of quantum-effect devices does not change the fact that we are dealing with computers where each gate is logically irreversible and where discarded information constantly is erased and turned into heat. A computer with quantum device components therefore does not make a quantum computer.

A quantum information processor has to be built on fundamentally reversible schemes with reversible gates where no information is discarded, and where all internal processes in the components are elastic. This issue is connected with the problem of the minimum energy needed for performing a calculation⁴³ (connected with the entropy change created by erasing the final result, i.e. reading the result and then clearing the register). A reversible information processor can in principle be built by classical means using adiabatically switched networks of different kinds. The principles were investigated in the 1980's and form a background for much of the work on quantum computation^{44,45,46,47,48,49,50}. Recently there has been some very interesting development of reversible computers (see^{51,52,53,54} and references therein). However, a reversible computer still does not make a quantum computer. What is characteristic for a quantum computer is that it is reversible and *quantum coherent*, meaning that one can build entangled non-classical multi-qubit states.

One can broadly distinguish between microscopic, mesoscopic and macroscopic qubits. Microscopic effective two-level systems are localized systems confined by natural or artificial constraining potentials. Natural systems then typically are atomic or molecular impurities utilizing electronic charge, or electronic or nuclear spins. These systems may be implanted^{55,56} or naturally occurring due to the material growth process⁵⁷. A related type of impurity qubit involves endohedral fullerenes, i.e. atoms implanted into C60 or similar cages⁵⁸, to be placed at specific positions on a surface prepared for control and readout.

Mesoscopic qubit systems typically involve geometrically defined confining potentials like quantum dots. Quantum dots (QD) for qubits⁵⁹ are usually made in semiconductor materials. One type of QD is a small natural or artificial semiconductor grain with quantized electronic levels. The electronic excitations may be excitonic (excitons,^{60,61} or biexcitons,⁶²), charge-like⁶³, or spin-like (e.g. singlet-triplet)^{64,65}. Another type of QD is geometrically defined in semiconductor 2DEG by electrostatic split-gate arrangements. Although the host materials are epitaxially layered semiconducting materials (e.g. GaAs/AlGaAs), the ungated 2DEG electronic system is metallic. A split-gate arrangement can then define a voltage-controlled system of quantum dots coupled to metallic reservoir electrodes, creating a system for electron charge and spin transport through quantum point contacts and (effective) two-level quantum dots^{64,65,66,67}.

There is also a potential qubit based on liquid He superfluid technology, namely "Electrons on Helium",

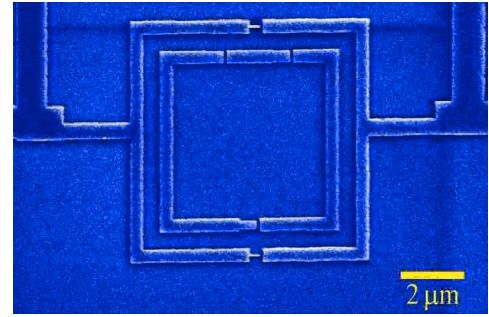


FIG. 1: 3-junction persistent current flux qubit (PCQ) (inner loop) surrounded by a 2-junction SQUID. *Courtesy of J.E. Mooij, TU Delft.*

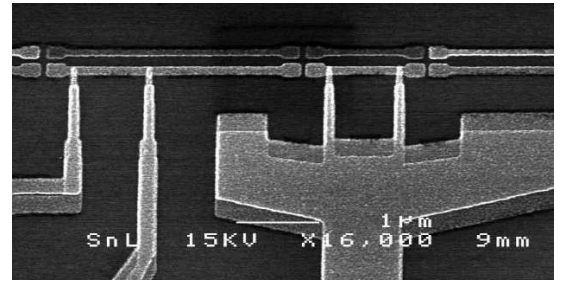


FIG. 2: Single Cooper pair box (SCB) (right) coupled to a single-electron transistor (SET) (left) for readout. *Courtesy of P. Delsing, Chalmers.*

EoH⁶⁸. This is really an atomic-like microscopic qubit: a thin film of liquid He is made to cover a Si surface, and electrons are bound by the image force above the He surface, forming an electronic two-level system. Qubits are laterally defined by electrostatic gate patterns in the Si substrate, which also defines circuits for qubit control, qubit coupling and readout.

Macroscopic superconducting qubits - the subject of this article - are based on electrical circuits containing Josephson junctions (JJ). Looking at two extreme examples, the principle is actually very simple. In one limit, the qubit is simply represented by the two rotation directions of the persistent supercurrent of Cooper pairs in a superconducting ring containing Josephson tunnel junctions (rf-SQUID)(flux qubit)^{6,7,8}, shown below in Fig. 1 for the Delft 3-junction flux qubit,

In another limit, the qubit is represented by the presence or absence of a Cooper pair on a small superconducting island (Single Cooper pair Box, SCB, or Transistor, SCT) (charge qubit)^{1,13,28,69}, as illustrated in Fig. 2. Hybrid circuits^{21,70,71} can in principle be tuned between these limits by varying the relations between the electrostatic charging energy E_C and the Josephson tunneling energy E_J .

All of these solid-state qubits have advantages and disadvantages, and only systematic research and development of multi-qubit systems will show the practical and ultimate limitations of various systems. The supercon-

ducting systems have presently the undisputable advantage of acutally existing, showing Rabi oscillations and responding to one- and two-qubit gate operations. In fact, even an elementary SCB two-qubit entangling gate creating Bell-type states has been demonstrated very recently³⁶. All of the non-superconducting qubits are so far, promising but still potential qubits. Several of the impurity electron spin qubits show impressive relaxation lifetimes in bulk measurements, but it remains to demonstrate how to read out individual qubit spins.

III. BASICS OF QUANTUM COMPUTATION

A. Conditions for quantum information processing

DiVincenzo⁷² has formulated a set of rules and conditions that need to be fulfilled in order for quantum computing to be possible:

1. Register of 2-level systems (qubits), $n = 2^N$ states $|101..01\rangle$ (N qubits)
2. Initialization of the qubit register: e.g. setting it to $|000..00\rangle$
3. Tools for manipulation: 1- and 2-qubit gates, e.g. Hadamard (H) gates to flip the spin to the equator, $U_H|0\rangle = (|0\rangle + |1\rangle)/2$, and Controlled-NOT ($CNOT$) gates to create entangled states, $U_{CNOT}U_H|00\rangle = (|00\rangle + |11\rangle)/2$ (Bell state)
4. Read-out of single qubits $|\psi\rangle = a|0\rangle + b e^{i\phi}|1\rangle \rightarrow a, b$ (spin projection; phase ϕ of qubit lost)
5. Long decoherence times: $> 10^4$ 2-qubit gate operations needed for error correction to maintain coherence "forever".
6. Transport qubits and to transfer entanglement between different coherent systems (quantum-quantum interfaces).
7. Create classical-quantum interfaces for control, read-out and information storage.

B. Qubits and entanglement

A qubit is a two-level quantum system characterized by the state vector

$$|\psi\rangle = \cos \frac{\theta}{2} |0\rangle + \sin \frac{\theta}{2} e^{i\phi} |1\rangle \quad (3.1)$$

Expressing $|0\rangle$ and $|1\rangle$ in terms of the eigenvectors of the Pauli matrix σ_z ,

$$|0\rangle = \begin{pmatrix} 1 \\ 0 \end{pmatrix}, \quad |1\rangle = \begin{pmatrix} 0 \\ 1 \end{pmatrix}. \quad (3.2)$$

this can be described as a rotation from the north pole of the $|0\rangle$ state,

$$|\psi\rangle = \begin{pmatrix} 1 & 0 \\ 0 & e^{i\phi} \end{pmatrix} \begin{pmatrix} \cos \frac{\theta}{2} & -\sin \frac{\theta}{2} \\ \sin \frac{\theta}{2} & \cos \frac{\theta}{2} \end{pmatrix} \begin{pmatrix} 1 \\ 0 \end{pmatrix} \quad (3.3)$$

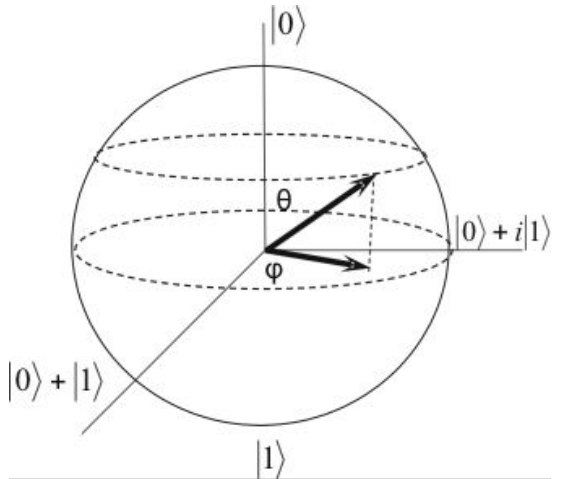


FIG. 3: The Bloch sphere. Points on the sphere correspond to the quantum states $|\psi\rangle$; in particular, the north and south poles correspond to the computational basis states $|0\rangle$ and $|1\rangle$; superposition cat-states $|\psi\rangle = |0\rangle + e^{i\phi}|1\rangle$ are situated on the equator.

can be characterised by a unit vector on the Bloch sphere:

The state vector can be represented as a unitary vector on the Bloch sphere, and general unitary (rotation) operations make it possible to reach every point on the Bloch sphere. The qubit is therefore an analogue object with a continuum of possible states. Only in the case of spin 1/2 systems do we have a true two-level system. In the general case, the qubit is represented by the lowest levels of a multi-level system, which means that the length of the state vector may not be conserved due to transitions to other levels. The first condition will therefore be to operate the qubit so that it stays on the Bloch sphere (fidelity). Competing with normal operation, noise from the environment may cause fluctuation of both qubit amplitude and phase, leading to relaxation and decoherence. It is a delicate matter to isolate the qubit from a perturbing environment, and desirable operation and unwanted perturbation (noise) easily go hand in hand. It is a major issue to design qubit control and read-out such that the necessary communication lines can be blocked when not in use.

The state of N independent qubits can be represented as a product state,

$$|\psi\rangle = |\psi_1\rangle|\psi_2\rangle\dots|\psi_N\rangle = |\psi_1\psi_2\dots\psi_N\rangle \quad (3.4)$$

involving any one of all of the configurations $|00\dots0\rangle$, $|00\dots1\rangle$, ..., $|11\dots1\rangle$. A general state of an N -qubit memory register (i.e. a many-body system) can then be written as a time-dependent superposition of many-particle configurations

$$|\psi(t)\rangle = c_1(t)|0\dots00\rangle + c_2(t)|0\dots01\rangle + c_3(t)|0\dots10\rangle + \dots + c_n(t)|1\dots11\rangle \quad (3.5)$$

where the amplitudes $c_i(t)$ are complex, providing phase information. This state represents a time-dependent superposition of $2N$ N-body configurations which in general cannot be written as a product of one-qubit states and then represents an entangled (quantum correlated) many-body state.

In the case of two qubits, the maximally entangled states are the so-called Bell states,

$$|\psi\rangle = (|00\rangle + |11\rangle)/2 \quad (3.6)$$

$$|\psi\rangle = (|00\rangle - |11\rangle)/2 \quad (3.7)$$

$$|\psi\rangle = (|01\rangle + |10\rangle)/2 \quad (3.8)$$

$$|\psi\rangle = (|01\rangle - |10\rangle)/2 \quad (3.9)$$

where the last one is the singlet state. In the case of three qubits, the corresponding maximally entangled ("cat") states are the Greenberger-Horne-Zeilinger (GHZ) states⁷³

$$|\psi\rangle = (|000\rangle \pm |111\rangle)/\sqrt{8} \quad (3.10)$$

Another interesting entangled three-qubit state appears in the teleportation process,

$$\begin{aligned} |\psi\rangle = & [|00\rangle(a|0\rangle + b|1\rangle) + |01\rangle(a|0\rangle - b|1\rangle) \\ & + |10\rangle(b|0\rangle + a|1\rangle) + |11\rangle(b|0\rangle - a|1\rangle)]/\sqrt{8} \end{aligned} \quad (3.11)$$

C. Operations and gates

Quantum computation basically means allowing the N -body state to develop in a fully coherent fashion through unitary transformations acting on all N qubits. The time evolution of the many-body system of N two-level subsystems can be described by the Schrödinger equation for the N -level state vector $|\psi(t)\rangle$,

$$i\hbar\partial_t|\psi\rangle = \hat{H}|\psi\rangle. \quad (3.12)$$

in terms of the time-evolution operator characterizing by the time-dependent many-body Hamiltonian $\hat{H}(t)$ of the system determined by the external control operations and the perturbing noise from the environment,

$$|\psi(t)\rangle = U(t, t_0)|\psi(t_0)\rangle. \quad (3.13)$$

The solution of Schrödinger equation for $U(t, t_0)$

$$i\hbar\partial_t U(t, t_0) = \hat{H}U(t, t_0) \quad (3.14)$$

may be written as

$$U(t, t_0) = 1 - \frac{i}{\hbar} \int_{t_0}^t \hat{H}(t')U(t', t_0)dt', \quad (3.15)$$

and finally, in terms of the time-ordering operator T , as

$$U(t, t_0) = T e^{-\frac{i}{\hbar} \int_{t_0}^t \hat{H}(t')dt'}, \quad (3.16)$$

describing the time evolution of the entire N -particle state in the interval $[t, t_0]$. If the total Hamiltonian commutes with itself at different times, the time ordering can be omitted,

$$U(t, t_0) = e^{-\frac{i}{\hbar} \int_{t_0}^t \hat{H}(t')dt'}. \quad (3.17)$$

This describes the time-evolution controlled by a homogeneous time-dependent potential or electromagnetic field, e.g. dc or ac pulses with finite rise times but having no space-dependence. If the Hamiltonian is constant in the interval $[t_0, t]$, then the evolution operator takes the simple form

$$U(t, t_0) = e^{-\frac{i}{\hbar} \hat{H}(t-t_0)}, \quad (3.18)$$

describing the time-evolution controlled by square dc pulses.

The time-development will depend on how many terms are switched on in the Hamiltonian during this time interval. In the ideal case, usually not realizable, all terms are switched off except for those selected for the specific computational step. A single qubit gate operation then involves turning on a particular term in the Hamiltonian for a specific qubit, while a two-qubit gate involves turning on an interaction term between two specific qubits. In principle one can perform an N -qubit gate operation by turning on interactions for all N qubits. In practical cases, many terms in the Hamiltonian are turned on all the time, leading to a "background" time development that has to be taken into account.

The basic model for a two-level qubit is the spin-1/2 in a magnetic field. A system of interacting qubits can then be modelled by a collection of interacting spins, described by the Heisenberg Hamiltonian

$$\hat{H}(t) = \sum \mathbf{h}_i(t) \mathbf{S}_i + \frac{1}{2} \sum J_{ij}(t) \mathbf{S}_i \mathbf{S}_j \quad (3.19)$$

controlled by a time-dependent external magnetic field $\mathbf{h}_i(t)$ and by a time-dependent spin-spin coupling $J_{ij}(t)$.

Expressing the Hamiltonian in Cartesian components, $\mathbf{h}_i(t) = (h_x, h_y, h_z)$, $\mathbf{S}_i(t) = (S_x, S_y, S_z)$ and introducing the Pauli σ -matrices, $(S_x, S_y, S_z) = \frac{1}{2}\hbar(\sigma_x, \sigma_y, \sigma_z)$ we obtain a general N -qubit Hamiltonian with general qubit-qubit coupling:

$$\begin{aligned} \hat{H} = & -\frac{1}{2} \sum_i (\epsilon_i \sigma_{zi} + Re\Delta_i \sigma_{xi} + Im\Delta_i \sigma_{yi}) \\ & + \frac{1}{2} \sum_{ij;\nu} \lambda_{\nu,ij}(t) \sigma_{\nu i} \sigma_{\nu j} \\ & + \sum_i (f_i(t) \sigma_{zi} + g_{xi}(t) \sigma_{xi} + g_{yi}(t) \sigma_{yi}) \end{aligned} \quad (3.20)$$

We have here introduced time-independent components of the external field defining qubit energy level splittings ϵ_i , $Re\Delta_i$ and $Im\Delta_i$ along the z and x,y axes, as well as time-dependent components $f_i(t)$ and $g_i(t)$ explicitly describing qubit operation and readout signals and noise.

Inserted into Eq.(3.17), this Hamiltonian determines the time evolution of the many-qubit state. In the ideal case one can turn on and off each individual term of the Hamiltonian, including the two-body interaction, giving complete control of the evolution of the state.

It has been shown that any unitary transformation can be achieved through a quantum network of sequential application of one- and two-qubit gates. Moreover, the size of the coherent workspace of the multi-qubit memory can be varied (in principle) by switching on and off qubit-qubit interactions.

In the common case of NMR applied to molecules^{74,75,76}, one has no control of the fixed, direct spin-spin coupling. With an external magnetic field one can control the qubit Zeeman level splittings (no control of individual qubits). Individual qubits can be addressed by external RF-fields since the qubits have different resonance frequencies (due to different chemical environments in a molecule). Two-qubit coupling can be induced by simultaneous resonant excitation of two qubits.

In the case of engineered solid state JJ-circuits, individual qubits can be addressed by local gates, controlling the local electric or magnetic field. Extensive single-qubit operation has recently been demonstrated by Collin et al.²³. Regarding two-qubit coupling, the field is just starting up, and different options are only beginning to be tested. The most straightforward approaches involve fixed capacitive^{35,36,40} or inductive^{37,38} coupling; such systems could be operated in NMR style, by detuning specific qubit pairs into resonance. Moreover, there are various solutions for controlling the direct physical qubit-qubit coupling strength, as will be described in Section IX.

D. Readout and state preparation

External perturbations, described by $f_i(t)$ and $g_i(t)$ in Eq.(3.20) can influence the two-level system in typically two ways: (i) shifting the individual energy levels, which may change the transition energy and the phase of the qubit; and (ii) inducing transitions between the levels, changing the level populations. These effects arise both from desirable control operations and from unwanted noise (see^{42,77,78,79} for a discussion of superconducting circuits, and Grangier et al.⁸⁰ for a discussion of state preparation and quantum non-demolition (QND) measurements).

To control a qubit register, the important thing is to control the decoherence during qubit operation and readout, and in the memory state. In the qubit memory state, the qubit must be isolated from the environment. Operation and read-out devices should be decoupled from the qubit and, ideally, not cause any dephasing or relaxation. The resulting intrinsic qubit life times should be long compared to the duration of the calculation. In the operation and readout state, the qubit must be connected

to the operation fields. This also opens up the system to a noisy environment, which puts great demands on signal-to-noise ratios.

The readout operation is a particularly critical step. The ultimate purpose is to perform a "single-shot" quantum non-demolition (QND) measurement, determining the state ($|0\rangle$ or $|1\rangle$) of the qubit in a single measurement and then leaving the qubit in that very state. During the measurement time, the back-action noise from the "meter" will cause relaxation and mixing, changing the qubit state. The "meter" must then be sensitive enough to detect the qubit state on a time scale shorter than the induced relaxation time T_1^* in the presence of the dissipative back-action of the "meter" itself. Under these conditions it is possible to detect the qubit projection in a single measurement (single shot read-out). Performing a single-shot projective measurement in the qubit eigenbasis then provides a QND measurement (note the "trivial" fact that the phase is irreversibly lost in the measurement process under any circumstances).

The readout/measurement processes described above can be related to the Stern-Gerlach (SG) experiment⁸⁰. A SG spin filter acts as a beam splitter for flying qubits, creating separate paths for spin-up and spin-down atoms, preparing for the measurement by making it possible in principle to distinguish spatially between the two states of the qubit. The measurement is then performed by particle counters: a click in, say, the spin-up path collapses the atom to the spin-up state in a single shot. There is essentially no decohering back-action from the detector until the atom is detected. However, after detection of the spin-up atom the state is thoroughly destroyed: this qubit has not only decohered and relaxed, but is removed from the system. However, if it was entangled with other qubits, these are left in a specific eigenstate. For example, if the qubit was part of the Bell pair $|\psi\rangle = (|00\rangle + |11\rangle)/\sqrt{2}$, detection of spin up ($|0\rangle$) selects $|00\rangle$ and leaves the other qubit in state $|0\rangle$. If instead the qubit was part of the Bell pair $|\psi\rangle = (|01\rangle + |10\rangle)/\sqrt{2}$, detection of spin up ($|0\rangle$) selects $|01\rangle$ and leaves the other qubit in the spin-down state $|1\rangle$. Furthermore, for the 3-qubit GHZ state $|\psi\rangle = (|000\rangle \pm |111\rangle)/\sqrt{8}$, detection of the first qubit in the spin up ($|0\rangle$) state leaves the remaining 2-qubit system in the $|00\rangle$ state.

Finally, in the case of the three-qubit entangled state in the teleportation process, Eq.(3.11), detection of the first qubit in the spin up state $|0\rangle$, leaves the remaining 2-qubit system in the entangled state $[|0\rangle(a|0\rangle + b|1\rangle) + |1\rangle(a|0\rangle - b|1\rangle)]/2$. Moreover, detection of also the second qubit in the spin-up state $|0\rangle$ will leave the third qubit in the state $(a|0\rangle + b|1\rangle)/\sqrt{2}$. In this way, *measurement can be used for state preparation*.

Applying this discussion to the measurement and readout of JJ-qubit circuits, an obvious difference is that the JJ-qubits are not flying particles. The detection can therefore not be turned on simply by the qubit flying into the detector. Instead, the detector is part of the JJ-qubit circuitry, and must be turned on to discriminate between

the two qubit states. These are not spatially separated and therefore sensitive to level mixing by detector noise with frequency around the qubit transition energy. The sensitivity of the detector determines the time scale T_m of the measurement, and the detector-on back-action determines the time scale of qubit relaxation T_1^* . Clearly $T_m \ll T_1^*$ is needed for single-shot discrimination of $|0\rangle$ and $|1\rangle$. This requires a detector signal-to-noise (S/N) ratio $\gg 1$, in which case one will have the possibility also to turn off the detector and leave the qubit in the determined eigenstate, now relaxing on the much longer time scale T_1 of the "isolated" qubit. This would then be the ultimate QND measurement.

Note that in the above discussion, the qubit dephasing time ("isolated" qubit) does not enter because it is assumed to be much longer than the measurement time, $T_m \ll T_\phi$. This condition is obviously essential for utilizing the measurement process for state preparation and error correction.

IV. DYNAMICS OF TWO-LEVEL SYSTEMS

To perform computational tasks one must be able to put a qubit in an arbitrary state. This is usually done in two steps. The first step, initialization, consists of relaxation of the initial qubit state to the equilibrium state due to interaction with environment. At low temperature, this state is close to the ground state. During the next step, time dependent dc- or rf-pulses are applied to the controlling gates: electrostatic gate in the case of charge qubits, bias flux in the case of flux qubits, and bias current in the case of the JJ qubit. Formally, the pulses enter as time-dependent contributions to the Hamiltonian and the state evolves under the action of the time-evolution operator. To study the dynamics of a single qubit two-level system we therefore first describe the two-level state, and then the evolution of this state under the influence of the control pulses ("perturbations").

A. The two-level state

The general 1-qubit Hamiltonian has the form

$$\hat{H} = -\frac{1}{2}(\epsilon \sigma_z + \Delta \sigma_x) \quad (4.1)$$

The qubit eigenstates are to be found from the stationary Schrödinger equation

$$\hat{H}|\psi\rangle = E|\psi\rangle \quad (4.2)$$

To solve the S-equation we expand the 1-qubit state in a complete basis, e.g. the basis states of the σ_z operator,

$$|\psi\rangle = \sum_k a_k |k\rangle = c_0|0\rangle + c_1|1\rangle \quad (4.3)$$

and project onto the basis states

$$\hat{H} \sum_m |m\rangle \langle m|\psi\rangle = E|\psi\rangle \quad (4.4)$$

obtaining the usual matrix equation

$$\sum_m \langle k|\hat{H}|m\rangle a_m = E a_k \quad (4.5)$$

where $a_k = \langle k|\psi\rangle$, and

$$H_{qp} = -\frac{\epsilon}{2}\langle k|\sigma_z|m\rangle - \frac{\Delta}{2}\langle k|\sigma_x|m\rangle \quad (4.6)$$

giving the Hamiltonian matrix

$$\hat{H} = -\frac{1}{2} \begin{pmatrix} \epsilon & \Delta \\ \Delta & -\epsilon \end{pmatrix} \quad (4.7)$$

The Schrödinger equation is then given by

$$(\hat{H} - E)|\psi\rangle = -\frac{1}{2} \begin{pmatrix} \epsilon + 2E & \Delta \\ \Delta & -\epsilon + 2E \end{pmatrix} \begin{pmatrix} a_1 \\ a_2 \end{pmatrix} = 0 \quad (4.8)$$

The eigenvalues are determined by

$$\det(\hat{H} - E) = E^2 - \frac{1}{4}(\epsilon^2 + \Delta^2) = 0 \quad (4.9)$$

with the result

$$E_{1,2} = \pm \frac{1}{2} \sqrt{\epsilon^2 + \Delta^2} \quad (4.10)$$

The eigenvectors are given by:

$$a_2 = -a_1 \frac{\Delta}{\epsilon + 2E} \quad (4.11)$$

After normalisation

$$a_1 = 1/\sqrt{1 + \left(\frac{\Delta}{\epsilon + 2E}\right)^2} = \frac{1}{\sqrt{2}} \sqrt{1 \pm \frac{\epsilon}{|2E|}} \quad (4.12)$$

$$a_2 = \pm \sqrt{1 - a_1^2} = \pm \frac{1}{\sqrt{2}} \sqrt{1 \mp \frac{\epsilon}{|2E|}} \quad (4.13)$$

We finally simplify the notation by fixing the signs of the amplitudes,

$$a_1 = \frac{1}{\sqrt{2}} \sqrt{1 + \frac{\epsilon}{|2E|}} ; a_2 = \frac{1}{\sqrt{2}} \sqrt{1 - \frac{\epsilon}{|2E|}} ; \quad (4.14)$$

and explicitly writing down all the energy eigenstates,

$$|E_1\rangle = a_1|0\rangle + a_2|1\rangle \quad (4.15)$$

$$|E_2\rangle = a_2|0\rangle - a_1|1\rangle \quad (4.16)$$

where

$$E_1 = -\frac{1}{2}\sqrt{\epsilon_1^2 + \Delta_1^2}; E_2 = +\frac{1}{2}\sqrt{\epsilon_1^2 + \Delta_1^2} \quad (4.17)$$

The sign of $|E_2\rangle$ has been chosen to give the familiar expression for the superposition at the degeneracy point $\epsilon_1 = 0$ where $|a_1| = |a_2| = 1/\sqrt{2}$,

$$|E_1\rangle = \frac{1}{\sqrt{2}}(|0\rangle + |1\rangle) \quad (4.18)$$

$$|E_2\rangle = \frac{1}{\sqrt{2}}(|0\rangle - |1\rangle) \quad (4.19)$$

B. The state evolution on the Bloch sphere

To study the time-evolution of a general state, a convenient way is to expand in the basis of energy eigenstates,

$$|\psi(t)\rangle = c_1|E_1\rangle e^{-iE_1 t} + c_2|E_2\rangle e^{-iE_2 t} \quad (4.20)$$

If we know the coefficients at $t = 0$, then we know the time evolution. On the Bloch sphere this time evolution is represented by rotation of the Bloch vector with constant angular speed $(E_1 - E_2)/\hbar$ around the direction defined by the energy eigenbasis. Indeed, by introducing parameterization, $c_1 = \cos\theta'$, $c_2 = \sin\theta' e^{i\phi'}$, we see that according to Eq. (4.20) the polar angle remains constant, $\theta' = \text{const}$, while the azimuthal angle grows, $\phi'(t)\phi'(0) + (E_1 - E_2)t/\hbar$. The primed angles here refer to a new coordinate system on the Bloch sphere related to the energy eigenbasis, which is obtained by rotation from the earlier introduced computational basis, Eq. (3.1).

The dynamics on the Bloch sphere is conveniently described in terms of the density matrix for a pure quantum state⁸¹,

$$\hat{\rho} = |\psi\rangle\langle\psi|. \quad (4.21)$$

This is a 2×2 Hermitian matrix whose diagonal elements ρ_1 and ρ_2 define occupation probabilities of the basis states, hence satisfying the normalization condition $\rho_1 + \rho_2 = 1$, while the off-diagonal elements give information about the phase. The density matrix can be mapped on a real 3-vector by means of the standard expansion in terms of σ -matrices,

$$\hat{\rho} = \frac{1}{2}(1 + \rho_x\sigma_x + \rho_y\sigma_y + \rho_z\sigma_z). \quad (4.22)$$

Direct calculation of the density matrix Eq.(4.21) using Eq.(3.1) and comparing with Eq.(4.22) shows that the vector $\rho = (\rho_x, \rho_y, \rho_z)$ coincides with the Bloch vector,

$$\rho = (\sin\theta \cos\phi, \sin\theta \sin\phi, \cos\theta) \quad (4.23)$$

introduced in Fig. 3 and also shown in Fig. 4. In the same σ -matrix basis, the general two-level Hamiltonian takes the form

$$\hat{H} = (H_x\sigma_x + H_y\sigma_y + H_z\sigma_z). \quad (4.24)$$

giving a 3-vector representation for the Hamiltonian,

$$\mathbf{H} = (H_x, H_y, H_z). \quad (4.25)$$

shown in Fig. 4.

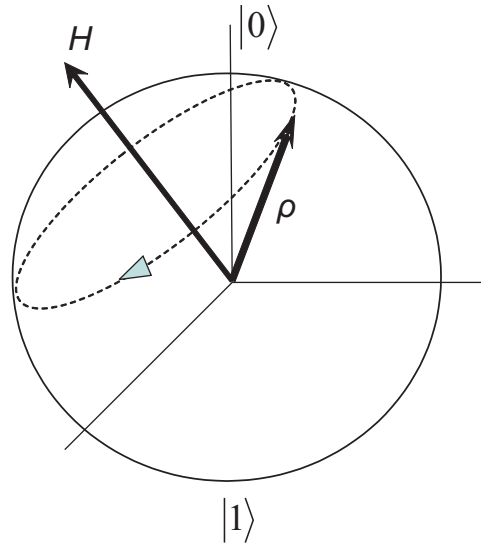


FIG. 4: The Bloch sphere: the Bloch vector ρ represents the states of the two-level system (same as in Fig. 3). The poles of the Bloch sphere correspond to the energy eigenstates; the vector H represents the two-level Hamiltonian.

The time evolution of the density matrix is given by the Liouville equation,

$$i\hbar\partial_t\hat{\rho} = [\hat{H}, \hat{\rho}]. \quad (4.26)$$

The vector form of the Liouville equation is readily derived by inserting Eqs.(4.24),(4.25) and using the commutation relations among the Pauli matrices,

$$\partial_t\rho = \frac{1}{\hbar}[\mathbf{H} \times \rho]. \quad (4.27)$$

This equation coincides with the Bloch equation for a magnetic moment evolving in a magnetic field, the role of the magnetic moment being played by the Bloch vector ρ which rotates around the effective "magnetic field" \mathbf{H} associated with the Hamiltonian of the qubit (plus any driving fields) (Fig. 4).

C. dc-pulses, sudden switching and free precession

To control the dynamics of the qubit system, one method is to apply dc (square) pulses which suddenly change the Hamiltonian and, consequently, the time-evolution operator. Sudden pulse switching means that the time-dependent Hamiltonian is changed so fast on the time scale of the evolution of the state vector that the state vector can be treated as time-independent - frozen - during the switching time interval. This implies

that the system is excited by a Fourier spectrum with an upper cut-off given by the inverse of the switching time.

In the specific scheme of sudden switching of different terms in the Hamiltonian using dc-pulses, the initial state is frozen during the switching event, and begins to evolve in time under the influence of the new

$$|0\rangle = |\psi(0)\rangle = c_1|E_1\rangle + c_2|E_2\rangle \quad (4.28)$$

To find the coefficients we project onto the charge basis, $k=0,1$

$$\langle 0|0\rangle = c_1\langle 0|E_1\rangle + c_2\langle 0|E_2\rangle \quad (4.29)$$

$$\langle 1|0\rangle = c_1\langle 1|E_1\rangle + c_2\langle 1|E_2\rangle \quad (4.30)$$

and use the explicit results for the energy eigenstates to calculate the matrix elements, obtaining

$$1 = c_1a_1 + c_2a_2 \quad (4.31)$$

$$0 = c_1a_2 - c_2a_1 \quad (4.32)$$

As a result,

$$|0\rangle = a_1|E_1\rangle + a_2|E_2\rangle \quad (4.33)$$

This stationary state then develops in time governed by the constant Hamiltonian as

$$|\psi(t)\rangle = a_1e^{-iE_1t}|E_1\rangle + a_2e^{-iE_2t}|E_2\rangle \quad (4.34)$$

Inserting the energy eigenstates we finally obtain the time evolution in the charge basis,

$$|\psi(t)\rangle = |0\rangle [a_1^2e^{-iE_1t} + a_2^2e^{iE_1t}] + |1\rangle [a_1a_2(e^{-iE_1t} - e^{iE_1t})] \quad (4.35)$$

The probability amplitudes of finding the system in one of the two charge states is then

$$\langle 0|\psi(t)\rangle = [a_1^2e^{-iE_1t} + a_2^2e^{iE_1t}] \quad (4.36)$$

$$\langle 1|\psi(t)\rangle = [a_1a_2(e^{-iE_1t} - e^{iE_1t})] \quad (4.37)$$

If the system is driven to the degeneracy point $\epsilon_1 = 0$, where $|a_1| = |a_2| = 1/\sqrt{2}$, then

$$\langle 0|\psi(t)\rangle = \cos E_1 t \quad (4.38)$$

$$\langle 1|\psi(t)\rangle = \sin E_1 t \quad (4.39)$$

In particular, the probability of finding the system in state $|1\rangle$ (level 2) oscillates like

$$p_2(t) = |\langle 1|\psi(t)\rangle| = \sin^2 E_1 t = \frac{1}{2}[1 - \cos(E_2 - E_1)t] \quad (4.40)$$

with the frequency of the interlevel distance. On the Bloch sphere, this describes free precession around the X -axis.

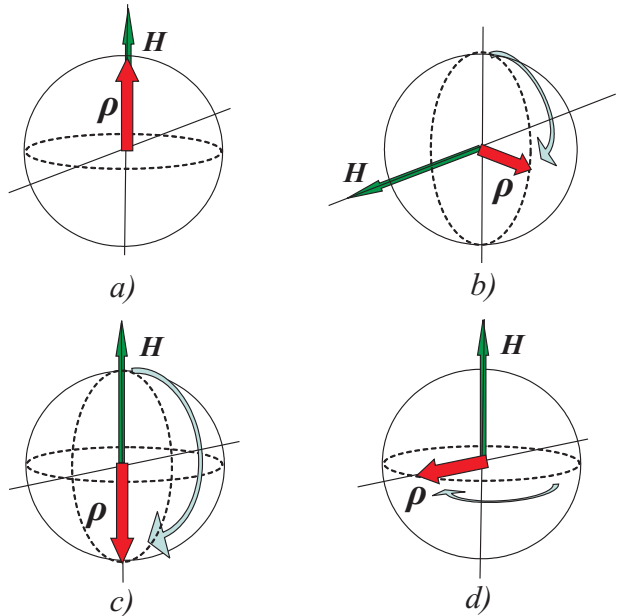


FIG. 5: Qubit operations with dc-pulses: the vector H represents the qubit Hamiltonian, and the vector ρ represents the qubit state. a) The qubit is initialized to the ground state; b) the Hamiltonian vector H is suddenly rotated towards x -axis, and the qubit state vector ρ starts to precess around H ; c) when qubit vector reaches the south pole of the Bloch sphere, the Hamiltonian vector H is switched back to the initial position; the vector ρ remains at the south pole, indicating complete inversion of the level population (π -pulse); d) if the Hamiltonian vector H is switched back when the qubit vector reaches the equator of the Bloch sphere ($\pi/2$ -pulse), then the ρ vector remains precessing at the equator, representing equal-weighted superposition of the qubit states (cat states) $|\psi\rangle = |0\rangle + e^{i\phi}|1\rangle$; this operation is the basis for the Hadamard gate.

Let us consider, for example, the diagonal qubit Hamiltonian, $\hat{H} = (\epsilon/2)\sigma_z$, and apply a pulse $\delta\epsilon$ during a time τ . This operation will shift phases of the qubit eigenstates by, $\pm\delta\epsilon\tau/2\hbar$. If the applied pulse is such that ϵ is switched off, and instead, the σ_x component, Δ , is switched on, Fig 5, then the state vector will rotate around the x -axis, and after the time $\Delta\tau/2\hbar = \pi$ (π -pulse) the ground state, $|+\rangle$, will flip and become, $|+\rangle \rightarrow |-\rangle$. This manipulation corresponds to the quantum NOT operation. Furthermore, if the pulse duration is twice smaller ($\pi/2$ -pulse), then the ground state vector will approach the equator of the Bloch sphere and precess along it after the end of the operation. Such state is an equal-weighted superposition of the basis states (cat state).

D. Adiabatic switching

Adiabatic switching represents the opposite limit to sudden switching, namely that the state develops so fast

on the time scale of the Hamiltonian that this can be regarded as "frozen", i.e. the time-dependence of the Hamiltonian becomes parametric. This implies that energy is conserved and no transitions are induced - the system stays in the same energy level (although the state changes).

E. Harmonic perturbation and Rabi oscillation

A particularly interesting and practically important case concerns harmonic perturbation with small amplitude λ and resonant frequency $\hbar\omega = E_2 - E_1$. Let us consider the situation when the harmonic perturbation is added to the z -component of the Hamiltonian corresponding to a modulation of the qubit bias with a microwave field.

In the eigenbasis of the non-perturbed qubit, $|E_1\rangle$, $|E_2\rangle$, the Hamiltonian will take the form,

$$\hat{H} = E_1\sigma_z + \cos\omega t (\lambda_z\sigma_z + \lambda_x\sigma_x), \quad (4.41)$$

$$\lambda_z = \lambda \frac{\epsilon}{E_2}, \quad \lambda_x = \lambda \frac{\Delta}{E_2}. \quad (4.42)$$

The first perturbative term determines small periodic oscillations of the qubit energy splitting, while the second term will induce interlevel transitions. Despite the amplitude of the perturbation being small, $\lambda/E_2 \ll 1$, the system will be driven far away from the initial state because of the resonance. Indeed, let us consider the wave function of the driven qubit on the form

$$|\psi\rangle = a(t)e^{-iE_1t/\hbar}|E_1\rangle + b(t)e^{-iE_2t/\hbar}|E_2\rangle. \quad (4.43)$$

Substituting this ansatz into the Schrödinger equation,

$$i\hbar|\dot{\psi}\rangle = \hat{H}(t)|\psi\rangle, \quad (4.44)$$

we get the following equations for the coefficients,

$$\begin{aligned} i\hbar\dot{a} &= \lambda_x \cos\omega t e^{i(E_1-E_2)t/\hbar} b, \\ i\hbar\dot{b} &= \lambda_x \cos\omega t e^{i(E_2-E_1)t/\hbar} a. \end{aligned} \quad (4.45)$$

(Here we have neglected a small diagonal perturbation, λ_z .)

Let us now focus on the slow evolution of the coefficients on the time scale of qubit precession, and average Eqs.(4.45) over the period of the precession. This approximation is known in the theory of two-level systems as the "rotating wave approximation (RWA)". Then, taking into account the resonance condition, we get the simple equations,

$$i\hbar\dot{a} = \frac{\lambda_x}{2} b, \quad i\hbar\dot{b} = \frac{\lambda_x}{2} a, \quad (4.46)$$

whose solutions read,

$$\begin{aligned} a^{(1)}(t) &= b^{(1)}(t) = e^{-i\lambda_x t/2\hbar}, \\ a^{(2)}(t) &= -b^{(2)}(t) = e^{i\lambda_x t/2\hbar}. \end{aligned} \quad (4.47)$$

Thus, the dynamics of a driven qubit is characterized by a linear combination of the two wave functions,

$$\begin{aligned} |\psi^{(1)}\rangle &= \frac{1}{\sqrt{2}}e^{-i\lambda_x t/2\hbar} \left(e^{-iE_1 t/\hbar}|E_1\rangle + e^{-iE_2 t/\hbar}|E_2\rangle \right), \\ |\psi^{(2)}\rangle &= \frac{1}{\sqrt{2}}e^{i\lambda_x t/2\hbar} \left(e^{-iE_1 t/\hbar}|E_1\rangle - e^{-iE_2 t/\hbar}|E_2\rangle \right). \end{aligned} \quad (4.48)$$

Let us assume that the qubit was initially in the ground state, $|E_1\rangle$, and that the perturbation was switched on instantly. Then the wave function of the driven qubit will take the form,

$$|\psi\rangle = \cos \frac{\lambda_x t}{2\hbar} e^{-iE_1 t/\hbar}|E_1\rangle + i \sin \frac{\lambda_x t}{2\hbar} e^{-iE_2 t/\hbar}|E_2\rangle. \quad (4.49)$$

Correspondingly, the probabilities of the level occupations will oscillate in time,

$$\begin{aligned} P_1 &= \cos^2 \frac{\lambda_x t}{2\hbar} = \frac{1}{2} \left(1 + \cos \frac{\lambda_x t}{\hbar} \right), \\ P_2 &= \sin^2 \frac{\lambda_x t}{2\hbar} = \frac{1}{2} \left(1 - \cos \frac{\lambda_x t}{\hbar} \right), \end{aligned} \quad (4.50)$$

with small frequency $\Omega_R = \lambda_x/\hbar \ll \omega$, Rabi oscillations, illustrated in Fig. 6.

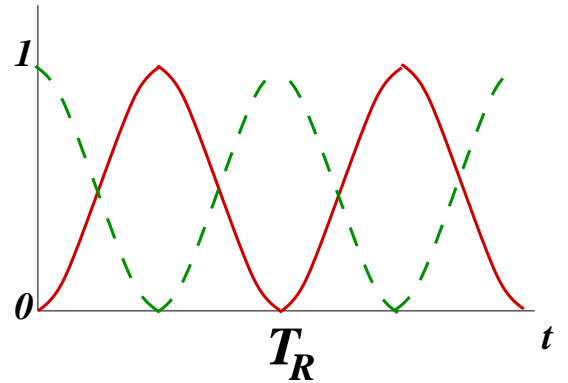


FIG. 6: Rabi oscillation of populations of lower level (full line) and upper level (dashed line) at exact resonance (zero detuning). $T_R = 2\pi/\Omega_R$ is the period of Rabi oscillations.

F. Decoherence of qubit systems

Descriptions of the qubit dynamics in terms of the density matrix and Liouville equation are more general than descriptions in terms of the wave function, allowing the effects of dissipation to be included. The density matrix defined in Section IV B for a pure quantum state possesses the projector operator property, $\hat{\rho}^2 = \hat{\rho}$. This assumption can be lifted, and then the density matrix describes a statistical mixture of pure states, say energy

eigenstates,

$$\hat{\rho} = \sum_i \rho_i |E_i\rangle\langle E_i|. \quad (4.51)$$

The density matrix acquires off-diagonal elements when the basis rotates away from the energy eigenbasis. Such a mixed state cannot be represented by the vector on the Bloch sphere; however, its evolution is still described by the Liouville equation (4.26),

$$i\hbar\partial_t\hat{\rho} = [\hat{H}, \hat{\rho}]. \quad (4.52)$$

The density matrix in Eq. (4.51) is the stationary solution of the Liouville equation. The evolution of an arbitrary density matrix, off-diagonal in the energy eigenbasis, is given by the equations,

$$\rho_1, \rho_2 = \text{const}, \quad \rho_{12} \propto e^{i(E_1 - E_2)t/\hbar}. \quad (4.53)$$

Dissipation is included in the density matrix description by extending the qubit Hamiltonian and including interaction with an environment. The environment for macroscopic superconducting qubits basically consists of various dissipative elements in external circuits which provide bias, control, and measurement of the qubit. The "off-chip" parts of these circuits are usually kept at room temperature and produce significant noise. Examples are the fluctuations in the current source producing magnetic field to bias flux qubits and, similarly, fluctuations of the voltage source to bias gate of the charge qubits. Electromagnetic radiation from the qubit during operation is another dissipative mechanisms. There are also intrinsic microscopic mechanisms of decoherence, such as fluctuating trapped charges in the substrate of the charge qubits, and fluctuating trapped magnetic flux in the flux qubits, believed to produce dangerous 1/f noise. Another intrinsic mechanism is possibly the losses in the tunnel junction dielectric layer. Various kinds of environment are commonly modelled with an infinite set of linear oscillators in thermal equilibrium (thermal bath), linearly coupled to the qubit (Caldeira-Leggett model^{2,3}). The extended qubit-plus-environment Hamiltonian has the form in the qubit energy eigenbasis⁸²,

$$\hat{H} = -\frac{1}{2}E\sigma_z + \sum_i (\lambda_{iz}\sigma_z + \lambda_{i\perp}\sigma_{\perp})X_i + \sum_i \left(\frac{\hat{P}_i^2}{2m} + \frac{m\omega_i^2 X_i^2}{2} \right), \quad (4.54)$$

where $E = E_1 - E_2$. The physical effects of the two coupling terms in Eq. (4.54) are quite different. The "transverse" coupling term proportional to λ_{\perp} induces interlevel transitions and eventually leads to the relaxation. The "longitudinal" coupling term proportional to λ_z commutes with the qubit Hamiltonian and thus does not induce interlevel transitions. However, it randomly changes the level spacing, which eventually leads to the loss of phase coherence, dephasing. The effect of both

processes, relaxation and dephasing, are referred to as decoherence.

Coupling to the environment leads, in the simplest case, to the following modification of the Liouville equation^{83,84},

$$\partial_t \rho_z = -\frac{1}{T_1}(\rho_z - \rho_z^{(0)}), \quad (4.55)$$

$$\partial_t \rho_{12} = \frac{i}{\hbar}E \rho_{12} - \frac{1}{T_2} \rho_{12}. \quad (4.56)$$

This equation is known as the Bloch-Redfield equation. The first equation describes relaxation of the level population to the equilibrium form, $\rho_z^{(0)} = -(1/2) \tanh(E/2kT)$, T_1 being the relaxation time. The second equation describes disappearance of the off-diagonal matrix element during characteristic time T_2 , dephasing.

The relaxation time is determined by the spectral density of the environmental fluctuations at the qubit frequency,

$$\frac{1}{T_1} = \frac{\lambda_{\perp}^2}{2} S_{\phi}(\omega = E). \quad (4.57)$$

The particular form of the spectral density depends on the properties of the environment, which are frequently expressed via the impedance (response function) of the environment. The most common environment consists of a pure resistance, in this case, $S_{\phi}(\omega) \propto \omega$, at low frequencies.

The dephasing time consists of two parts,

$$\frac{1}{T_2} = \frac{1}{2T_1} + \frac{1}{T_{\phi}}. \quad (4.58)$$

The first part is generated by the relaxation process, while the second part results from the pure dephasing due to the longitudinal coupling to the environment. This pure dephasing part is proportional to the spectral density of the fluctuation at zero frequency.

$$\frac{1}{T_{\phi}} = \frac{\lambda_z^2}{2} S_{\phi}(\omega = 0). \quad (4.59)$$

There is already a vast recent literature on decoherence and noise in superconducting circuits, qubits and detectors, and how to engineer the qubits and environment to minimize decoherence and relaxation^{20,42,86,87,88,89,90,91,92,93,94,95,96,97,98,99,100,101,102,103,104,105,106}. Many of these issues will be at the focus of this article.

V. CLASSICAL SUPERCONDUCTING CIRCUITS

In this section we describe a number of elementary superconducting circuits with tunnel Josephson junctions,

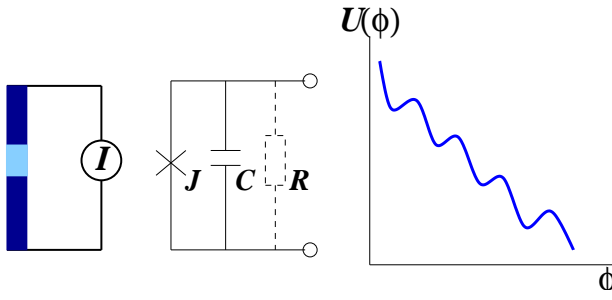


FIG. 7: Current-biased Josephson junction (JJ) (left), equivalent circuit (center), and effective (washboard-like) potential (right). The superconducting leads are indicated with dark color, and the tunnel junction with light color.

which are used as building blocks in qubit applications. These basic circuits are: single current biased Josephson junction; single Josephson junction (JJ) included in a superconducting loop (rf SQUID); two Josephson junctions included in a superconducting loop (dc SQUID); and an ultra-small superconducting island connected to a massive superconducting electrode via tunnel Josephson junction (Single Cooper pair Box, SCB).

A. Current biased Josephson junction

The simplest superconducting circuit, shown in Fig. 7, consists of a tunnel junction with superconducting electrodes, a tunnel Josephson junction, connected to a current source. An equivalent electrical circuit, which represents the junction consists of the three lumped elements connected in parallel: the junction capacitance C , the junction resistance R , which generally differs from the normal junction resistance R_N and strongly depends on temperature and applied voltage, and the Josephson element associated with the tunneling through the junction.

The current-voltage relations for the junction capacitance and resistance have standard forms, $I_C = C(dV/dt)$, and $I_R = V/R$. To write down a similar relation for the Josephson element, it is necessary to introduce the superconducting phase difference $\phi(t)$ across the junction, often simply referred to as the superconducting phase, which is related to the voltage drop across the junction,

$$\phi(t) = \frac{2e}{\hbar} \int V dt + \phi, \quad (5.1)$$

where ϕ is the time-independent part of the phase difference. The phase difference can be also related to a magnetic flux,

$$\phi = \frac{2e}{\hbar} \Phi = 2\pi \frac{\Phi}{\Phi_0}, \quad (5.2)$$

where $\Phi_0 = h/2e$ is the magnetic flux quantum. The

current through the Josephson element has the form⁸⁵,

$$I_J = I_c \sin \phi, \quad (5.3)$$

where I_c is the critical Josephson current, i.e. the maximum non-dissipative current that may flow through the junction. The microscopic theory of superconductivity^{111,112,113} gives the following equation for the Josephson current,

$$I_c = \frac{\pi \Delta}{2eR_N} \tanh \frac{\Delta}{2T}, \quad (5.4)$$

where Δ is the superconducting order parameter, and T is the temperature. Using these relations and expressing voltage through the superconducting phase, we can write down Kirchhoff's rule for the circuit,

$$\frac{\hbar}{2e} C \ddot{\phi} + \frac{\hbar}{2eR} \dot{\phi} + I_c \sin \phi = I_e, \quad (5.5)$$

where I_e is the bias current. This equation describes the dynamics of the phase, and it has the form of a damped non-linear oscillator. The role of the non-linear inductance is here played by the Josephson element.

The dissipation determines the qubit lifetime, and therefore circuits suitable for qubit applications must have extremely small dissipation. Let us assume zero level of the dissipation, dropping the resistive term in Eq. (5.5). Then the circuit dynamic equations, using the mechanical analogy, can be presented in the Lagrangian form, and, equivalently, in the Hamiltonian form. The circuit Lagrangian consists of the difference between the kinetic and potential energies, the electrostatic energy of the junction capacitors playing the role of kinetic energy, while the energy of the Josephson current plays the role of potential energy.

The kinetic energy corresponding to the first term in the Kirchhoff equation (5.5) reads,

$$K(\dot{\phi}) = \left(\frac{\hbar}{2e} \right)^2 \frac{C \dot{\phi}^2}{2}. \quad (5.6)$$

This energy is equal to the electrostatic energy of the junction capacitor, $CV^2/2$. It is convenient to introduce the charging energy of the junction capacitor charged with one electron pair (Cooper pair),

$$E_C = \frac{(2e)^2}{2C}, \quad (5.7)$$

in which case Eq. (5.6) takes the form

$$K(\dot{\phi}) = \frac{\hbar^2 \dot{\phi}^2}{4E_C}. \quad (5.8)$$

The potential energy corresponds to the last two terms in Eq. (5.5), and consists of the energy of the Josephson current, and the magnetic energy of the bias current,

$$U(\phi) = E_J(1 - \cos \phi) - \frac{\hbar}{2e} I_e \phi, \quad (5.9)$$

where $E_J = \hbar/2e I_c$ is the Josephson energy. This potential energy has a form of a washboard (see Fig. 7). In the absence of bias current this potential corresponds to a pendulum with the frequency of small-amplitude oscillations given by

$$\omega_J = \sqrt{\frac{2eI_c}{\hbar C}}. \quad (5.10)$$

This frequency is known as the plasma frequency of the Josephson junction. When current bias is applied, the pendulum potential becomes tilted, its minima becoming more shallow, and finally disappearing when the bias current becomes equal to the critical current, $I_e = I_c$. At this point, the plasma oscillations become unstable, which physically corresponds to switching to the dissipative regime and the voltage state.

Now we are ready to write down the Lagrangian for the circuit, which is the difference between the kinetic and potential energies. Combining Eqs. (5.8) and (5.9), we get,

$$L(\phi, \dot{\phi}) = \frac{\hbar^2 \dot{\phi}^2}{4E_C} - E_J(1 - \cos \phi) + \frac{\hbar}{2e} I_e \phi. \quad (5.11)$$

It is straightforward to check that the Kirchhoff equation (5.5) coincides with the dynamic equation following from the Lagrangian (5.11), using

$$\frac{d}{dt} \frac{\partial L}{\partial \dot{\phi}} - \frac{\partial L}{\partial \phi} = 0. \quad (5.12)$$

It is important to emphasize, that the resistance of the junction can only be neglected for low temperatures, and also only for slow time evolution of the phase; both the temperature and the characteristic frequency must be small compared to the magnitude of the energy gap in the superconductor: $T, \hbar\omega \ll \Delta$. The physical reason behind this constraint concerns the amount of generated quasi-particle excitations in the system: if the constraint is fulfilled, the amount of equilibrium and non-equilibrium excitations will be exponentially small. Otherwise, the gap in the spectrum will not play any significant role, dissipation becomes large, and the advantage of the superconducting state compared to the normal conducting state will be lost.

B. rf-SQUID

The rf-SQUID is the next important superconducting circuit. It consists of a tunnel Josephson junction inserted in a superconducting loop, as illustrated in Fig. 8. This circuit realizes magnetic flux bias for the Josephson junction¹¹³. To describe this circuit, we introduce the current associated with the inductance L of the leads,

$$I_L = \frac{\hbar}{2eL}(\phi - \phi_e), \quad \phi_e = \frac{2e}{\hbar} \Phi_e \quad (5.13)$$

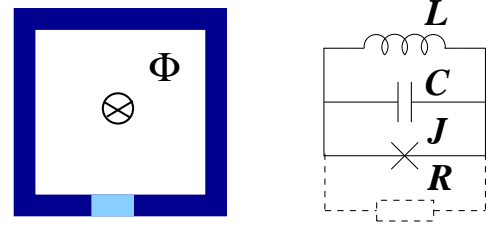


FIG. 8: Superconducting quantum interference device - SQUID (left) consists of a superconducting loop (dark) interrupted by a tunnel junction (light); magnetic flux Φ is sent through the loop. Right: equivalent circuit.

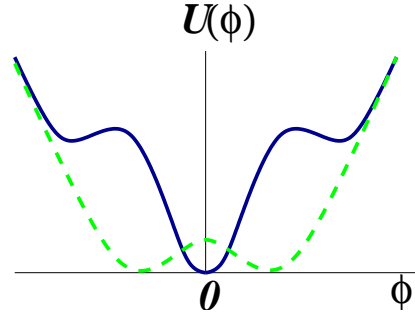


FIG. 9: SQUID potential: the full (dark) curve corresponds to integer bias flux (in units of flux quanta), while the dashed (light) curve corresponds to half-integer bias flux.

where Φ_e is the external magnetic flux threading the SQUID loop. The Kirchhoff rule for this circuit takes the form

$$\frac{\hbar}{2e} C \ddot{\phi} + \frac{\hbar}{2eR} \dot{\phi} + I_c \sin \phi + \frac{\hbar}{2eL} (\phi - \phi_e) = 0. \quad (5.14)$$

While neglecting the Josephson tunneling ($I_c = 0$), this equation describes a damped linear oscillator of a conventional LC-circuit. The resonant frequency is then,

$$\omega_{LC} = \frac{1}{\sqrt{LC}}, \quad (5.15)$$

and the (weak) damping is $\gamma = 1/RC$.

In the absence of dissipation, it is straightforward to write down the Lagrangian of the rf-SQUID,

$$L(\phi, \dot{\phi}) = \frac{\hbar^2 \dot{\phi}^2}{4E_C} - E_J(1 - \cos \phi) - E_L \frac{(\phi - \phi_e)^2}{2}. \quad (5.16)$$

The last term in this equation corresponds to the energy of the persistent current circulating in the loop,

$$E_L = \frac{\Phi_0^2}{4\pi^2 L}. \quad (5.17)$$

The potential energy $U(\phi)$ corresponding to the last two terms in Eq. (5.16) is sketched in Fig. 9.

For bias flux equal to integer number of flux quanta, or $\phi_e 2\pi n$, the potential energy of the SQUID has one absolute minimum at $\phi = \phi_e$. For half integer flux quanta

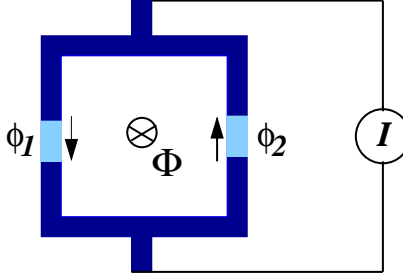


FIG. 10: dc SQUID consists of two tunnel junctions included in a superconducting loop; arrows indicate the direction of the positive Josephson current.

the potential energy has two degenerate minima, which correspond to the two persistent current states circulating in the SQUID loop in the opposite directions. This configuration of the potential energy provides the basis for constructing a persistent-current flux qubit (PCQ).

C. dc SQUID

We now consider consider the circuit shown in Fig. 10 consisting of two Josephson junctions coupled in parallel to a current source. The new physical feature here, compared to a single current-biased junction, is the dependence of the effective Josephson energy of the double junction on the magnetic flux threading the SQUID loop.

Let us evaluate the effective Josephson energy. Now the circuit has two dynamical variables, superconducting phases, $\phi_{1,2}$ across the two Josephson junctions. Defining phases as shown in the figure, and applying considerations from Sections V A and V B we find for the static Josephson currents,

$$I_{c1} \sin \phi_1 - I_{c2} \sin \phi_2 = I_e, \quad (5.18)$$

where I_e is the biasing current. Let us further assume small inductance of the SQUID loop and neglect the magnetic energy of circulating currents. Then the total voltage drop over the two junctions is zero, $V_1 + V_2 = 0$, and therefore, $\phi_1 + \phi_2 = \phi_e$, where ϕ_e is the biasing phase related to biasing magnetic flux. Introducing new variables,

$$\phi_{\pm} = \frac{\phi_1 \pm \phi_2}{2}, \quad (5.19)$$

and taking into account that $2\phi_+ = \phi_e$, we rewrite equation (5.18) on the form,

$$I_c(\phi_e) \sin(\phi_- + \alpha) = I_e, \quad (5.20)$$

where

$$I_c(\phi_e) = \sqrt{I_{c1}^2 + I_{c2}^2 + I_{c1}I_{c2} \cos \phi_e}, \quad (5.21)$$

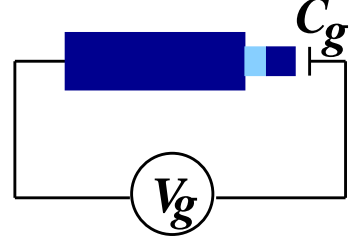


FIG. 11: Single Cooper pair box (SCB): a small superconducting island connected to a bulk superconductor via a tunnel junction; the island potential is controlled by the gate voltage V_g .

and

$$\tan \alpha = \frac{I_{c1} - I_{c2}}{I_{c1} + I_{c2}} \tan \frac{\phi_e}{2}. \quad (5.22)$$

For a symmetric SQUID with $I_{c1} = I_{c2}$, giving $\alpha = 0$, Eq. (5.20) reduces to the form

$$2I_c \cos(\phi_e/2) \sin \phi_- = I_e. \quad (5.23)$$

The potential energy generated by Eq. (5.20) has the form,

$$U(\phi) = 2E_J \cos\left(\frac{\phi_e}{2}\right) (1 - \cos \phi_-) - \frac{\hbar}{2e} I_e \phi_-, \quad (5.24)$$

which indeed is similar to the potential energy of a single current biased junction, Eq. (5.9) and Fig. 9, but with flux-controlled critical current. This property of the SQUID is used in qubit applications for controlling the Josephson coupling, and also for measuring the qubit flux.

The kinetic energy of the SQUID can readily be written down noticing that it is associated with the charging energy of the two junction capacitances connected in parallel,

$$K(\dot{\phi}) = \left(\frac{\hbar}{2e}\right)^2 (C_1 + C_2) \frac{\dot{\phi}^2}{2}. \quad (5.25)$$

Thus the Lagrangian for the SQUID has a form similar to Eq. (5.11) where $E_C = (2e)^2/2(C_1 + C_2)$,

$$L(\phi, \dot{\phi}) = \frac{\hbar^2 \dot{\phi}^2}{4E_C} - 2E_J \cos\left(\frac{\phi_e}{2}\right) (1 - \cos \phi) + \frac{\hbar}{2e} I_e \phi. \quad (5.26)$$

D. Single Cooper Pair Box (SCB)

There is a particularly important Josephson junction circuit consisting of a small superconducting island connected via a Josephson tunnel junction to a large superconducting reservoir (see Fig. 11).

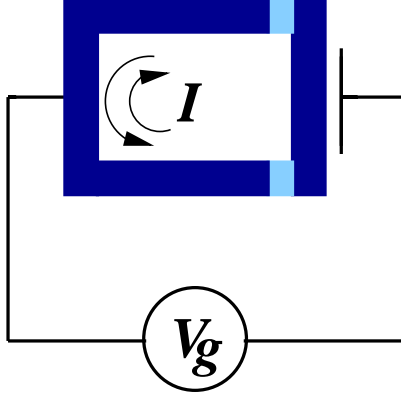


FIG. 12: Single Cooper pair transistor (SCT): SCB with loop-shape bulk electrodes; charge fluctuations on the island produces current fluctuation in the loop.

The island is capacitively coupled to another massive electrode, which may act as an electrostatic gate. The voltage source V_g controls the gate potential. In the normal state, such a circuit is named a Single Electron Box (SEB)¹¹⁴ for the following reason: if the junction resistance exceeds the quantum resistance $R_q \approx 26 \text{ k}\Omega$, and the temperature is small compared to the charging energy of the island, the system is in a Coulomb blockade regime^{1,115} where the electrons can only be transferred to the island one by one, the number of electrons on the island being controlled by the gate voltage. In the superconducting state, the same circuit is called a Single Cooper pair Box (SCB)^{116,117}; for a review see the book¹¹⁸. An experimental SCB device is shown in Fig. 2. In this section we consider a classical Lagrangian for the circuit. Since the structure now has two capacitances, one from the tunnel junction, C , and another one from the gate, C_g , the electrostatic term in the Hamiltonian must be reconsidered.

Let us first evaluate the electrostatic energy of the SCB. It has the form,

$$\frac{CV^2}{2} + \frac{C_g(V_g - V)^2}{2}, \quad (5.27)$$

where V is the voltage over the tunnel junction. Then the Lagrangian can be written (omitting the constant term),

$$L(\phi, \dot{\phi}) = \frac{C_\Sigma}{2} \left(\frac{\hbar}{2e} \dot{\phi} - \frac{C_g}{C_\Sigma} V_g \right)^2 - E_J(1 - \cos \phi), \quad (5.28)$$

where $C_\Sigma = C + C_g$.

The interferometer effect of two Josephson junctions connected in parallel (Fig. 12) can be used to control the Josephson energy of the single Cooper pair box. This setup can be viewed as a flux-biased dc SQUID where Josephson junctions have very small capacitances and are placed very close to each other so that the island confined between them has large charging energy. The gate electrode is connected to the island to control the charge.

The effect of the gate electrode is only essential for the kinetic term, and repeating previous analysis we arrive at the following equation for the kinetic energy (assuming for simplicity identical junctions),

$$K(\dot{\phi}_-) = \frac{C_\Sigma}{2} \left(\frac{\hbar}{2e} \dot{\phi}_- - \frac{C_g}{C_\Sigma} V_g \right)^2, \\ C_\Sigma = 2C + C_g. \quad (5.29)$$

Combining this kinetic energy with the potential energy derived in previous subsection, we arrive at the Lagrangian of the SCB (cf. Eq. (5.28)) where both the charging energy and the Josephson energy can be controlled,

$$L = \frac{C_\Sigma}{2} \left(\frac{\hbar}{2e} \dot{\phi}_- - \frac{C_g}{C_\Sigma} V_g \right)^2 \\ + 2E_J \cos \left(\frac{\phi_e}{2} \right) \cos \phi_-. \quad (5.30)$$

VI. QUANTUM SUPERCONDUCTING CIRCUITS

One may look upon the Kirchhoff rules, as well as the circuit Lagrangians, as the equations describing the dynamics of electromagnetic field in the presence of the electric current. Generally, this electromagnetic field is a quantum object, and therefore there must be a quantum generalization of the equations in the previous section. At first glance, the idea of quantization of an equation describing a macroscopic circuit containing a huge amount of electrons may seem absurd. To convince ourselves that the idea is reasonable, it is useful to recall an early argument in favor of the quantization of electron dynamics in atoms, and to apply it to the simplest circuit, an rf-SQUID: When the current oscillations are excited in the SQUID, it works as an antenna radiating electromagnetic waves. Since EM waves are quantized, the same should apply to the antenna dynamics.

To quantize the circuit equation, we follow the conventional way of canonical quantization: first we introduce the Hamiltonian and then change the classical momentum to the momentum operator. The Hamiltonian is related to the Lagrangian as

$$H(p, \phi) = p\dot{\phi} - L, \quad (6.1)$$

where p is the canonical momentum conjugated to coordinate ϕ ,

$$p = \frac{\partial L}{\partial \dot{\phi}}. \quad (6.2)$$

For the simplest case of a single junction, Eq. (5.6), the momentum reads,

$$p = \left(\frac{\hbar}{2e} \right)^2 C \dot{\phi}. \quad (6.3)$$

The so defined momentum has a simple interpretation: it is proportional to the charge $q = CV$ on the junction capacitor, $p = (\hbar/2e)q$, or the number n of electronic pairs on the junction capacitor,

$$p = \hbar n. \quad (6.4)$$

The Hamiltonian for the current-biased junction has the form (omitting a constant),

$$H = E_C n^2 - E_J \cos \phi - \frac{\hbar}{2e} I_e \phi. \quad (6.5)$$

Similarly, the Hamiltonian for the SQUID circuit has the form

$$H(n, \phi) = E_C n^2 - E_J \cos \phi + E_L \frac{(\phi - \phi_e)^2}{2}. \quad (6.6)$$

The dc SQUID considered in the previous Section V C has two degrees of freedom. The Hamiltonian can be written by generalizing Eqs. (6.5), (6.6) for the phases ϕ_{\pm} . In the symmetric case we have,

$$\begin{aligned} H = & E_C n_+^2 + E_C n_-^2 - 2E_J \cos \phi_+ \cos \phi_- \\ & + E_L \frac{(2\phi_+ - \phi_e)^2}{2} + \frac{\hbar}{2e} I_e \phi_-. \end{aligned} \quad (6.7)$$

For the SCB, Eq. (5.28), the conjugated momentum has the form,

$$p = \frac{\hbar C_{\Sigma}}{2e} \left(\frac{\hbar}{2e} \dot{\phi} - \frac{C_g}{C_{\Sigma}} V_g \right), \quad (6.8)$$

and the Hamiltonian reads,

$$H = E_C (n - n_g)^2 - E_J \cos \phi, \quad (6.9)$$

where now $E_C = (2e)^2/2C_{\Sigma}$, and $n = p/\hbar$ has the meaning of the number of electron pairs (Cooper pairs) on the island electrode. $n_g = -C_g V_g / 2e$ is the charge on the gate capacitor (in units of Cooper pairs (2e)), which can be tuned by the gate potential, and which therefore plays the role of external controlling parameter.

The quantum Hamiltonian results from Eq. (6.2) by substituting the classical momentum p for the differential operator,

$$\hat{p} = -i\hbar \frac{\partial}{\partial \phi}. \quad (6.10)$$

Similarly, one can define the charge operator,

$$\hat{q} = -2ei \frac{\partial}{\partial \phi}, \quad (6.11)$$

and the operator of the pair number,

$$\hat{n} = -i \frac{\partial}{\partial \phi}. \quad (6.12)$$

The commutation relation between the phase operator and the pair number operator has a particularly simple form,

$$[\phi, \hat{n}] = i. \quad (6.13)$$

The meaning of the quantization procedure is the following: the phase and charge dynamical variables can not be exactly determined by means of physical measurements; they are fundamentally random variables with the probability of realization of certain values given by the modulus square of the wave function of a particular state,

$$\langle \phi \rangle = \int \psi^*(\phi) \phi \psi(\phi) d\phi, \quad \langle q \rangle = \int \psi^*(\phi) \hat{q} \psi(\phi) d\phi. \quad (6.14)$$

The time evolution of the wave function is given by the Schrödinger equation,

$$i\hbar \frac{\partial \psi(\phi, t)}{\partial t} = \hat{H} \psi(\phi, t) \quad (6.15)$$

where \hat{H} is the circuit quantum Hamiltonian. The explicit form of the quantum Hamiltonian for the circuits considered above, is the following:

rf-SQUID:

$$\hat{H} = E_C \hat{n}^2 - E_J \cos \phi + E_L \frac{(\phi - \phi_e)^2}{2}; \quad (6.16)$$

Current biased JJ:

$$\hat{H} = E_C \hat{n}^2 - E_J \cos \phi + \frac{\hbar}{2e} I_e \phi; \quad (6.17)$$

dc-SQUID:

$$\begin{aligned} \hat{H} = & E_C \hat{n}_+^2 + E_C \hat{n}_-^2 - 2E_J \cos \phi_+ \cos \phi_- \\ & + E_L \frac{(2\phi_+ - \phi_e)^2}{2} + \frac{\hbar}{2e} I_e \phi_-. \end{aligned} \quad (6.18)$$

and finally the *single Cooper pair box (SCB)*:

$$\hat{H} = E_C (\hat{n} - n_g)^2 - E_J \cos \phi, \quad (6.19)$$

For junctions connecting macroscopically large electrodes, the charge on the junction capacitor is a continuous variable. This implies that no specific boundary conditions on the wave function are imposed. The situation is different for the SCB: in this case one of the electrodes, the island, is supposed to be small enough to show pronounced charging effects. If tunneling is forbidden, electrons are trapped on the island, and their number is always integer (the charge quantization condition). However, there is a difference between the energies of even and odd numbers of electrons on the island: while an electron pair belongs to the superconducting condensate and has the additional energy E_C , a single electron forms an excitation and thus its energy consists of the charging energy, $E_C/2$ plus the excitation energy,

Δ (parity effect)¹¹⁶. To prevent the appearance of individual electrons on the island and to provide the SCB regime, the condition $\Delta \gg E_C/2$ must be fulfilled. Thus when the tunneling is switched on, only Josephson tunneling is allowed since it transfers Cooper pairs and the number of electrons on the island must change pairwise, $n_- = \text{integer}$. In order to provide such a constraint, periodic boundary conditions on the SCB wave function are imposed,

$$\psi(\phi) = \psi(\phi + 2\pi). \quad (6.20)$$

This implies that arbitrary state of the SCB is a superposition of the charge states with integer amount of the Cooper pairs,

$$\psi(\phi) = \sum_n a_n e^{in\phi}. \quad (6.21)$$

The uncertainty of the dynamical variables are not important as long as the relative mean deviations of dynamical variables are small, i.e. the amplitudes of the quantum fluctuations are small. In this case, the particle behaves as a classical particle. It is known from quantum mechanics, that this corresponds to large mass of the particle, in our case, to large junction capacitance. Thus we conclude that the quantum effects in the circuit dynamics are essential when the junction capacitances are sufficiently small. The qualitative criterion is that the charging energy must be larger than, or comparable to, the Josephson energy of the junction, $E_C \sim E_J$.

Typical Josephson energies of the tunnel junctions in qubit circuits are of the order of a few degrees Kelvin or less. Bearing in mind that the insulating layers of the junctions have the thickness of few atomic distances, and modeling the junction as a planar capacitor, the estimated junction area should be smaller than a few square micrometers to observe the circuit quantum dynamics.

One of most important consequences of the quantum dynamics is quantization of the energy of the circuit. Let us consider, for example, the LC circuit. In the classical case, the amplitude of the plasma oscillations has continuous values. In the quantum case the amplitude of oscillation can only have certain discrete values defined through the energy spectrum of the oscillator. The linear oscillator is well studied in the quantum mechanics, and its energy spectrum is very well known,

$$E_n = \hbar\omega_{LC}(n + 1/2), \quad n = 0, 1, 2, \dots \quad (6.22)$$

One may ask, why is quantum dynamics never observed in ordinary electrical circuits? After all, in high-frequency applications, frequencies up to THz are available, which corresponds to a distance between the quantized oscillator levels of order 10K, which can be observed at sufficiently low temperature. For an illuminative discussion on this issue see the paper by Martinis, Devoret and Clarke¹²³. According to Ref. 2 it is the dissipation that kills quantum fluctuations: as known from classical mechanics, the dissipation (normal resistance) broadens the resonance, and good resonators must have small

resonance width, $\gamma = 1/RC$ compared to the resonance frequency, $\gamma \ll \omega_{LC}$. It is intuitively clear that the quantization effect will be destroyed when the level broadening exceeds the level spacing. For quantum behavior of the circuit, narrow resonances, $\gamma \ll \omega_{LC}$, are therefore essential. However, even in this case it is hard to observe the quantum dynamics in linear circuits such as LC-resonators¹²³ because the expectation values of the linear oscillator follow the classical time evolution. Thus the presence of non-linear circuit elements is essential.

The linear oscillator provides the simplest example of a quantum energy level spectrum: it only consists of discrete levels with equal distance between the levels. The level spectrum of the Josephson junction associated with a pendulum potential is more complicated. Firstly, because of the non-linearity (non-parabolic potential wells), the energy spectrum is non-equidistant (anharmonic), the high-energy levels being closer to each other than the low-energy levels. Moreover, for energies larger than the amplitude of the potential (top of the barrier), E_J , the spectrum is continuous. Secondly, one has to take into account the possibility of a particle tunneling between neighboring potential wells: this will produce broadening of the energy levels into energy bands. The level broadening is determined by the overlap of the wave function tails under the potential barriers, and it must be small for levels lying very close to the bottom of the potential wells. Such a situation may only exist if the level spacing, given by the plasma frequency of the tunnel junction is much smaller than the Josephson energy, $\hbar\omega_J \ll E_J$, i.e. when $E_C \ll E_J$. This almost classical regime with Josephson tunneling dominating over charging effects, is called the phase regime, because phase fluctuations are small and the superconducting phase is well defined. In the opposite case, $E_C \gg E_J$, the lowest energy level lies well above the potential barrier, and this situation corresponds to wide energy bands separated by small energy gaps. In this case, the wave function far from the gap edges can be well approximated with a plane wave,

$$\psi_q(\phi) = \exp \frac{iq\phi}{2e}. \quad (6.23)$$

This wave function corresponds to an eigenstate of the charge operator with well defined value of the charge, q . Such a regime with small charge fluctuations is called the charge regime.

VII. BASIC QUBITS

The quantum superconducting circuits considered above contain a large number of energy levels, while for qubit operation only two levels are required. Moreover, these two qubit levels must be well decoupled from the other levels in the sense that transitions between qubit levels and the environment must be much less probable than the transitions between the qubit levels itself. Typically that means that the qubit should involve a low-lying

pair of levels, well separated from the spectrum of higher levels, and not being close to resonance with any other transitions.

A. Single Josephson Junction (JJ) qubit

The simplest qubit realization is a current biased JJ with large Josephson energy compared to the charging energy. In the classical regime, the particle representing the phase either rests at the bottom of one of the wells of the "washboard" potential (Fig. 7), or oscillates within the well. Due to the periodic motion, the average voltage across the junction is zero, $\dot{\phi} = 0$. Strongly excited states, where the particle may escape from the well, correspond to the dissipative regime with non-zero average voltage across the junction, $\dot{\phi} \neq 0$.

In the quantum regime described by the Hamiltonian (6.5),

$$\hat{H} = E_C \hat{n}^2 - E_J \cos \phi - \frac{\hbar}{2e} I_e \phi, \quad (7.1)$$

particle confinement, rigorously speaking, is impossible because of macroscopic quantum tunneling (MQT) through the potential barrier, see Fig. 13. However, the probability of MQT is small and the tunneling may be neglected if the particle energy is close to the bottom of the local potential well, i.e. when $E \ll E_J$. To find the conditions for such a regime, it is convenient to approximate the potential with a parabolic function, $U(\phi) \approx (1/2)E_J \cos \phi_0 (\phi - \phi_0)^2$, where ϕ_0 corresponds to the potential minimum, $E_J \sin \phi_0 = (\hbar/2e)I_e$. Then the lowest energy levels, $E_k = \hbar\omega_p(k + 1/2)$ are determined by the plasma frequency, $\omega_p = 2^{1/4}\omega_J(1 - I_e/I_c)^{1/4}$. It then follows that the levels are close to the bottom of the potential if $E_C \ll E_J$, i.e. when the Josephson junction is in the phase regime, and moreover, if the bias current is not too close to the critical value, $I_e < I_c$.

It is essential for qubit operation that the spectrum in the well is not equidistant. Then the two lowest energy levels, $k = 0, 1$ can be employed for the qubit operation. Truncating the full Hilbert space of the junction to the subspace spanned by these two states, $|0\rangle$ and $|1\rangle$, we may write the qubit Hamiltonian on the form,

$$H_q = -\frac{1}{2}\epsilon\sigma_z, \quad (7.2)$$

where $\epsilon = E_1 - E_0$.

The interlevel distance is controlled by the bias current. When bias current approaches the critical current, level broadening due to MQT starts to play a role, $E_k \rightarrow E_k + i\Gamma_k/2$. The MQT rate for the lowest level is given by⁸²

$$\Gamma_{MQT} = \frac{52\omega_p}{2\pi} \sqrt{\frac{U_{max}}{\hbar\omega_p}} \exp\left(-\frac{7.2U_{max}}{\hbar\omega_p}\right), \quad (7.3)$$

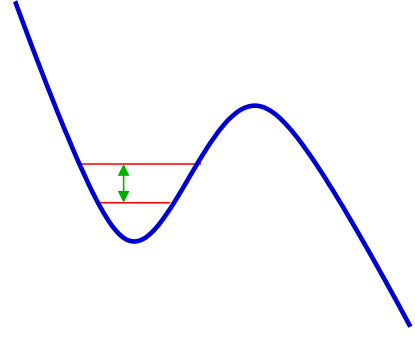


FIG. 13: Quantized energy levels in the potential of a current biased Josephson Junction

where $U_{max} = 2\sqrt{2}(\Phi_0/2\pi)(1 - I_e/I_c)^{3/2}$ is the height of the potential barrier at given bias current.

B. Charge qubits

1. Single Cooper pair Box - SCB

An elementary charge qubit can be made with the SCB operating in the charge regime, $E_C \gg E_J$. Neglecting the Josephson coupling implies the complete isolation of the island of the SCB, with a specific number of Cooper pairs trapped on the island. Correspondingly, the eigenfunctions,

$$E_C(\hat{n} - n_g)^2 |n\rangle = E_n |n\rangle, \quad (7.4)$$

correspond to the charge states $n = 0, 1, 2, \dots$, with the energy spectrum $E_n = E_C(n - n_g)^2$, as shown in Fig. 14. The ground state energy oscillates with the gate voltage, and the number of Cooper pairs in the ground state increases. There are, however, specific values of the gate voltage, e.g. $n_g = 1/2$ where the charge states $|0\rangle$ and $|1\rangle$ become degenerate. Switching on a small Josephson coupling will then lift the degeneracy, forming a tight two-level system.

The qubit Hamiltonian is derived by projecting the full Hamiltonian (6.19) on the two charge states, $|0\rangle$, $|1\rangle$, leading to

$$\hat{H}_{SCB} = -\frac{1}{2}(\epsilon \sigma_z + \Delta \sigma_x), \quad (7.5)$$

where $\epsilon = E_C(1 - 2n_g)$, and $\Delta = E_J$. The qubit level energies are then given by the equation

$$E_{1,2} = \mp \frac{1}{2} \sqrt{E_C^2(1 - 2n_g)^2 + E_J^2}, \quad (7.6)$$

the interlevel distance being controlled by the gate voltage. At the degeneracy point, $n_g = 1/2$, the diagonal part of the qubit Hamiltonian vanishes, the levels being separated by the Josephson energy, E_J , and the qubit eigenstates corresponding to the cat states,

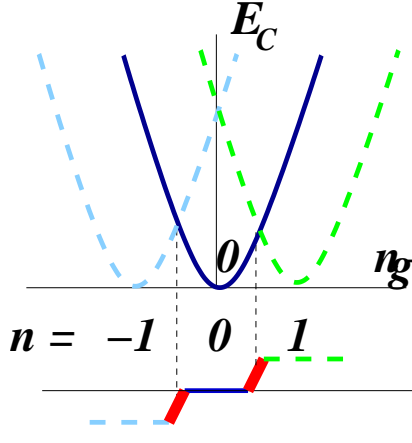


FIG. 14: Single Cooper pair box (SCB): charging energy (upper panel), and charge on the island (lower panel) vs gate potential. Washed-out onsets of the charge steps indicate quantum fluctuations of the charge on the island.

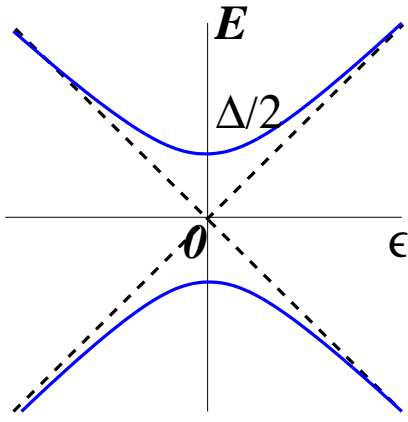


FIG. 15: Energy spectrum of the SCB (solid lines): it results from hybridization of the charge states (dashed lines).

$|E_1\rangle, |E_2\rangle = |0\rangle \mp |1\rangle$. For these states, the average charge on the island is zero, while it changes to $\mp 2e$ far from the degeneracy point, where the qubit eigenstates approach pure charge states.

The SCB was first experimentally realized by Lafarge et al.¹¹⁷, observing the Coulomb staircase with steps of $2e$ and the superposition of the charge states, see also¹³. Realization of the first charge qubit by manipulation of the SCB and observation of Rabi oscillations was done by Nakamura et al.^{1,119,120}, and further investigated theoretically by Choi et al.¹²¹.

2. Single Cooper pair Transistor - SCT

In the SCB, charge fluctuations on the island generate fluctuating current between the island and large electrode. In the two-junction setup discussed at the end of Section VD, an interesting question concerns how the

current is distributed between the two junctions. The answer to this question is apparently equivalent to evaluating the persistent current circulating in the SQUID loop. This current was neglected so far because the associated induced flux $\tilde{\phi} = 2\phi_+ - \phi_e$ was assumed to be frozen, $\tilde{\phi} = 0$, in the limit of infinitely small SQUID inductance, $L = 0$. Let us now lift this assumption and allow fluctuation of the induced flux; the Hamiltonian will then take the form (6.7), in which a gate potential is included in the charging term of the SCB, and the term containing external current is dropped,

$$\hat{H}_{SCT} = E_C(\hat{n}_- - n_g)^2 + E_C\hat{n}_+^2 - 2E_J \cos\phi_+ \cos\phi_- + E_L \frac{(2\phi_+ - \phi_e)^2}{2}. \quad (7.7)$$

($\hat{n}_+ = -i\partial/\partial\phi_+$). For small but non-zero inductance, the amplitude of the induced phase is small, $\tilde{\phi} = 2\phi_+ - \phi_e \ll 1$, and the cosine term containing ϕ_+ can be expanded, yielding the equation

$$\hat{H}_{SCT} = \hat{H}_{SCB}(\phi_-) + \hat{H}_{osc}(\tilde{\phi}) + \hat{H}_{int}. \quad (7.8)$$

$\hat{H}_{SCB}(\phi_-)$ is the SCB Hamiltonian (6.19) with the flux dependent Josephson energy, $E_J(\phi_e) = 2E_J \cos(\phi_e/2)$. $\hat{H}_{osc}(\tilde{\phi})$ describes the linear oscillator associated with the variable $\tilde{\phi}$,

$$\hat{H}_{osc}(\tilde{\phi}) = 4E_C\hat{n}^2 + E_L \frac{\tilde{\phi}^2}{2}, \quad (7.9)$$

and the interaction term reads,

$$\hat{H}_{int} = E_J \sin\left(\frac{\phi_e}{2}\right) \cos(\phi_-) \tilde{\phi}. \quad (7.10)$$

Thus, the circuit consists of the non-linear oscillator of the SCB linearly coupled to the linear oscillator of the SQUID loop. This coupling gives the possibility to measure the charge state of the SCB by measuring the persistent currents and the induced flux.

Truncating Eq. (7.8) we finally arrive at the Hamiltonian which is formally equivalent to the spin-oscillator Hamiltonian,

$$\hat{H}_{SCT} = -\frac{1}{2}(\epsilon\sigma_z + \Delta(\phi_e)\sigma_x) + \lambda\tilde{\phi}\sigma_x + H_{osc}. \quad (7.11)$$

In this equation, $\Delta(\phi_e) = 2E_J \cos(\phi_e/2)$, and $\lambda = E_J \sin(\phi_e/2)$.

C. Flux qubit

1. Quantum rf-SQUID

An elementary flux qubit can be constructed from an rf-SQUID operating in the phase regime, $E_J \gg E_C$. Let us consider the Hamiltonian (6.6) at $\phi_e = \pi$, i.e. at half

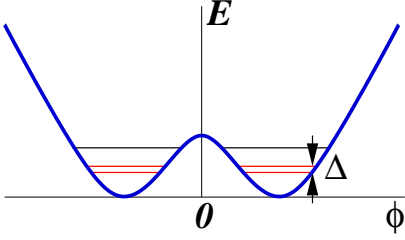


FIG. 16: Double-well potential of the rf-SQUID with degenerate quantum levels in the wells (black). Macroscopic quantum tunneling (MQT) through the potential barrier introduces a level splitting Δ , and the lowest level pair forms a qubit.

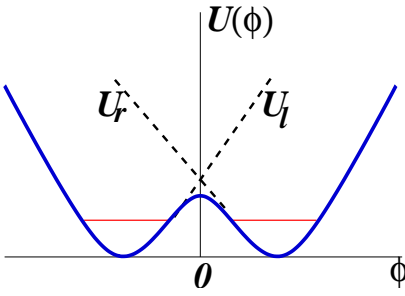


FIG. 17: Flux qubit: truncation of the junction Hamiltonian; dashed lines indicate potentials of the left and right wells with ground energy levels.

integer bias magnetic flux. The potential, $U(\phi)$, shown in Fig. 16 has two identical wells with equal energy levels when MQT between the wells is neglected (phase regime, $\omega_J \ll E_J$). These levels are connected with current fluctuations within each well around averaged values corresponding to clockwise and counterclockwise persistent currents circulating in the loop (the flux states). Let us consider the lowest, doubly degenerate, energy level. When the tunneling is switched on, the levels split, and a tight two-level system is formed with the level spacing determined by the MQT rate, which is much smaller than the level spacing in the well. In the case that the tunneling barrier is much smaller than the Josephson energy, the potential in Eq. (5.9) can be approximated,

$$\begin{aligned} U(\phi) &= E_J(1 - \cos \phi) + E_L \frac{(\phi - \phi_e)^2}{2} \\ &\approx E_L \left(-\varepsilon \frac{\tilde{\phi}^2}{2} - f\tilde{\phi} + \frac{1 + \varepsilon}{24} \tilde{\phi}^4 \right), \end{aligned} \quad (7.12)$$

where $\tilde{\phi} = \phi - \pi$, $f = \phi_e - \pi$, and where

$$\varepsilon = \frac{E_J}{E_L} - 1 \ll 1. \quad (7.13)$$

determines the height of the tunnel barrier.

The qubit Hamiltonian is derived by projecting the whole Hilbert space of the full Hamiltonian (6.6) on the

subspace spanned by these two levels. The starting point of the truncation procedure is to approximate the double well potential with U_l and U_r , as shown in Fig. 17, to confine the particle to the left or to the right well, respectively. The corresponding ground state wave functions $|l\rangle$ and $|r\rangle$ satisfy the stationary Schrödinger equation,

$$\hat{H}_l |l\rangle = E_l |l\rangle, \quad \hat{H}_r |r\rangle = E_r |r\rangle. \quad (7.14)$$

The averaged induced flux for these states, ϕ_l and ϕ_r have opposite signs, manifesting opposite directions of the circulating persistent currents. Let us allow the bias flux to deviate slightly from the half integer value, $\phi_e = \pi + f$, so that the ground state energies are not equal but still close to each other, $E_l \approx E_r$. The tunneling will hybridize the levels, and we can approximate the true eigenfunction, $|E\rangle$,

$$\hat{H}|E\rangle = E|E\rangle, \quad (7.15)$$

with a superposition,

$$|E\rangle = a|l\rangle + b|r\rangle. \quad (7.16)$$

The qubit Hamiltonian is given by the matrix elements of the full Hamiltonian, Eq. (7.15), with respect to the states $|l\rangle$ and $|r\rangle$,

$$\begin{aligned} H_{ll} &= E_l + \langle l|U - U_l|l\rangle, \\ H_{rr} &= E_r + \langle r|U - U_r|r\rangle, \\ H_{rl} &= E_l \langle r|l\rangle + \langle r|U - U_l|l\rangle. \end{aligned} \quad (7.17)$$

In the diagonal matrix elements, the second terms are small because the wave functions are exponentially small in the region where the deviation of the approximated potential from the true one is appreciable. The off diagonal matrix element is exponentially small because of small overlap of the ground state wave functions in the left and right wells, and also here the main contribution comes from the first term. Since the wave functions can be chosen real, the truncated Hamiltonian is symmetric, $H_{lr} = H_{rl}$. Then introducing $\epsilon = E_r - E_l$, and $\Delta/2 = H_{rl}$, we arrive at the Hamiltonian of the flux qubit,

$$\hat{H} = -\frac{1}{2}(\epsilon \sigma_z + \Delta \sigma_x). \quad (7.18)$$

The Hamiltonian of the flux qubit is formally equivalent to that of the charge qubit, Eq. (7.5), but the physical meaning of the terms is rather different. The flux qubit Hamiltonian is written in the flux basis, i.e. the basis of the states with certain averaged induced flux, ϕ_l and ϕ_r (rather than the charge basis of the charge qubit).

The energy spectrum of the flux qubit is obviously the same as that of the charge qubit,

$$E_{1,2} = \mp \frac{1}{2} \sqrt{\epsilon^2 + \Delta^2}, \quad (7.19)$$

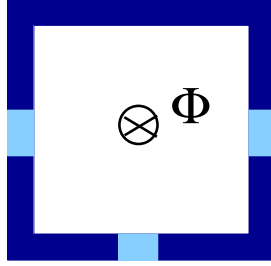


FIG. 18: Persistent current flux qubit (PCQ) with 3 junctions. The side junctions are identical, while the central junction has smaller area.

as shown in Fig. 15. However, for the flux qubit the dashed lines indicate persistent current states in the absence of macroscopic tunneling, and the current degeneracy point ($\epsilon = 0$) corresponds to a half-integer bias flux. The energy levels are controlled by the bias magnetic flux (instead of the gate voltage for the charge qubit).

At the flux degeneracy point, $f = 0$ ($\phi_e = \pi$), the level spacing is determined by the small amplitude of tunneling through macroscopic potential barrier, and the wave functions correspond to the cat states, which are equally weighted superpositions of the flux states. Far from the degeneracy point, the qubit states are almost pure flux states.

The possibility to achieve quantum coherence of macroscopic current states in an rf-SQUID with a small capacitance Josephson junction was first pointed out in 1984 by Leggett¹²². However, successful experimental observation of the effect was achieved only in 2000 by Friedman et al.⁸.

2. 3-junction SQUID - persistent current qubit (PCQ)

The main drawback of the flux qubit with a single Josephson junction (rf-SQUID) described above concerns the large inductance of the qubit loop, the energy of which must be comparable to the Josephson energy to form the required double-well potential profile. This implies large size of the qubit loop, which makes the qubit vulnerable to dephasing by magnetic fluctuations of the environment. One way to overcome this difficulty was pointed out by Mooij et al.⁶, replacing the large loop inductance by the Josephson inductance of an additional tunnel junction, as shown in Fig. 18. The design employs three tunnel junctions connected in series in a superconducting loop. The inductive energy of the loop is chosen to be much smaller than the Josephson energy of the junctions. The two junctions are supposed to be identical while the third junction is supposed to have smaller area, and therefore smaller Josephson and larger charging energy. The Hamiltonian has the form,

$$\hat{H} = E_C[\hat{n}_1^2 + \hat{n}_2^2 + \hat{n}_3^2/(1/2 + \epsilon)] - E_J[\cos \phi_1 + \cos \phi_2 + (1/2 + \epsilon) \cos \phi_3]. \quad (7.20)$$

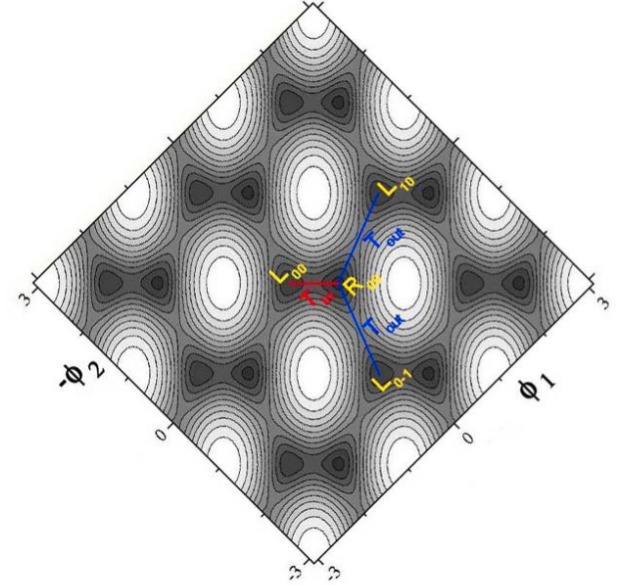


FIG. 19: Potential energy landscape $U(\phi_1, \phi_2) = U(\phi_+, \phi_-)$ of the Delft qubit as a function of the two independent phase variables ϕ_1 and ϕ_2 , or equivalently, ϕ_+ (horizontal axis) and ϕ_- (vertical axis). Black represents the bottom of the potential wells, and white the top of the potential barriers. The qubit double-well potential is determined by the potential landscape centered around the origin in the horizontal direction, and typically has the shape shown in Fig. 16. *Courtesy of C.H. van der Wal.*

To explain the idea, let us consider the potential energy. The three phases are not independent and satisfy the relation $\phi_1 + \phi_2 + \phi_3 = \phi_e$. Let us suppose that the qubit is biased at half integer flux quantum, $\phi_e = \pi$. Then introducing new variables, $\phi_{\pm} = (\phi_1 \pm \phi_2)/2$, we have

$$U(\phi_+, \phi_-) = -E_J[2 \cos \phi_- \cos \phi_+ - (1/2 + \epsilon) \cos 2\phi_+]. \quad (7.21)$$

The potential landscape is shown in Fig. 19, and the qubit potential consists of the double well structure near the points $(\phi_+, \phi_-) = (0, 0)$. An approximate form of the potential energy is given by

$$U(\phi_+, 0) \approx E_J \left(-2\epsilon \phi_+^2 + \frac{\phi_+^4}{4} \right). \quad (7.22)$$

Each well in this structure corresponds to clock- and counterclockwise currents circulating in the loop. The amplitude of the structure is given by the parameter ϵE_J , and for $\epsilon \ll 1$ the tunneling between these wells dominates. Thus this qubit is qualitatively similar to the single-junction qubit described above, but the quantitative parameters are different and can be significantly optimized.

D. Potential qubits

The superconducting qubits that have been discussed in previous sections exploit the fundamental quantum uncertainty between electric charge and magnetic flux. This uncertainty appears already in the dynamics of a single Josephson junction (JJ), which is the basis for elementary JJ qubits. There are however other possibilities. One of them is to delocalize quantum information in a JJ network by choosing global quantum states of the network as a computational basis. Recently, some rather complicated JJ networks have been discussed, which have the unusual property of degenerate ground state, which might be employed for efficient qubit protection against decoherence^{124,125}.

An alternative possibility of further miniaturization of superconducting qubits could be to replace the standard Josephson junction by a quantum point contact (QPC), using the microscopic conducting modes in the JJ QPC, the bound Andreev states, as a computational basis, allowing control of intrinsic decoherence inside the junction^{105,126}.

To explain the physics of this type of qubit, let us consider an rf SQUID (see Fig. 8) with a junction that has such a small cross section that the quantization of electronic modes in the (transverse) direction perpendicular to the current flow becomes pronounced. In such a junction, quantum point contact (QPC), the Josephson current is carried by a number of independent conducting electronic modes, each of which can be considered an elementary microscopic Josephson junction characterized by its own transparency. The number of modes is proportional to the ratio of the junction cross section and the area of the atomic cell (determined by the Fermi wavelength) of the junction material. In atomic-sized QPCs with only a few conducting modes, the Josephson current can be appreciable if the conducting modes are transparent (open modes). If the junction is fully transparent (reflectivity $R = 0$) then current is a well defined quantity. This will correspond to a persistent current with certain direction circulating in the qubit loop. On the other hand, for a finite reflectivity ($R \neq 0$), the electronic back scattering will induce hybridization of the persistent current states giving rise to strong quantum fluctuation of the current.

Such a quantum regime is distinctly different from the macroscopic quantum coherent regime of the flux qubit described in Section VII, where the quantum hybridization of the persistent current states is provided by charge fluctuations on the junction capacitor. Clearly, charging effects will not play any essential role in quantum point contacts, and the leading role belongs to the microscopic mechanism of electron back scattering. This mechanism is only pronounced in quantum point contacts: in classical (large area) contacts, such as junctions of macroscopic qubits with areas of several square micrometers, the current is carried by a large number ($> 10^4$) of statistically independent conducting modes, and fluctuation of the

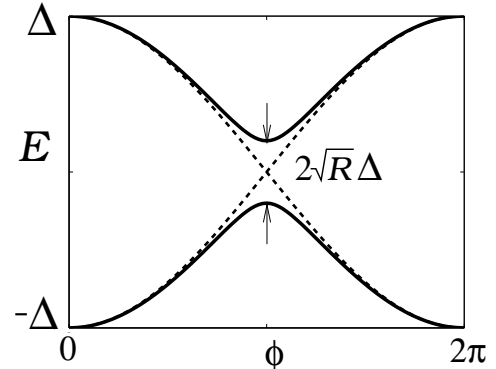


FIG. 20: Energy spectrum of microscopic bound Andreev levels; the level splitting is determined by the contact reflectivity.

net Josephson current is negligibly small.

In QPCs, the Josephson effect is associated with microscopic Andreev levels, localized in the junction area, which transport Cooper pairs from one junction electrode to the other^{127,128}. As shown in Fig. 20, the Andreev levels, two levels per conducting mode, lie within the superconducting gap and have the phase-dependent energy spectrum,

$$E_a = \pm \Delta \sqrt{\cos^2(\phi/2) + R \sin^2(\phi/2)}, \quad (7.23)$$

(here Δ is the superconducting order parameter in the junction electrodes). For very small reflectivity, $R \ll 1$, and phase close to π (half integer flux bias) the Andreev two-level system is well isolated from the continuum states. The expectation value for the Josephson current carried by the level is determined by the Andreev level spectrum,

$$I_a = \frac{2e}{\hbar} \frac{dE_a}{d\phi_e}, \quad (7.24)$$

and it has different sign for the upper and lower level. Since the state of the Andreev two-level system is determined by the phase difference and related to the Josephson current, the state can be manipulated by driving magnetic flux through the SQUID loop, and read out by measuring circulating persistent current^{129,130}.

This microscopic physics underlines recent proposal for Andreev level qubit^{105,126}. The qubit is similar to the macroscopic flux qubits with respect to how it is manipulated and measured, but the great difference is that the quantum information is stored in the microscopic quantum states. This difference is reflected in the more complex form of the qubit Hamiltonian, which consists of the two-level Hamiltonian of the Andreev levels strongly coupled to the quantum oscillator describing phase fluctuations,

$$\hat{H} = \Delta e^{-i\sigma_x \sqrt{R} \phi/2} \left(\cos \frac{\phi}{2} \sigma_z + \sqrt{R} \sin \frac{\phi}{2} \sigma_y \right) + \hat{H}_{osc}[\phi], \quad (7.25)$$

$\hat{H}_{osc}[\phi] = E_C \hat{n} + (E_L/2)(\phi - \phi_e)^2$. Comparing this equation with e.g. the SCT Hamiltonian (7.8), we find that the truncated Hamiltonian of the SCB is replaced here by the Andreev level Hamiltonian.

VIII. QUBIT READOUT AND MEASUREMENT OF QUANTUM INFORMATION

In this section we present a number of proposed, and realized, schemes for measuring quantum states of various superconducting qubits.

A. Readout: why, when and how?

As already mentioned in Section III D, the ultimate objective of a qubit readout device is to distinguish the *eigenstates* of a qubit in a single measurement "without destroying the qubit", a so called "single-shot" quantum non-demolition (QND) projective measurement. This objective is essential for several reasons: state preparation for computation, readout for error correction during the calculation, and readout of results at the end of the calculation. Strictly speaking, the QND property is only needed if the qubit must be left in an eigenstate after the readout. In a broader sense, readout of a specific qubit must of course not destroy any other qubits in the system.

It must be carefully noted that one cannot "read out the *state* of a qubit" in a single measurement - this is prohibited by quantum mechanics. It takes repeated measurements on a large number of replicas of the quantum state to characterize the state of the qubit (Eq. (3.1)) - "quantum tomography"¹³¹.

The measurement connects the qubit with the open system of the detector, which collapses the combined system of qubit and measurement device to one of its common eigenstates. If the coupling between the qubit and the detector is weak, the eigenstates are approximately those of the qubit. In general however, one must consider the eigenstates of the total qubit-detector system and manipulate gate voltages and fluxes such that the readout measurement is performed in a convenient energy eigenbasis (see e.g.^{42,79}).

Even under ideal conditions, a single-shot measurement can only determine the population of an eigenstate if the system is prepared in an eigenstate: then the answer will always be either "0" or "1". If an ideal single-shot measurement is used to read out a qubit superposition state, e.g. during Rabi oscillation, then again the answer can only be "0" or "1". To determine the qubit population (i.e. the $|a_1|^2$ and $|a_2|^2$ probabilities) requires repetition of the measurement to obtain the expectation value. During the intermediate stages of quantum computation one must therefore not perform a measurement on a qubit unless one knows, because of the design and timing of the algorithm, that this qubit is in an energy

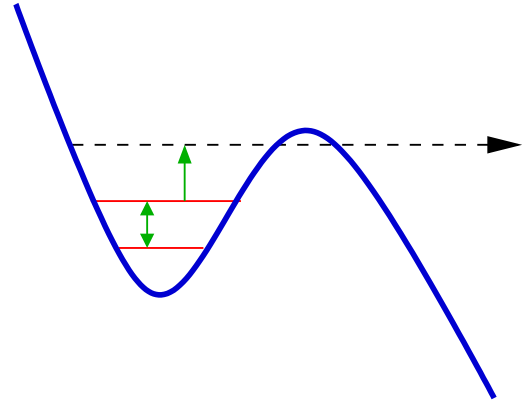


FIG. 21: Measurement of the phase qubit. Long-living levels form the qubit, while the dashed line indicates a leaky level with large energy.

eigenstate. Then the value is predetermined and the qubit left in the eigenstate (Stern-Gerlach-style).

On the other hand, to extract the desired final result it may be necessary to create an ensemble of calculations to be able to perform a complete measurement to determine the expectation values of variables of interest, performing quantum state tomography¹³¹.

B. Direct qubit measurement

Direct destructive measurement of the qubit can be illustrated with the example of a single JJ (phase) qubit, Section VII A. After the manipulation has been performed (e.g. Rabi oscillation), the qubit is left in a superposition of the upper and lower energy states. To determine the probability of the upper state, one slowly increases the bias current until it reaches such a value that the upper energy level equals (or gets close to) the top of the potential barrier, see Fig. 21. Then the junction, being at the upper energy level, will switch from the Josephson branch to the dissipative branch, and this can be detected by measuring the finite average voltage appearing across the junction (voltage state). If the qubit is in the lower energy state the qubit will remain on the Josephson branch and a finite voltage will not be detected (zero-voltage state). An alternative method to activate switching³⁰ is to apply an rf signal with resonant frequency (instead of tilting the junction potential) in order to excite the upper energy level and to induce the switching event, see Fig. 21 (also illustrating a standard readout method in atomic physics).

It is obvious that, in this example, the qubit upper energy state is always destroyed by the measurement. Single-shot measurement is possible provided the MQT rate for the lower energy level is sufficiently small to prevent the junction switching during the measurement time. It is also essential to keep a sufficiently small rate of interlevel transitions induced by fluctuations of the bias

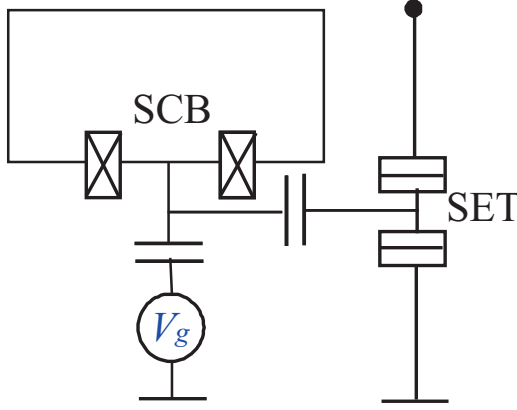


FIG. 22: Single Electron Transistor (SET) capacitively coupled to an SCB.

current and by the current ramping.

A similar kind of direct destructive measurement was performed by Nakamura et al.¹ to detect the state of the charge qubit. The qubit operation was performed at the charge degeneracy point, $u_g = 1$, where the level splitting is minimal. An applied gate voltage then shifted the SCB working point (Fig. 15), inducing a large level splitting of the pure charge states $|0\rangle$ and $|1\rangle$ (the measurement preparation stage). In this process the upper $|1\rangle$ charge state went above the threshold for Cooper pair decay, creating two quasi-particles which immediately tunnel out via the probe junction into the leads. These quasi-particles were measured as a contribution to the classical charge current by repeating the experiment many times. Obviously, this type of measurement is also destructive.

C. Measurement of charge qubit with SET

Non-destructive measurement of the charge qubit has been implemented by connecting the qubit capacitively to a SET electrometer⁶⁹. The idea of this method is to use a qubit island as an additional SET gate (Fig. 22), controlling the dc current through the SET depending on the state of the qubit. When the measurement is to be performed, a driving voltage is applied to the SET, and the dc current is measured. Another version of the measurement procedure is to apply rf bias to the SET (rf-SET^{69,133,134,135}) in Fig. 22, and to measure the dissipative or inductive response. In both cases the transmissivity will show two distinct values correlated with the two states of the qubit. Yet another version has recently been developed by the NEC group¹³⁶ to perform single-shot readout: the Cooper pair on the SCB island then tunnels out onto a trap island (instead of the leads) used as a gate to control the current through the SET.

The physics of the SET-based readout has been extensively studied theoretically (see^{42,137,138} and references therein). A similar idea of controlling the transmission of a quantum point contact (QPC) (instead of an SET)

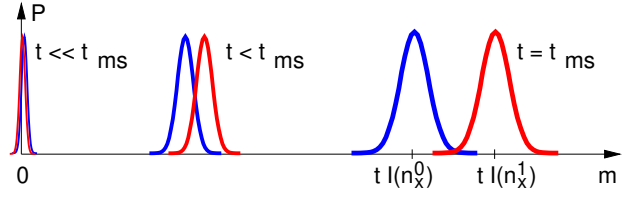


FIG. 23: Probability distributions P of counted electrons as functions of time after the turning on the measurement beam of electrons. *Courtesy of G. Johansson, Chalmers.*

capacitively coupled to a charge qubit has also been extensively discussed in literature^{132,139,140,141,142,143,144}.

The induced charge on the SET gate depends on the state of the qubit, affecting the SET working point and determining the conductivity and the average current. The development of the probability distributions of counted electrons with time is shown in Fig. 23.

As the number of counted electrons grows, the distributions separate and become distinguishable, the distance between the peaks developing as $\sim N$ and the width $\sim \sqrt{N}$. Detailed investigations¹⁴⁴ show that the two electron-number probability distributions correlate with the probability of finding the qubit in either of two energy levels. The long-time development depends on the intensity and frequency distribution of the back-action noise from the electron current. With very weak detector back action, the qubit can relax to $|0\rangle$ during the natural relaxation time T_1 . With very strong back-action noise at the qubit frequency, the qubit may become saturated in a 50/50 mixed state.

D. Measurement via coupled oscillator

Another method of qubit read out that has attracted much attention concerns the measurement of the properties of a linear or non-linear oscillator coupled to a qubit. This method is employed for the measurement of induced magnetic flux and persistent current in the loop of flux qubits and charge-phase qubits, as well as for charge measurement on charge qubits. With this method, the qubit affects the characteristics of the coupled oscillator, e.g. changes the shape of the oscillator potential, after which the oscillator can be probed to detect the changes. There are two versions of the method: resonant spectroscopy of a linear tank circuit/cavity, and threshold detection using biased JJ or SQUID magnetometer.

The first method uses the fact that the resonance frequency of a linear oscillator weakly coupled to the qubit undergoes a shift depending on the qubit state. The effect is most easily explained by considering the SCT Hamiltonian, Eq. (11.1),

$$\begin{aligned} \hat{H}_{SCT} = & -\frac{1}{2}(\epsilon\sigma_z + \Delta(\phi_e)\sigma_x) + \lambda(\phi_e)\tilde{\phi}\sigma_x \\ & + 4E_C\hat{n}^2 + \frac{1}{2}E_L\tilde{\phi}^2. \end{aligned} \quad (8.1)$$

Let us proceed to the qubit energy basis, in which case the qubit Hamiltonian takes the form $-(E/2)\sigma_z$, $E = \sqrt{\epsilon^2 + \Delta^2}$. The interaction term in the qubit eigenbasis will consist of two parts, the longitudinal part, $\lambda_z \dot{\phi} \sigma_z$, $\lambda_z = (\Delta/E)\lambda$, and the transverse part, $\lambda_x \dot{\phi} \sigma_x$, $\lambda_x = (\epsilon/E)\lambda$. In the limit of weak coupling the transverse part of interaction is the most essential. In the absence of interaction ($\phi_e = 0$), the energy spectrum of the qubit + oscillator system is

$$E_{n\mp} = \mp \frac{E}{2} + \hbar\omega(n + \frac{1}{2}), \quad (8.2)$$

where $\hbar\omega = \sqrt{8E_C E_L}$ is the plasma frequency of the oscillator. The effect of weak coupling is enhanced in the vicinity of the resonance, when the oscillator plasma frequency is close to the qubit level spacing, $\hbar\omega \approx E$. Let us assume, however, that the coupling energy is smaller than the deviation from the resonance, $\lambda_x \ll |\hbar\omega - E|$. Then the spectrum of the interacting system in the lowest perturbative order will acquire a shift,

$$\delta E_{n\pm} = \pm (n + 1) \frac{\lambda_x^2 \hbar\omega}{E_L(\hbar\omega - E)}. \quad (8.3)$$

This shift is proportional to the first power of the oscillator quantum number n , which implies that the oscillator frequency acquires a shift (the frequency of the qubit is also shifted^{145,146,147,148,149}). Since the sign of the oscillator frequency shift is different for the different qubit states, it is possible to distinguish the state of the qubit by probing this frequency shift.

In the case of the SCT, the LC oscillator is a generic part of the circuit. It is equally possible to use an additional LC oscillator inductively coupled to a qubit. This type of device has been described by Zorin⁷¹ for SCT readout, and recently implemented for flux qubits by Il'ichev et al.^{27,39}

Figure 24 illustrates another case, namely a charge qubit capacitively coupled to an oscillator, again providing energy resolution for discriminating the two qubit levels¹⁵⁰. Analysis of this circuit is similar to the one discussed below in the context of qubit coupling via oscillators, Section IX. The resulting Hamiltonian is similar to Eq. (9.20), namely,

$$\hat{H} = \hat{H}_{SCB} + \lambda \sigma_y \phi + \hat{H}_{osc}. \quad (8.4)$$

In comparison with the case of the SCT, Eq. (8.4) has a different form of the coupling term, which does not change during rotation to the qubit eigenbasis. Therefore the coupling constant λ directly enters Eq. (8.3). Recently, this type of read out has been implemented for a charge qubit by capacitively coupling the SCB of the qubit to a superconducting strip resonator^{151,152,153}.

E. Threshold detection

To illustrate the threshold-detection method, let us consider an SCT qubit with a third Josephson junction

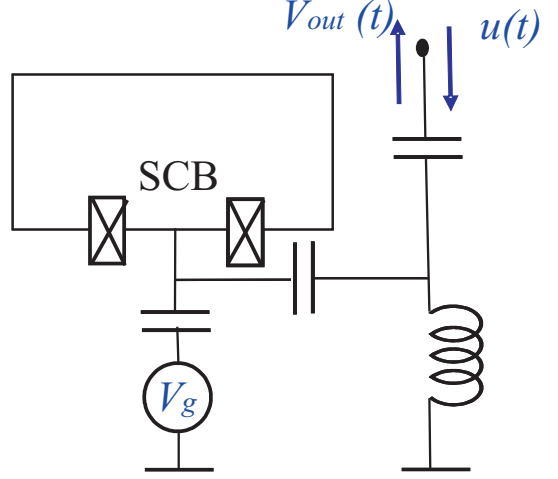


FIG. 24: SCT qubit coupled to a readout oscillator. The qubit is operated by input pulses $u(t)$. The readout oscillator is controlled and driven by ac microwave pulses $V_g(t)$. The output signal will be ac voltage pulses $V_{out}(t)$, the amplitude or phase of which may discriminate between the qubit "0" and "1" states.

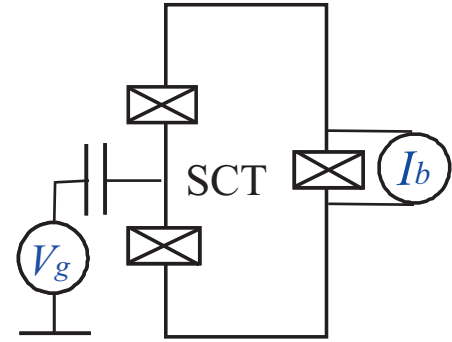


FIG. 25: SCT qubit coupled to a JJ readout quantum oscillator. The JJ oscillator is controlled by dc/ac current pulses $I_b(t)$ adding to the circulating currents in the loop due to the SCT qubit. The output will be dc/ac voltage pulses $V_{out}(t)$ discriminating between the qubit "0" and "1" states.

inserted in the qubit loop, as shown in Fig. 25.

When the measurement of the qubit state is to be performed, a bias current is sent through the additional junction. This current is then added to the qubit-state dependent persistent current circulating in the qubit loop. If the qubit and readout currents flow in the same direction, the critical current of the readout JJ is exceeded, which induces the junction switching to the resistive branch, sending out a voltage pulse. This effect is used to distinguish the qubit states. The method has been extensively used experimentally by Vion et al.^{21,22,23}.

To describe the circuit, we add the Lagrangian of a biased JJ, Eq. (5.11),

$$L = \frac{\hbar^2 \dot{\phi}^2}{4E_C^m} + E_J^m \cos \phi + \frac{\hbar}{2e} I_e \phi, \quad (8.5)$$

to the SCT Lagrangian (generalized Eq. (5.30), cf. Eqs. (6.7), (7.7)),

$$L_{SCT} = \frac{\hbar^2}{4E_C} \left(\dot{\phi}_- - \frac{2eC_g}{\hbar C_\Sigma} V_g \right)^2 + \frac{\hbar^2}{4E_C} \dot{\phi}_+^2 - 2E_J \cos \phi_+ \cos \phi_- - \frac{1}{2} E_L \dot{\phi}^2 \quad (8.6)$$

(here we have neglected a small contribution of the gate capacitance to the qubit charging energy). The phase quantization condition will now read: $2\phi_+ + \phi = \phi_e + \tilde{\phi}$. The measurement junction will be assumed in the phase regime, $E_J^m \gg E_C^m$, and moreover, the inductive energy will be the largest energy in the circuit, $E_L \gg E_J^m$. The latter implies that the induced phase is negligibly small and can be dropped from the phase quantization condition. We also assume that $\phi_e = 0$, thus $2\phi_+ + \phi = 0$. Then, after having omitted the variable ϕ_+ , the kinetic energy term of the qubit can be combined with the much larger kinetic energy of the measurement junction leading to insignificant renormalization of the measurement junction capacitance, $C^m + C/4 \rightarrow C^m$. As a result, the total Hamiltonian of the circuit will take the form,

$$\hat{H} = E_C (\hat{n}_- - n_g)^2 - 2E_J \cos \left(\frac{\phi}{2} \right) \cos \phi_- + E_C^m \hat{n}^2 - E_J^m \cos \phi - \frac{\hbar}{2e} I_e \phi. \quad (8.7)$$

Since the measurement junction is supposed to be almost classical, its phase is fairly close to the minimum of the junction potential. During qubit operation, the bias current is zero; hence the phase of the measurement junction is zero. When the measurement is made, the current is ramped to a large value close to the critical current of the measurement junction, $I_e = (2e/\hbar)E_J^m - \delta I$, tilting the junction potential and shifting the minimum towards $\pi/2$. Introducing a new variable $\phi = \pi + \theta$, we expand the potential with respect to small $\theta \ll 1$ and, truncating the qubit part, we obtain

$$\hat{H} = -\frac{\epsilon}{2} \sigma_z - \frac{\Delta}{2} \left(1 - \frac{\theta}{2} \right) \sigma_x + E_C^m \hat{n}^2 - E_J^m \frac{\theta^3}{6} + \frac{\hbar}{2e} \delta I \theta, \quad (8.8)$$

where $\Delta = 2\sqrt{E_J}$. The ramping is supposed to be adiabatic so that the phase remains at the minimum point. Let us analyze the behavior of the potential minimum by omitting a small kinetic term and diagonalizing the Hamiltonian (8.8). The corresponding eigenenergies depend on θ ,

$$E_{\pm}(\theta) = \mp \frac{E}{2} - E_J^m \frac{\theta^3}{6} + \left(\frac{\hbar}{2e} \delta I \pm \frac{\Delta^2}{4E} \right) \theta, \quad (8.9)$$

as shown in Fig. 26. Then within the interval of the bias currents, $|\delta I| \leq -(2e/\hbar)(\Delta^2/4E)$, the potential energy corresponding to the ground state has a local minimum,

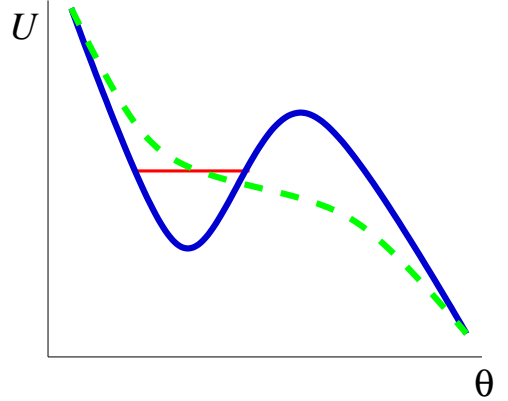


FIG. 26: Josephson potential energy of the measurement junction during the measurement: for the "0" qubit eigenstate there is a well (full line) confining a level, while for the "1" qubit state there is no well (dashed line).

while for the excited state it does not. This implies that when the junction is in the ground state, no voltage will be generated. However, if the junction is in the excited state, it will switch to the resistive branch, generating a voltage pulse that can be detected.

With the discussed setup the direction of the persistent current is measured. It is also possible to arrange the measurement of the flux by using a dc SQUID as a threshold detector. Such a setup is suitable for the measurement of flux qubits. Let us consider, for example, the three junction flux qubit from Section VII C inductively coupled to a dc SQUID. Then, under certain assumptions, the Hamiltonian of the system can be reduced to the following form:

$$\hat{H} = -\frac{1}{2}(\epsilon \sigma_z + \Delta \sigma_x) + E_J^s \hat{n}^2 - (E_J^s + \lambda \sigma_z) \cos \phi - \frac{\hbar}{2e} \delta I \phi, \quad (8.10)$$

where E_J^s is an effective (bias flux dependent) Josephson energy of the SQUID, Eq. (5.24), and λ is an effective coupling constant proportional to the mutual inductance of the qubit and the SQUID loops.

IX. PHYSICAL COUPLING SCHEMES FOR TWO QUBITS

A. General principles

A generic scheme for coupling qubits is based on the physical interaction of linear and non-linear oscillators constituting a superconducting circuit. The Hamiltonians for the SCB, rf-SQUID, and plain JJ contain quadratic terms representing the kinetic and potential energies plus the non-linear Josephson energy term, which is quadratic when expanded to lowest order,

$$\hat{H} = E_C (\hat{n} - n_g)^2 + E_J (1 - \cos \phi) \quad (9.1)$$

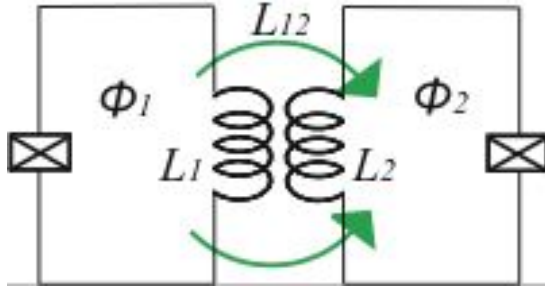


FIG. 27: Fixed inductive (flux) coupling of elementary flux qubit. The loops can be separate, or have a common leg like in the figure.

$$\hat{H} = E_C \hat{n}^2 + E_J (1 - \cos \phi) + E_L \frac{(\phi - \phi_e)^2}{2} \quad (9.2)$$

$$\hat{H} = E_C \hat{n}^2 + E_J (1 - \cos \phi) + \frac{\hbar}{2e} I_e \phi. \quad (9.3)$$

In a multi-qubit system the induced gate charge in the SCB, or the flux through the SQUID loop, or the phase in the Josephson energy, will be a sum of contributions from several (in principle, all) qubits. The energy of the system can therefore not be described as the sum of two independent qubits because of the quadratic dependence, and the cross terms represent interaction energies of different kinds: capacitive, inductive and phase/current. Moreover, using JJ circuits as non-linear coupling elements we have the advantage that the direct physical coupling strength may be controlled, e.g. tuning the inductance via current biased JJs, or tuning the capacitance by a voltage biased SCB.

B. Inductive coupling of flux qubits

A common way of coupling flux qubits is the inductive coupling: magnetic flux induced by one qubit threads the loop of another qubit, changing the effective external flux. This effect is taken into account by introducing the inductance matrix L_{ik} , which connects flux in the i -th loop with the current circulating in the k -th loop,

$$\Phi_i = \sum_k L_{ik} I_k. \quad (9.4)$$

The off-diagonal element of this matrix, L_{12} , is the mutual inductance which is responsible for the interaction. By using the inductance matrix, the magnetic part of the potential energy in Eq. (6.16) can be generalized to the case of two coupled qubits,

$$\frac{1}{2} \left(\frac{\hbar}{2e} \right)^2 \sum_{ik} (L^{-1})_{ik} (\phi_i - \phi_{ei})(\phi_k - \phi_{ek}). \quad (9.5)$$

Then following the truncation procedure explained in Section VII C, we calculate the matrix elements,

$$\langle l | \tilde{\phi} - f | l \rangle, \quad \langle r | \tilde{\phi} - f | r \rangle, \quad \langle l | \tilde{\phi} - f | r \rangle, \quad (9.6)$$

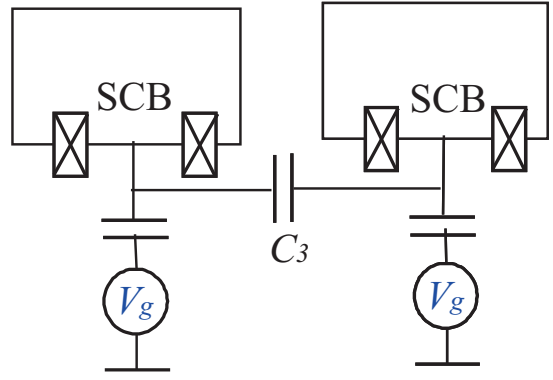


FIG. 28: Fixed capacitive coupling of charge qubits

for each qubit. The last matrix element is exponentially small, while the first two ones are approximately equal to the minimum points of the potential energy, ϕ_l and ϕ_r , respectively. This implies that the truncated interaction basically has the zz -form,

$$\hat{H}_{int} = \lambda \sigma_{z1} \sigma_{z2},$$

$$\lambda = \frac{1}{8} \left(\frac{\hbar}{2e} \right)^2 (L^{-1})_{12} (\phi_l - \phi_r)_1 (\phi_l - \phi_r)_2. \quad (9.7)$$

C. Capacitive coupling of charge qubits

One of the simplest coupling schemes is the capacitive coupling of charge qubits. Such a coupling is realized by connecting the islands of two SCBs via a small capacitor, as illustrated in Fig. 28. This will introduce an additional term in the Lagrangian of the two non-interacting SCBs, Eq. (5.27), namely the charging energy of the capacitor C_3 ,

$$\delta L = \frac{C_3 V_3^2}{2}. \quad (9.8)$$

The voltage drop V_3 over the capacitor is expressed via the phase differences across the qubit junctions,

$$V_3 = \frac{\hbar}{2e} (\dot{\phi}_1 - \dot{\phi}_2), \quad (9.9)$$

and thus the kinetic part of the Lagrangian (5.28) will take the form

$$K(\dot{\phi}_1, \dot{\phi}_2) = \frac{1}{2} \left(\frac{\hbar}{2e} \right)^2 \sum_{i,k} C_{ik} \dot{\phi}_i \dot{\phi}_k - \frac{\hbar}{2e} \sum_i^2 C_{gi} V_{gi} \dot{\phi}_i, \quad (9.10)$$

where the capacitance matrix elements are $C_{ii} = C_{\Sigma i} + C_3$, and $C_{12} = C_3$. Then proceeding to the circuit quantum Hamiltonian as described in Section VI, we find the interaction term,

$$\hat{H}_{int} = 2e^2 (C^{-1})_{12} \hat{n}_1 \hat{n}_2. \quad (9.11)$$

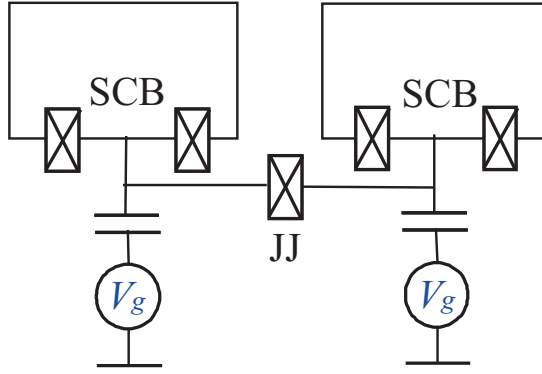


FIG. 29: Fixed phase coupling of charge qubits

This interaction term is diagonal in the charge basis, and therefore leads to the zz -interaction after truncation,

$$\hat{H}_{int} = \lambda \sigma_{z1} \sigma_{z2}, \quad \lambda = \frac{e^2}{2} (C^{-1})_{12}. \quad (9.12)$$

The qubit Hamiltonians are given by Eq. (7.5) with charging energies renormalized by the coupling capacitor.

D. JJ phase coupling of charge qubits

Instead of the capacitor, the charge qubits can be connected via a Josephson junction¹⁵⁴, as illustrated in Fig. 29,

In this case, the Josephson energy of the coupling junction $E_{J3} \cos(\phi_1 - \phi_2)$ must be added to the Lagrangian in addition to the charging energy. This interaction term is apparently off-diagonal in the charge basis and, after truncation, gives rise to xx - and yy -couplings,

$$\hat{H}_{int} = \lambda (\sigma_{x1} \sigma_{x2} + \sigma_{y1} \sigma_{y2}), \quad \lambda = \frac{E_{J3}}{4}, \quad (9.13)$$

or equivalently,

$$\hat{H}_{int} = 2\lambda (\sigma_{+,1} \sigma_{-,2} + \sigma_{-,1} \sigma_{+,2}). \quad (9.14)$$

E. Capacitive coupling of single JJs

Capacitive coupling of JJ qubits, illustrated in Fig. 30, is described in a way similar to the charge qubit, in terms of the Lagrangian Eqs. (9.8), (9.9), and the resulting interaction Hamiltonian has the form given in Eq. (9.11).

Generally, in the qubit eigenbasis, $|0\rangle$ and $|1\rangle$, all matrix elements of the interaction Hamiltonian are non-zero. However, if we adopt a parabolic approximation for the Josephson potential, then the diagonal matrix elements turn to zero, $n_{00} = n_{11} = 0$, while the off-diagonal matrix elements remain finite, $n_{01} = -n_{10} = -i(E_J/E_C)^{1/4}$. Then, after truncation, the charge number operator \hat{n}

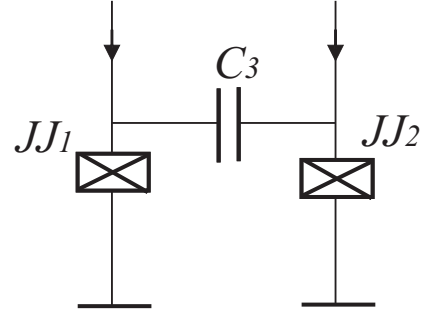


FIG. 30: Capacitive coupling of single JJ qubits

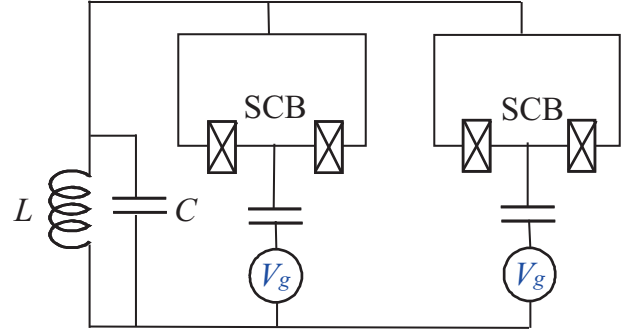


FIG. 31: Two charge qubits coupled to a common LC-oscillator.

turns to σ_y , and the qubit-qubit interaction takes the yy -form,

$$\hat{H}_{int} = \lambda \sigma_{y1} \sigma_{y2}, \quad \lambda = 2e^2 \sqrt{\frac{\hbar^2 \omega_{p1} \omega_{p2}}{E_{C1} E_{C2}}} (C^{-1})_{12}. \quad (9.15)$$

F. Coupling via oscillators

Besides the direct coupling schemes described above, several schemes of coupling qubits via auxiliary oscillators have been considered⁴². Such schemes provide more flexibility, e.g. to control qubit interaction, to couple two remote qubits, and to connect several qubits. Moreover, in many advanced qubits, the qubit variables are generically connected to the outside world via an oscillator (e.g. the Delft and Saclay qubits). To explain the principles of such a coupling, we consider the coupling scheme for charge qubits suggested by Shnirman et al.¹⁴.

1. Coupling of charge (SCB, SCT) qubits

In this circuit the island of each SCB is connected to ground via a common LC -oscillator, as illustrated in Fig. 31. The kinetic energy (5.27) of a single qubit should now be modified taking into account the additional phase

difference ϕ across the oscillator,

$$K(\dot{\phi}_{-,i}; \dot{\phi}) = \frac{1}{2} \left(\frac{\hbar}{2e} \right)^2 \left[2C\dot{\phi}_{-,i}^2 + C_g(V_{gi} - \dot{\phi} - \dot{\phi}_{-,i})^2 \right]. \quad (9.16)$$

The cross term in this equation can be made to vanish by a change of qubit variable,

$$\phi_{-,i} = \phi_i - a\phi, \quad a = \frac{C_g}{C_\Sigma}. \quad (9.17)$$

The kinetic energy will then split into two independent parts, the kinetic energy of the qubit in Eq. (5.28), and an additional quadratic term,

$$\frac{1}{2} \left(\frac{\hbar}{2e} \right)^2 \frac{CC_g}{C_\Sigma} \dot{\phi}^2, \quad (9.18)$$

which should be combined with the kinetic energy of the oscillator, leading to renormalization of oscillator capacitance.

Expanding the Josephson energy, after the change of variable, gives

$$E_{Ji} \cos(\phi_i - a\phi) \approx E_{Ji} \cos \phi_i - E_{Ji} a\phi \sin \phi_i. \quad (9.19)$$

provided the amplitude of the oscillations of ϕ is small. The last term in this equation describes the linear coupling of the qubit to the LC -oscillator.

Collecting all the terms in the Lagrangian and performing quantization and truncation procedures, we arrive at the following Hamiltonian of the qubits coupled to the oscillator (this is similar to Eq. (8.4) for the SCT),

$$\hat{H} = \sum_{i=1,2} (\hat{H}_{SCB,i} + \lambda_i \sigma_{yi} \phi) + \hat{H}_{osc}, \quad (9.20)$$

where $\hat{H}_{SCB}^{(i)}$ is given by Eq. (7.5), and

$$\lambda_i = \frac{E_{Ji} C_g}{C_\Sigma}, \quad (9.21)$$

is the coupling strength, and

$$\hat{H}_{osc} = E_{Cosc} \hat{n}^2 + E_L \phi^2 / 2, \quad (9.22)$$

is the oscillator Hamiltonian where the term in Eq. (9.18) has been included.

The physics of the qubit coupling in this scheme is the following: quantum fluctuation of the charge of one qubit produces a displacement of the oscillator, which perturbs the other qubit. If the plasma frequency of the LC oscillator is much larger than the frequencies of all qubits, then virtual excitation of the oscillator will produce a direct effective qubit-qubit coupling, the oscillator staying in the ground state during all qubit operations. To provide a small amplitude of the zero-point fluctuations, the oscillator plasma frequency should be small compared to the inductive energy, or $E_{Cosc} \ll E_L$. Then the fast fluctuations can be averaged out. Noticing that

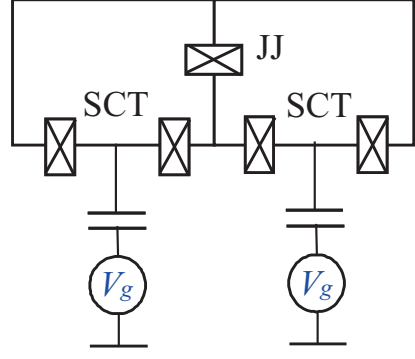


FIG. 32: Charge (charge-phase) qubits coupled via a common Josephson junction providing phase coupling of the two circuits

the displacement does not change the oscillator ground state energy, which then drops out after the averaging, we finally arrive at the Hamiltonian of the direct effective qubit coupling,

$$\hat{H}_{int} = -\frac{\lambda_1 \lambda_2}{E_L} \sigma_{y1} \sigma_{y2}. \quad (9.23)$$

for the oscillator-coupled charge qubits in Fig. 31.

2. Current coupling of SCT qubits

Charge qubits based on SCTs can be coupled by connecting loops of neighboring qubits by a large Josephson junction in the common link^{155,156,157,158,159,160,161}, as illustrated in Fig. 32,

The idea is similar to the previous one: to couple qubit variables to a new variable, the phase of the coupling Josephson junction, then to arrange the phase regime for the junction with large plasma frequency ($E_{Ccoupl} \ll E_{Jcoupl}$), and then to average out the additional phase. Technically, the circuit is described using the SCT Hamiltonian, Eqs. (7.7), (7.8), for each qubit,

$$\begin{aligned} \hat{H}_{SCT} = & E_C (\hat{n}_- - n_g)^2 + E_C \hat{n}_+^2 \\ & - 2E_J \cos \phi_+ \cos \phi_- + E_L \frac{(2\phi_+ - \phi_e)^2}{2}, \end{aligned} \quad (9.24)$$

and adding the Hamiltonian of the coupling junction,

$$\hat{H}_c = E_{C,c} \hat{n}_c^2 - E_{J,c} \cos \phi_c. \quad (9.25)$$

The phase ϕ_c across the coupling junction must be added to the flux quantization condition in each qubit loop; e.g., for the first qubit $2\phi_{+,1} + \phi_c = \phi_{e,1} + \phi_1$ (for the second qubit the sign of ϕ_c will be minus). Assuming small inductive energy, $E_L \ll E_{J,c}$, we may neglect $\tilde{\phi}$; then assuming the flux regime for the coupling Josephson junction we adopt a parabolic approximation for the junction potential, $E_{J,c} \phi_c^2 / 2$.

With these approximations, the Hamiltonian of the first qubit plus coupling junction will take form similar to Eq. (9.24) where $E_{J,c}$ will substitute for E_L , and ϕ_c will substitute for $2\phi_+ - \phi_e$. Finally assuming the amplitude of the ϕ_c -oscillations to be small, we proceed as in the previous subsection, i.e. expand the cosine term obtaining linear coupling between the SCB and the oscillator, truncate the full Hamiltonian, and average out the oscillator. This will yield the following interaction term,

$$\hat{H}_{int} = \frac{\lambda_1 \lambda_2}{E_{J,c}} \sigma_{x1} \sigma_{x2}, \quad \lambda_i = E_J \sin \frac{\phi_i}{2} \quad (9.26)$$

This coupling scheme also applies to flux qubits: in this case, the coupling will have the same form as in Eq. (9.7), but the strength will be determined by the Josephson energy of the coupling junction, cf. Eq. (9.26), rather than by the mutual inductance.

G. Variable coupling schemes

Computing with quantum gate networks basically assumes that one-and two-qubit gates can be turned on and off at will. This can be achieved by tuning qubits with fixed, finite coupling in and out of resonance, in NMR-style computing¹⁶².

Here we shall discuss an alternative way, namely to vary the strength of the physical coupling between nearest-neighbour qubits, as discussed in a number of recent papers^{155,156,158,159,160,163,164,165,166}.

1. Variable inductive coupling

To achieve variable inductive coupling of flux qubits one has to be able to control the mutual inductance of the qubit loops. This can be done by different kinds of controllable switches (SQUIDS, transistors)¹⁶³ in the circuit. In a recent experiment, a variable flux transformer was implemented as a coupling element (see Fig. 33) by controlling the transforming ratio¹⁶⁷. The flux transformer is a superconducting loop strongly inductively coupled to the qubit loops, which are distant from each other so that the direct mutual qubit inductance is negligibly small. Because of the effect of quantization of magnetic flux in the transformer loop¹¹², the local variation of magnetic flux Φ_1 induced by one qubit will affect a local magnetic flux Φ_2 in the vicinity of the other qubit creating effective qubit-qubit coupling. When a dc SQUID is inserted in the transformer loop, as shown in Fig. 33, it will shortcircuit the transformer loop, and the transformer ratio Φ_2/Φ_1 will change. The effect depends on the current flowing through the SQUID, and is proportional to the critical current of the SQUID. The latter is controlled by applying a magnetic flux Φ_{cx} to the SQUID loop, as explained in Section V C and shown in Fig. 33. Quantitatively, the dependence of the transformer ratio

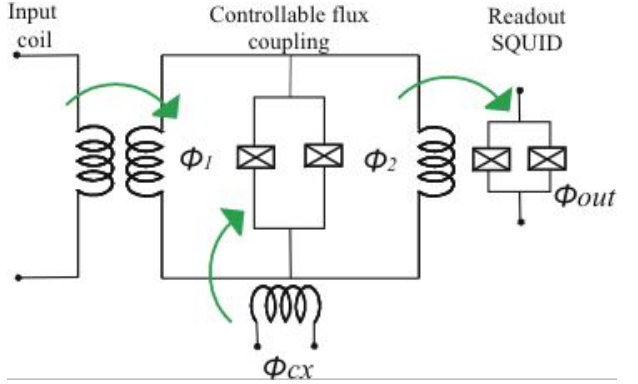


FIG. 33: Flux transformer with variable coupling controlled by a SQUID.

on the controlling flux is given by the equation¹⁶⁷,

$$\frac{\Phi_2}{\Phi_1} = \left(1 + \frac{E_J}{E_L} \cos \frac{\pi \Phi_{cx}}{\Phi_0} \right)^{-1}, \quad (9.27)$$

where E_J is the Josephson energy of the SQUID junction, and E_L is the inductive energy of the transformer.

2. Variable Josephson coupling

A variable Josephson coupling is obtained when a single Josephson junction is substituted by a symmetric dc SQUID whose effective Josephson energy $2E_J \cos(\phi_e/2)$ depends on the magnetic flux threading the SQUID loop (see the discussion in Section V C). This property is commonly used to control level spacing in both flux and charge qubits introduced in Section V D, and it can also be used to switch on and off qubit-qubit couplings. For example, the coupling of the charge-phase qubits via Josephson junction in Fig. 32 can be made variable by substituting the single coupling junction with a dc SQUID^{155,156}.

The coupling scheme discussed in Section IX F 1 is made controllable by using a dc SQUID design for the SCB as explained in Section V D). Indeed, since the coupling strength depends on the Josephson energy of the qubit junction, Eq. (9.21), this solution provides variable coupling of the qubits. Similarly, the coupling of the SCTs considered in Section IX F 2 can be made controllable by employing a dc SQUID as a coupling element. A disadvantage of this solution is that the qubit parameters will vary simultaneously with varying of the coupling strength. A more general drawback of the dc SQUID-based controllable coupling is the necessity to apply magnetic field locally, which might be difficult to achieve without disturbing other elements of the circuit. This is however an experimental question, and what are practical solutions in the long run remains to be seen.

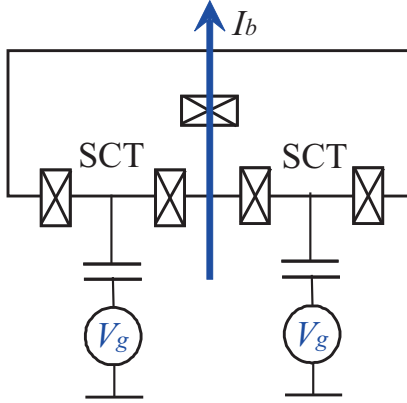


FIG. 34: Coupled charge qubits with current-controlled phase coupling: the arrow indicates the direction of the controlling bias current.

3. Variable phase coupling

An alternative solution for varying the coupling is based on the idea of controlling the properties of the Josephson junction by applying external dc current^{158,159,160}, as illustrated in Fig. 34.

Let us consider the coupling scheme of Section IX F 2: the coupling strength here depends on the plasma frequency of the coupling Josephson junction, which in turn depends on the form of the local minimum of the junction potential energy. This form can be changed by tilting the junction potential by applying external bias current (Fig. 34), as discussed in Section V A. The role of the external phase bias, ϕ_e , will now be played by the minimum point ϕ_0 of the tilted potential determined by the applied bias current, $E_{J,c} \sin \phi_0 = (\hbar/2e)I_e$. Then the interaction term will read,

$$\hat{H}_{int} = \lambda \sigma_{x1} \sigma_{x2}, \quad \lambda = \frac{E_J^2 \sin^2(\phi_0/2)}{E_{J,c} \cos \phi_0}, \quad (9.28)$$

and local magnetic field biasing is not required.

4. Variable capacitive coupling

Variable capacitive coupling of charge qubits based on a quite different physical mechanism of interacting SCB charges has been proposed in Ref.¹⁶⁵. The SCBs are then connected via the circuit presented in Fig. 35.

The Hamiltonian of this circuit, including the charge qubits, has the form

$$\hat{H} = \sum_i \hat{H}_{SCB,i} + E_C (\hat{n} - q(\hat{n}_1 + \hat{n}_2))^2 - E_J \cos \phi, \quad (9.29)$$

where E_C and $E_J \sim E_c$ are the charging and Josephson energies of the coupling junction, and \hat{n} and ϕ are the charge and the phase of the coupling junction. The function q is a linear function of the qubit charges, \hat{n}_1 , and

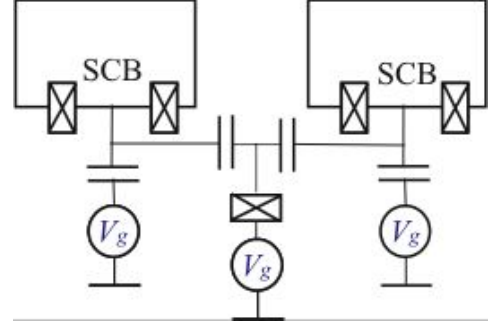


FIG. 35: Variable capacitance tuned by a voltage-controlled SCB.

\hat{n}_2 , and it also depends on the gate voltages of the qubits and the coupling junction. In contrast to the previous scheme, here the coupling junction is not supposed to be in the phase regime; however, it is still supposed to be fast, $E_J \gg E_{Ji}$. Then the energy gap in the spectrum of the coupling junction is much bigger than the qubit energy, and the junction will stay in the ground state during qubit operations. Then after truncation, and averaging out the coupling junction, the Hamiltonian of the circuit will take the form,

$$\hat{H} = \sum_i \hat{H}_{SCB,i} + \epsilon_0 (\sigma_{z1} + \sigma_{z2}), \quad (9.30)$$

where the qubit Hamiltonian is given by Eq. (7.5), and the function ϵ_0 is the ground state energy of the coupling junction. The latter can be generally presented as a linear combination of terms proportional to $\sigma_{z1}\sigma_{z2}$ and $\sigma_{z1} + \sigma_{z2}$,

$$\epsilon_0 (\sigma_{z1} + \sigma_{z2}) = \alpha + \nu \sigma_{z1} \sigma_{z2} + \beta (\sigma_{z1} + \sigma_{z2}). \quad (9.31)$$

with coefficients depending on the gate potentials. The second term in this expression gives the zz -coupling (in the charge basis), and the coupling constant ν may, according to the analysis of Ref.¹⁶⁵, take on both positive and negative values depending on the coupling junction gate voltage. In particular it may turn to zero, implying qubit decoupling.

H. Two qubits coupled via a resonator

In the previous discussion, the coupling oscillator plays a passive role, being enslaved by the qubit dynamics. However, if the oscillator is tuned into resonance with a qubit, then the oscillator dynamics will become essential, leading to qubit-oscillator entanglement. In this case, the approximation of direct qubit-qubit coupling is not appropriate; instead, manipulations explicitly involving the oscillator must be considered.

Let us consider, as an example, operations with two charge qubits capacitively coupled to the oscillator. Assuming the qubits to be biased at the degeneracy point

and proceeding to the qubit eigenbasis (phase basis in this case), we write the Hamiltonian on the form (cf. Eq. (7.10)),

$$\hat{H} = - \sum_{i=1,2} \left(\frac{\Delta_i}{2} \sigma_{zi} - \lambda_i \sigma_x \phi_i \right) + \hat{H}_{osc}[\phi]. \quad (9.32)$$

Let us consider the following manipulation involving the variation of the oscillator frequency (cf. Ref¹⁶⁴): at time $t = 0$, the oscillator frequency is off-resonance with both qubits,

$$\hbar\omega(0) < \Delta_1 < \Delta_2. \quad (9.33)$$

Then the frequency is rapidly ramped so that the oscillator becomes resonant with the first qubit,

$$\hbar\omega(t_1) = \Delta_1, \quad (9.34)$$

the frequency remaining constant for a while. Then the frequency is ramped again and brought into resonance with the second qubit,

$$\hbar\omega(t_2) = \Delta_2. \quad (9.35)$$

Finally, after a certain time it is ramped further so that the oscillator gets out of resonance with both qubits at the end,

$$\hbar\omega(t > t_3) > \Delta_2. \quad (9.36)$$

When passing through the resonance, the oscillator is hybridized with the corresponding qubit, and after passing the resonance, the oscillator and qubit have become entangled. For example, let us prepare our system at $t = 0$ in the *excited* state $\psi(0) = |100\rangle = |1\rangle|0\rangle|0\rangle$, where the first number denotes the state of the oscillator (first excited level), and the last numbers denote the (ground) states of the first and second qubits, respectively. After the first operation, the oscillator will be entangled with the first qubit,

$$\psi(t_1 < t < t_2) = (\cos \theta_1 |10\rangle + \sin \theta_1 e^{i\alpha} |01\rangle) |0\rangle. \quad (9.37)$$

After the second manipulation, the state $|100\rangle$ will be entangled with state $|001\rangle$,

$$\begin{aligned} \psi(t > t_3) = & \cos \theta_1 (\cos \theta_2 |100\rangle + \sin \theta_2 e^{i\beta} |001\rangle) \\ & + \sin \theta_1 e^{i\alpha} |010\rangle. \end{aligned} \quad (9.38)$$

To ensure that there are no more resonances during the described manipulations, it is sufficient to require $\hbar\omega(0) > \Delta_2 - \Delta_1$.

If the controlling pulses are chosen so that $\theta_2 = \pi/2$, then the initial excited state will be eliminated from the final superposition, and we'll get entangled states of the qubits, while the oscillator will return to the ground state,

$$\psi(t > t_3) = |0\rangle (\cos \theta_1 e^{i\beta} |01\rangle + \sin \theta_1 e^{i\alpha} |10\rangle). \quad (9.39)$$

The manipulation should not necessarily be step-like, it is sufficient to pass the resonance rapidly enough to provide the Landau-Zener transition, i.e. the speed of the frequency ramping should be comparable to the qubit level splittings.

References to recent work on the entanglement of qubits and oscillators will be given in Section IV C.

X. DYNAMICS OF MULTI-QUBIT SYSTEMS

A. General N-qubit formulation

A general N-qubit Hamiltonian with general qubit-qubit coupling can be written on the form

$$\hat{H} = - \sum_i \left(\frac{\epsilon_i}{2} \sigma_{zi} + \frac{\Delta_i}{2} \sigma_{xi} \right) + \frac{1}{2} \sum_{i,j;\nu} \lambda_{\nu,ij} \sigma_{\nu i} \sigma_{\nu j} \quad (10.1)$$

To solve the Schrödinger equation

$$\hat{H}|\psi\rangle = E|\psi\rangle \quad (10.2)$$

we expand the N-qubit state in a complete basis, e.g. the 2^N basis states of the $(\sigma_z)^N$ operator,

$$\begin{aligned} |\psi\rangle &= \sum a_q |q\rangle \\ &= a_0 |0..00\rangle + a_1 |0..01\rangle + a_2 |0..10\rangle + \dots a_{(2^N-1)} |1..11\rangle \end{aligned} \quad (10.3)$$

and project onto the basis states

$$\hat{H} \sum_p |p\rangle \langle p| \psi = E|\psi\rangle \quad (10.4)$$

obtaining the usual matrix equation

$$\sum_p \langle q | \hat{H} | p \rangle a_p = E a_q \quad (10.5)$$

where $a_q = \langle q | \psi \rangle$, with typical matrix elements given by

$$H_{qp} = \langle q | \hat{H} | p \rangle = \langle 1..01 | \hat{H} | 0..11 \rangle \quad (10.6)$$

B. Two qubits, longitudinal (diagonal) coupling

The first case is an Ising-type model Hamiltonian, relevant for capacitively or inductively coupled flux qubits,

$$H = - \sum_{i=1,2} \left(\frac{\epsilon_i}{2} \sigma_{zi} + \frac{\Delta_i}{2} \sigma_{xi} \right) + \lambda_{12} \sigma_{z1} \sigma_{z2} \quad (10.7)$$

We expand a general 2-qubit state in the the σ_z basis $q = \{kl\}$,

$$|\psi\rangle = a_1 |00\rangle + a_2 |01\rangle + a_3 |10\rangle + a_4 |11\rangle \quad (10.8)$$

With $q = \{kl\}$ and $p = \{mn\}$, we get

$$\begin{aligned} H_{qp} &= -\langle kl | \sum_{i=1,2} \frac{\epsilon_i}{2} \sigma_{zi} + \frac{\Delta_i}{2} \sigma_{xi} \rangle + \lambda_{12} \sigma_{z1} \sigma_{z2} | mn \rangle \\ &= -\left(\frac{\epsilon_1}{2} \langle k | \sigma_{z1} | m \rangle + \frac{\Delta_1}{2} \langle k | \sigma_{x1} | m \rangle\right) \langle l | n \rangle \\ &\quad -\langle k | m \rangle \left(\frac{\epsilon_2}{2} \langle l | \sigma_{z2} | n \rangle + \frac{\Delta_2}{2} \langle l | \sigma_{x2} | n \rangle\right) \\ &\quad + \lambda_{12} \langle k | \sigma_{z1} | m \rangle \langle l | \sigma_{z2} | n \rangle \end{aligned} \quad (10.9)$$

The longitudinal zz-coupling only connects basis states with the same indices (diagonal terms), $|kl\rangle \leftrightarrow |kl\rangle$. Evaluation of the matrix elements results in the Hamiltonian matrix (setting $\lambda_{12} = \lambda$, $\epsilon_1 + \epsilon_2 = 2\epsilon$, $\epsilon_1 - \epsilon_2 = 2\Delta\epsilon$)

$$\hat{H} = \begin{pmatrix} \epsilon + \lambda & -\frac{1}{2}\Delta_2 & -\frac{1}{2}\Delta_1 & 0 \\ -\frac{1}{2}\Delta_2 & \Delta\epsilon - \lambda & 0 & -\frac{1}{2}\Delta_1 \\ -\frac{1}{2}\Delta_1 & 0 & -\Delta\epsilon - \lambda & -\frac{1}{2}\Delta_2 \\ 0 & -\frac{1}{2}\Delta_1 & -\frac{1}{2}\Delta_2 & -\epsilon + \lambda \end{pmatrix} \quad (10.10)$$

The one-body operators can only connect single-particle states, and therefore the rest of the state must be unchanged (unit overlap). Zero overlap matrix elements

$$\langle k | m \rangle = \delta_{k,m}, \quad \langle l | n \rangle = \delta_{l,n} \quad (10.11)$$

therefore make some matrix elements zero.

The two-body operators describing the qubit-qubit coupling connect two-particle states with up to two different indices (single-particle basis states). In the present case, the qubit coupling Hamiltonian $H_2 = \lambda \sigma_{z1} \sigma_{z2}$ has the charge basis as eigenstates and cannot couple different charge states. It therefore only contributes to shifting the energy eigenvalues on the diagonal by $\pm\lambda$. In contrast, qubit coupling Hamiltonians involving $\sigma_{x1} \sigma_{x2}$ or $\sigma_{y1} \sigma_{y2}$ couplings contribute to the off-diagonal matrix elements (in the charge basis), and specifically remove the zero matrix elements above.

In the examples below we will specifically consider the case when $\epsilon_1 - \epsilon_2 = 2\Delta\epsilon = 0$, which can be achieved by tuning the charging energies via fabrication or gate voltage bias. The eigenvalues of the matrix Schrödinger equation with the Hamiltonian given by (10.10) are then determined by

$$\begin{aligned} \det(\hat{H} - E) = 0 &= [(\lambda^2 - E^2) + \frac{1}{4}(\Delta_1 + \Delta_2)^2] \\ &\times [(\lambda^2 - E^2) + \frac{1}{4}(\Delta_1 - \Delta_2)^2] - \epsilon^2 (\lambda + E)^2 \end{aligned} \quad (10.12)$$

1. Biasing far away from the degeneracy point

Far away from the degeneracy points in the limit $\epsilon \gg \Delta_1, \Delta_2$, the Hamiltonian matrix is diagonal and we are

dealing with pure charge states. The secular equation factorises according to

$$\begin{aligned} \det(\hat{H} - E) &= \\ &= [(\lambda^2 - E^2) + \epsilon(\lambda + E)][(\lambda^2 - E^2) - \epsilon(\lambda + E)] = 0 \end{aligned} \quad (10.13)$$

giving the eigenvalues

$$E_1 = \epsilon + \lambda, \quad E_{2,3} = -\lambda, \quad E_4 = -\epsilon + \lambda \quad (10.14)$$

The corresponding eigenvectors and 2-qubit states are given by

$$E_1 = \epsilon + \lambda :$$

$$a_2 = a_3 = a_4 = 0 \quad (10.15)$$

$$|\psi_1\rangle = |00\rangle \quad (10.16)$$

$$E_{2,3} = -\lambda :$$

$$a_1 = a_4 = 0 \quad (10.17)$$

$$|\psi_2\rangle = |01\rangle, \quad (a_3 = 0); \quad |\psi_3\rangle = |10\rangle, \quad (a_2 = 0) \quad (10.18)$$

$$E_4 = -\epsilon + \lambda :$$

$$a_1 = a_2 = a_3 = 0 \quad (10.19)$$

$$|\psi_4\rangle = |11\rangle \quad (10.20)$$

2. Biasing at the degeneracy point

Parking both qubits at the degeneracy point, $\epsilon = 0$, the secular equation factorises in a different way,

$$\begin{aligned} \det(\mathcal{H} - E) = 0 &= [(\lambda^2 - E^2) + \frac{1}{4}(\Delta_1 + \Delta_2)^2] \\ &\times [(\lambda^2 - E^2) + \frac{1}{4}(\Delta_1 - \Delta_2)^2] \end{aligned} \quad (10.21)$$

again giving a set of exact energy eigenvalues

$$E_{1,4} = \pm \sqrt{\lambda^2 + \frac{1}{4}(\Delta_1 + \Delta_2)^2} \quad (10.22)$$

$$E_{2,3} = \pm \sqrt{\lambda^2 + \frac{1}{4}(\Delta_1 - \Delta_2)^2} \quad (10.23)$$

where $E_1 < E_2 < E_3 < E_4$. For $E = E_{1,4}$, the corresponding eigenvectors and 2-qubit states are given by

$$a_1 = a_4, \quad a_2 = a_3; \quad a_2 = -a_1 \frac{\Delta_1 + \Delta_2}{\lambda + 2E} \quad (10.24)$$

$$|E_1\rangle = a_1(|00\rangle + |11\rangle) + a_2(|01\rangle + |10\rangle) \quad (10.25)$$

$$|E_4\rangle = a_2(|00\rangle + |11\rangle) - a_1(|01\rangle + |10\rangle) \quad (10.26)$$

After normalisation

$$a_1 = \frac{1}{2} \sqrt{1 + \frac{\lambda}{|2E_1|}}; \quad a_2 = \frac{1}{2} \sqrt{1 - \frac{\lambda}{|2E_1|}} \quad (10.27)$$

For $E = E_{2,3}$, the corresponding eigenvectors and 2-qubit states are given by

$$b_1 = -b_4, \quad b_2 = -b_3; \quad b_2 = -b_1 \frac{\Delta_1 - \Delta_2}{\lambda + 2E} \quad (10.28)$$

$$|E_2\rangle = b_1(|00\rangle - |11\rangle) + b_2(|01\rangle - |10\rangle) \quad (10.29)$$

$$|E_3\rangle = b_2(|00\rangle - |11\rangle) - b_1(|01\rangle - |10\rangle) \quad (10.30)$$

After normalisation

$$b_1 = \frac{1}{2} \sqrt{1 + \frac{\lambda}{|2E_2|}}; \quad b_2 = \frac{1}{2} \sqrt{1 - \frac{\lambda}{|2E_2|}} \quad (10.31)$$

3. Two-qubit dynamics under dc-pulse excitation

We now investigate the dynamics of the two-qubit state in the specific case that the dc-pulse is applied equally to both gates, $\epsilon_1(t) = \epsilon_2(t)$, where $\epsilon_1 = \epsilon_1(n_{g1}) = E_C(1 - 2n_{g1})$, $\epsilon_2 = \epsilon_2(n_{g2}) = E_C(1 - 2n_{g2})$, taking the system from the the pure charge-state region to the co-degeneracy point and back. This is the precise analogy of the single-qubit dc-pulse scheme discussed in Section IV C.

Since the charge state $|00\rangle$ of the starting point does not have time to evolve during the steep rise of the dc-pulse, it remains frozen and forms the initial state $|00\rangle$ at time $t = 0$ at the co-degeneracy point, where it can be expanded in the energy eigenbasis,

$$|00\rangle = |\psi(0)\rangle = c_1|E_1\rangle + c_2|E_2\rangle + c_3|E_3\rangle + c_4|E_4\rangle \quad (10.32)$$

To find the coefficients we project onto the charge basis, $kl=0,1$

$$\langle kl|00\rangle = c_1\langle kl|E_1\rangle + c_2\langle kl|E_2\rangle + c_3\langle kl|E_3\rangle + c_4\langle kl|E_4\rangle \quad (10.33)$$

and use the explicit results for the energy eigenstates to calculate the matrix elements, obtaining

$$|00\rangle = a_1|E_1\rangle + b_1|E_2\rangle - b_2|E_3\rangle - a_2|E_4\rangle \quad (10.34)$$

For $t > 0$ this stationary state then develops in time governed by the constant Hamiltonian as

$$|\psi(t)\rangle = a_1 e^{-iE_1 t} |E_1\rangle + b_1 e^{-iE_2 t} |E_2\rangle - b_2 e^{+iE_2 t} |E_3\rangle - a_2 e^{+iE_1 t} |E_4\rangle \quad (10.35)$$

Inserting the energy eigenstates from expressions (10.25), (10.26), (10.29), (10.30) we obtain the time evolution in the charge basis,

$$\begin{aligned} |\psi(t)\rangle = & |00\rangle [a_1^2 e^{-iE_1 t} + a_2^2 e^{iE_1 t} + b_1^2 e^{-iE_2 t} + b_2^2 e^{iE_2 t}] \\ & + |01\rangle [a_1 a_2 (e^{-iE_1 t} + e^{iE_1 t}) + b_1 b_2 (e^{-iE_2 t} + e^{iE_2 t})] \\ & + |10\rangle [a_1 a_2 (e^{-iE_1 t} + e^{iE_1 t}) - b_1 b_2 (e^{-iE_2 t} + e^{iE_2 t})] \\ & + |11\rangle [a_1^2 e^{-iE_1 t} + a_2^2 e^{iE_1 t} - b_1^2 e^{-iE_2 t} - b_2^2 e^{iE_2 t}] \end{aligned} \quad (10.36)$$

This state could be the input state for another gate operation, where some other part of the Hamiltonian is suddenly varied. It might also be that this is the state to be measured on. For that purpose one needs in principle the probabilities

$$p_1(t) = |\langle 00|\psi(t)\rangle|^2 \quad (10.37)$$

$$p_2(t) = |\langle 01|\psi(t)\rangle|^2 \quad (10.38)$$

$$p_3(t) = |\langle 10|\psi(t)\rangle|^2 \quad (10.39)$$

$$p_4(t) = |\langle 11|\psi(t)\rangle|^2 \quad (10.40)$$

As one example, we will calculate $p_3(t) + p_4(t)$, which represents the probability of finding the qubit 1 in the upper state $|1\rangle$, independently of the state of qubit 1 (the states of which are summed over).

$$p_3(t) = |[(a_1^2 + a_2^2) \cos E_1 t - (b_1^2 + b_2^2) \cos E_2 t] - i[(a_1^2 - a_2^2) \sin E_1 t - (b_1^2 - b_2^2) \sin E_2 t]|^2 \quad (10.41)$$

$$p_4(t) = |[2ia_1 a_2 \sin E_1 t - 2ib_1 b_2 \sin E_2 t]|^2 \quad (10.42)$$

Adding $p_3(t)$ and $p_4(t)$ we obtain

$$\begin{aligned} p_3(t) + p_4(t) = & \frac{1}{2} - \frac{1}{4} \cos E_1 t \cos E_2 t + \frac{1}{4} \chi \sin E_1 t \sin E_2 t \\ = & \frac{1}{2} - \frac{1}{4} (1 + \chi) \cos E_+ t + (1 - \chi) \cos E_- t \end{aligned} \quad (10.43)$$

where $E_+ = E_2 + E_1$, $E_- = E_2 - E_1$, and where $\chi = (1 - \frac{\lambda^2}{2|E_1 E_2|})$.

C. Two qubits, transverse x-x coupling

This model is relevant for charge qubits in current-coupled loops. The Hamiltonian is now given by

$$\hat{H} = - \sum_{i=1,2} \left(\frac{\epsilon_i}{2} \sigma_{zi} + \frac{\Delta_i}{2} \sigma_{xi} \right) + \lambda \sigma_{x1} \sigma_{x2} \quad (10.44)$$

Proceeding as before we have

$$H_{qp} = \langle kl| \sum_{i=1,2} \left(\frac{\epsilon_i}{2} \sigma_{zi} - \frac{\Delta_i}{2} \sigma_{xi} \right) + \lambda \sigma_{z1} \sigma_{z2} |mn\rangle$$

$$\begin{aligned}
&= \left(\frac{\epsilon_1}{2} \langle k | \sigma_z^{(1)} | m \rangle - \frac{\Delta_1}{2} \langle k | \sigma_{x1} | m \rangle \right) \langle l | n \rangle \\
&\quad + \langle k | m \rangle \left(\frac{\epsilon_2}{2} \langle l | \sigma_{z2} | n \rangle \right) \frac{\Delta_2}{2} \langle l | \sigma_{x2} | n \rangle \\
&\quad + \lambda \langle k | \sigma_{x1} | m \rangle \langle l | \sigma_{x2} | n \rangle
\end{aligned} \tag{10.45}$$

This coupling only connects basis states which differ in both indices ("anti-diagonal" terms), i.e. $|00\rangle \leftrightarrow |11\rangle$ and $|01\rangle \leftrightarrow |10\rangle$, meaning that interaction will only appear on the anti-diagonal. Evaluation of the matrix elements result in the Hamiltonian matrix (again setting $\lambda_{12} = \lambda$, $\epsilon_1 + \epsilon_2 = 2\epsilon$, $\epsilon_1 - \epsilon_2 = 2\Delta\epsilon$)

$$\hat{H} = \begin{pmatrix} \epsilon & -\frac{1}{2}\Delta_2 & -\frac{1}{2}\Delta_1 & \lambda \\ -\frac{1}{2}\Delta_2 & \Delta\epsilon_1 & \lambda & -\frac{1}{2}\Delta_1 \\ -\frac{1}{2}\Delta_1 & \lambda & -\Delta\epsilon & -\frac{1}{2}\Delta_2 \\ \lambda & -\frac{1}{2}\Delta_1 & -\frac{1}{2}\Delta_2 & -\epsilon \end{pmatrix}, \tag{10.46}$$

XI. EXPERIMENTS WITH SINGLE QUBITS AND READOUT DEVICES

In this section we shall describe a few experiments with single-qubits that represent the current state-of-the-art and quite likely will be central components in the development of multi-qubit systems during the next five to ten years. The first experiment presents Rabi oscillations induced and observed in the elementary phase qubit and readout oscillator formed by a single JJ-junction^{30,31,32,33,34}. The next example describes a series of recent experiments with a flux qubit²⁴ coupled to different kinds of SQUID oscillator readout devices^{25,26,168}. A further example will discuss the charge-phase qubit coupled to a JJ-junction oscillator²¹ and the recent demonstration of extensive NMR-style operation of this qubit²³. The last example will present the case of a charge qubit (single Cooper pair box, SCB) coupled to a microwave stripline oscillator^{147,148,151,152}, representing a solid-state analogue of "cavity QED".

Before describing experiments and results, however, we will discuss in some detail the measurement procedures that give information about resonance line profiles, Rabi oscillations, and relaxation and decoherence times. The illustrations will be chosen from Vion et al.²¹ and related work for the case of the charge-phase qubit, but the examples are relevant for all types of qubits, representing fundamental procedures for studying quantum systems.

A. Readout detectors

Before discussing some of the actual experiments, it is convenient to describe some of basic readout-detector principles which more or less the same for the SET, rf-SET, JJ and SQUID devices. A typical pulse scheme for exciting a qubit and reading out the response is shown in Fig. 36:

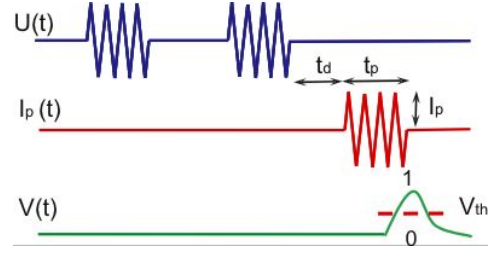


FIG. 36: Control pulse sequences involved in quantum state manipulations and measurement. Top: microwave voltage pulses $U(t)$ are applied to the control gate for state manipulation. Middle: a readout dc ac pulse (DCP) or ac pulse (ACP) $I_b(t)$ is applied to the threshold detector/discriminator a time t_d after the last microwave pulse. Bottom: output signal $V(t)$ from the detector. The occurrence of a output pulse depends on the occupation probabilities of the energy eigenstates. A discriminator with threshold V_{th} converts $V(t)$ into a boolean 0/1 output for statistical analysis.

In Fig. 36 the readout control pulse can be a dc pulse (DCP) or ac pulse (ACP). A DCP readout most often leads to an output voltage pulse, which may be quite destructive for the quantum system. An ACP readout presents a much weaker perturbation by probing the ac-response of an oscillator coupled to the qubit, creating much less back action, at best representing QND readout.

1. Spectroscopic detection of Rabi oscillation

In the simplest use of the classical oscillator, it does not discriminate between the two different qubit states, but only between energies of radiation emitted by a lossy resonator coupled to the qubit. In this way it is possible to detect the "low-frequency" Rabi oscillation of a qubit driven by *continuous* (i.e. not pulsed) high-frequency radiation tuned in the vicinity of the qubit transition energy. If the oscillator is tunable, the resonance window can be swept past the Rabi line. Alternatively, the Rabi frequency can be tuned and swept past the oscillator window by changing the qubit pumping power²⁷.

2. Charge qubit energy level occupation from counting electrons: rf-SET

In this case, the charge qubit is interacting with a beam of electrons passing through a single-electron transistor (SET) coupled to a charge qubit (e.g. the rf-SET,⁶⁹), as discussed in Section VIII and illustrated in Fig. 22. In these cases the transmissivity of the electrons will show two distinct values correlated with the two states of the qubit.

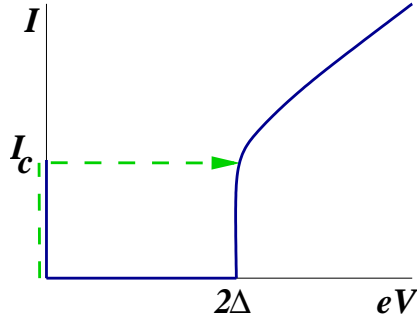


FIG. 37: Current-voltage characteristic of tunnel junction (solid line) consists of the Josephson branch - vertical line at $V = 0$, and the dissipative branch - curve at $eV \geq 2\Delta$. When the current is ramped, the junction stays at the Josephson branch and when the current approaches the critical value I_c , the junction switches to the dissipative branch (dashed line).

3. Coupled qubit-classical-oscillator system: switching detectors with dc-pulse (DCP) output

In Section VIII we analyzed the case of an SCT qubit current-coupled to a JJ-oscillator (Fig. 25) and discussed the Hamiltonian of the coupled qubit-JJ-oscillator system. The effect of the qubit was to deform the oscillator potential in different ways depending on the state of the qubit. The effect can then be probed in a number of ways, by input and output dc and ac voltage and current pulses, to determine the occupation of the qubit energy levels.

Using non-linear oscillators like single JJs or SQUIDS one can achieve threshold and switching behaviour where the JJ/SQUID switches out of the zero-voltage state, resulting in an output dc-voltage pulse.

Switching JJ: The method is based on the dependence of the critical current of the JJ on the state of the qubit, and consists of applying a short current DCP to the JJ at a value I_b during a time Δt , so that the JJ will switch out of its zero-voltage state with a probability $P_{sw}(I_b)$. For well-chosen parameters, the detection efficiency can approach unity. The switching probability then directly measures the qubit's energy level population.

Switching SQUID: In the experiments on flux qubits by the Delft group, two kinds of physical coupling of the SQUID to the qubit have been implemented, namely inductive coupling (Fig. 38 (left))^{7,168} and direct coupling (Fig. 38 (right))^{24,25,26}. The critical current of the SQUID depends on the flux threading the loop, and therefore is different for different qubit states. The problem is to detect a two percent variation in the SQUID critical current associated with a transition between the qubit states in a time shorter than the qubit energy relaxation time T_1 . The SQUID behaves as an oscillator with a characteristic plasma frequency $\omega_p = [(L + L_J)C_{sh}]^{-1/2}$. This frequency depends on the bias current I_b and on the critical current I_C via the Josephson inductance $L_J = \Phi_0/2\pi I_C \sqrt{1 - I_b^2/I_c^2}$ (the shunt capacitor with ca-

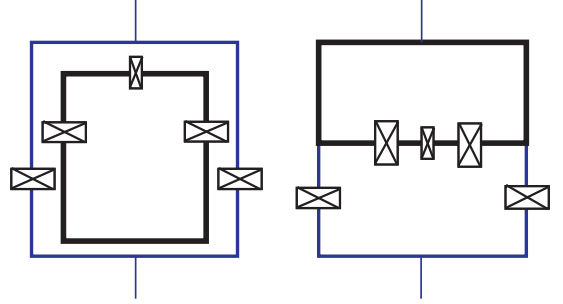


FIG. 38: Schematics of readout dc SQUID coupled to flux qubit; left - inductive coupling, right - direct phase coupling

pacitance C_{sh} and lead inductance L is used to "tune" ω_p). Thus, the plasma frequency takes different values $\omega_p^{(0)}$ or $\omega_p^{(1)}$ depending on the state of qubit, representing two different shapes of the SQUID oscillator potential.

In the dc-pulse-triggered switching SQUID^{7,24,25}, a dc-current readout-pulse is applied after the operation pulse(s) (Fig. 36), setting a switching threshold for the critical current. The circulating qubit current for one qubit state will then add to the critical current and make the SQUID switch to the voltage state, while the other qubit state will reduce the current and leave the SQUID in the zero-voltage state.

In an application of ac-pulse-triggered switching SQUID²⁶, readout relies on resonant activation by a microwave pulse at a frequency close to ω_p , adjusting the power so that the SQUID switches to the finite voltage state by resonant activation if the qubit is in state $|0\rangle$, whereas it stays in the zero-voltage state if it is in state $|1\rangle$. The resonant activation scheme is similar to the readout scheme used by Martinis et al.^{30,31,32,33}. (see Section XI C).

4. Coupled qubit-classical-oscillator system: ac-pulse (ACP) non-switching detectors

This implementation of ACP readout uses the qubit-SQUID combination⁷ shown in Fig. 38 (left), but with ACP instead of DCP readout, implementing a nondestructive dispersive method for the readout of the flux qubit¹⁶⁸. The detection is based on the measurement of the Josephson inductance of a dc-SQUID inductively coupled to the qubit. Using this method, Lupascu et al.¹⁶⁸ measured the spectrum of the qubit resonance line and obtained relaxation times around $80 \mu\text{s}$, much longer than observed with DCP.

A related readout scheme was recently implemented by Siddiqi et al.¹⁶⁹ using two different oscillation states of the non-linear JJ in the zero-voltage state.

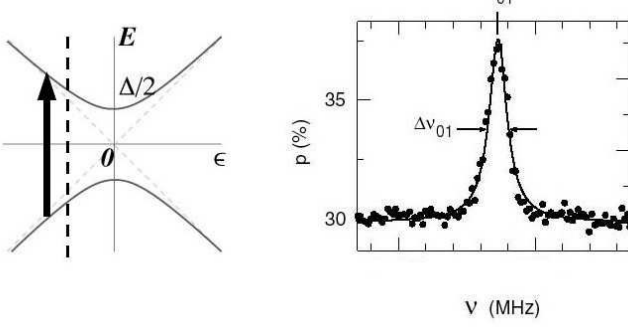


FIG. 39: Left: qubit energy level scheme. The vertical dashed line marks the qubit working point and transition energy. The arrow marks the detuned microwave excitation. Right: population of the upper level as a function of the detuning; the inverse of the half width (FWHM) of the resonance line gives the total decoherence time T_2 . *Courtesy of D. Esteve, CEA-Saclay.*

B. Operation and measurement procedures

A number of operation and readout pulses can be applied to a qubit circuit in order to measure various properties. The number of applied microwave pulses can vary depending on what quantities are to be measured: resonance line profile, relaxation time, Rabi oscillation, Ramsey interference or Spin Echo, as discussed below.

1. Resonance line profiles and T_2 decoherence times

To study the resonance line profile, one applies a single long weak microwave pulse with given frequency, followed by a readout pulse. The procedure is then repeated for a spectrum of frequencies. The Rabi oscillation amplitude, the upper state population, and the detector switching probability $p(t)$ will depend on the detuning and will grow towards resonance. The linewidth gives directly the total inverse decoherence lifetime $1/T_2 = 1/2T_1 + 1/T_\phi$. The decoherence-time contributions from relaxation ($1/T_1$) and dephasing ($1/T_\phi$) can be (approximately) separately measured, as discussed below.

2. T_1 relaxation times

To determine the T_1 relaxation time one measures the decay of the population of the upper $|1\rangle$ state after a long microwave pulse saturating the transition, varying the delay time t_d of the detector readout pulse. The measured $T_1 = 1.8$ microseconds is so far the best value for the Quantronium charge-phase qubit.

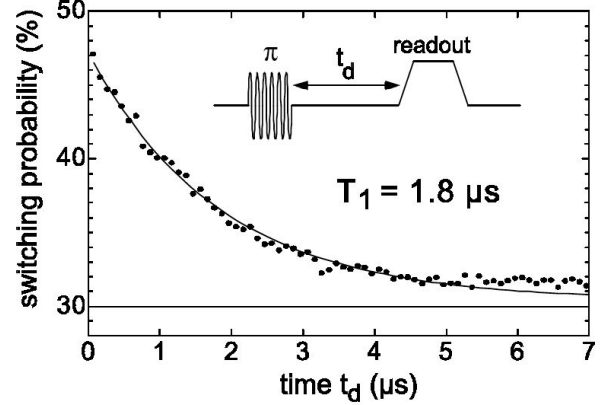


FIG. 40: Decay of the switching probability of the charge-qubit readout junction as a function of the delay time t_d between the excitation and readout pulses. *Courtesy of D. Esteve, CEA-Saclay.*

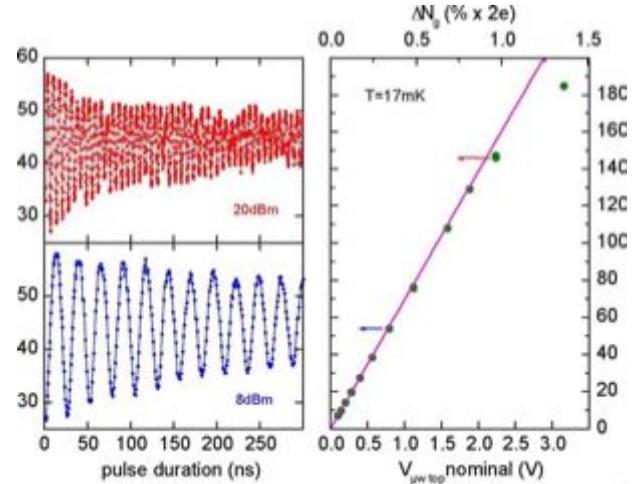


FIG. 41: Left: Rabi oscillations of the switching probability measured just after a resonant microwave pulse of duration. Right: Measured Rabi frequency (dots) varies linearly with microwave amplitude (voltage) as expected. *Courtesy of D. Esteve, CEA-Saclay.*

3. Rabi oscillations and $T_{2,Rabi}$ decoherence time

To study Rabi oscillations (frequency $\Omega \sim u$, the amplitude of driving field) one turns on a resonant microwave pulse for a given time $t_{\mu w}$ and measures the upper $|1\rangle$ state population (probability) $p_1(t)$ after a given (short) delay time t_d . If the system is perfectly coherent, the state vector will develop as $\cos \Omega t |0\rangle + \sin \Omega t |1\rangle$, and the population of the upper state will then oscillate as $\sin^2 \Omega t$ between 0 and 1. In the presence of decoherence, the amplitude of the oscillation of $p_1(t)$ will decay on a time scale T_{Rabi} towards the average value $p_1(t = \infty) = 0.5$. This corresponds to incoherent saturation of the 0 to 1 transition.

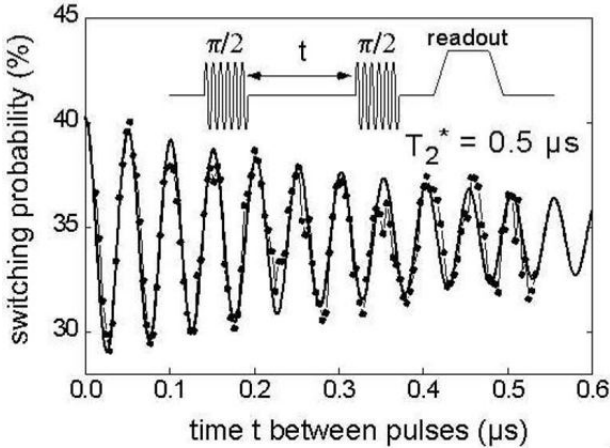


FIG. 42: Ramsey fringes of the switching probability after two phase-coherent microwave $\pi/2$ pulses separated by the time delay t . The continuous line represents a fit by exponentially damped cosine function with time constant $T_2^* = T_\phi = 0.5\mu\text{s}$. The oscillation period coincides with the inverse of the detuning frequency δ (here $\delta = \nu - \nu_{01} = 20.6$ MHz). *Courtesy of D. Esteve, CEA-Saclay.*

4. Ramsey interference, dephasing and $T_{2,\text{Ramsey}}$ decoherence time

The Ramsey interference experiment measures the decoherence time of the non-driven, freely precessing, qubit. In this experiment a $\pi/2$ microwave pulse around the x-axis induces Rabi oscillation that tips the spin from the north pole down to the equator. The spin vector rotates in the x-y plane, and after a given time Δt , another $\pi/2$ microwave pulse is applied, immediately followed by a readout pulse.

Since the $\pi/2$ pulses are detuned by δ from the qubit $|0\rangle \rightarrow |1\rangle$ transition frequency, the qubit will precess with frequency δ relative to the rotating frame of the driving field. Since the second microwave pulse will be applied in the plane of the rotating frame, it will have a projection $\cos \delta t$ on the qubit vector and will drive the qubit towards the north or south poles, resulting in a specific time-independent final superposition state $\cos \delta t |0\rangle + \sin \delta t |1\rangle$ of the qubit at the end of the last $\pi/2$ pulse. The readout pulse then catches the qubit in this superposition state and forces it to decay if the qubit is in the upper $|1\rangle$ state. The probability will oscillate with the detuning frequency, and a single-shot experiment will then detect the upper state with this probability. Repeating the experiment many times for different $\pi/2$ pulse separation Δt will then give $|0\rangle$ or $|1\rangle$ with probabilities $\cos^2 \delta t$ and $\sin^2 \delta t$. Taking the average, and then varying the pulse separation, will trace out the Ramsey interference oscillatory signal. Dephasing will make the signal decay on the timescale T_ϕ .

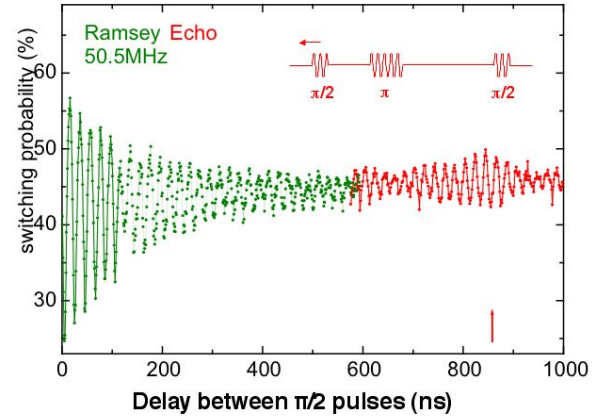


FIG. 43: Spin-echo experiment. The left part shows the basic Ramsey oscillation. The right part shows the echo signal appearing in the time window around twice the time delay between the first $\pi/2$ -pulse and the π -pulse. *Courtesy of D. Esteve, CEA-Saclay.*

5. Spin-echo

The spin-echo and Ramsey pulse sequences differ in that a π -pulse around the x-axis is added in between the two $\pi/2$ -pulses in the spin-echo experiment, as shown in Fig.43. As in the Ramsey experiment, the first $\pi/2$ -pulse makes the Bloch vector start rotating in the equatorial x-y plane with frequency $E/\hbar = \nu_{01}$. The effect of the π -pulse is now to flip the entire x-y plane with the rotating Bloch vector around the x-axis, reflecting the Bloch vector in the x-z plane. The Bloch vector then continues to rotate in the x-y plane in the same direction. Finally a second $\pi/2$ -pulse is applied to project the state on the z-axis.

If two Bloch vectors with slightly different frequency start rotating at the same time in the x-y plane, they will move with different angular speeds. The effect of the π -pulse at time Δt will be to permute the Bloch vectors, and then let the motion continue in the same direction. This is similar to reversing the motion and letting the Bloch vectors back-trace. The net result is that the two Bloch vectors re-align after time $2\Delta t$.

In NMR experiments, the different Bloch vectors correspond to different spins in the ensemble. In the case of a single qubit, the implication is that in a series of repeated experiments, the result will be insensitive to small variations δE of the qubit energy *between* measurements, as long as the energy (rotation frequency) is constant *during* one and the same measurement. If fluctuations occur during one measurement, then this cannot be corrected for. The spin-echo procedure can therefore remove the measurement-related line-broadening associated with slow fluctuations of the qubit precession, and allow observation of the intrinsic coherence time of the qubit.

C. NIST Current-biased Josephson Junction Qubit

Several experimental groups have realized the Josephson Junction (JJ) qubit^{29,30,31,32,33,34}. Here we describe the experiment performed at NIST^{32,33}. In this experiment the junction parameters and bias current were chosen such that a small number of well defined levels were formed in the potential well (Fig. 21), with the inter-level frequencies, $\omega_{01}/2\pi = 6.9\text{GHz}$ and $\omega_{12}/2\pi=6.28\text{GHz}$, the quality factor was $Q=380$. The experiment was performed at very low temperature, $T= 25\text{ mK}$.

The qubit was driven from the ground state, $|0\rangle$, to the upper state, $|1\rangle$, by the resonance rf pulse with frequency ω_{01} , and then the occupation of the upper qubit level was measured. The measurement was performed by exciting qubit further from the upper level to the auxiliary level with higher escape rate by applying the second resonance pulse with frequency ω_{12} . During the whole operation, across the junction only oscillating voltage develops with zero average value over the period. When the tunneling event occurred, the junction switched to the dissipative regime, and finite dc voltage appeared across the junction, which was detected. Alternatively, post-measurement classical states "0" and "1" differ in flux by Φ_0 , which is readily measured by a readout SQUID.

The relaxation rate was measured in the standard way by applying a Rabi pumping pulse followed by a measuring pulse with a certain delay. Non-exponential relaxation was observed, first rapid, $\sim 20\text{ nsec}$, and then more slow, $\sim 300\text{ nsec}$. By reducing the length of the pumping pulse down to 25 nsec, i.e. below the relaxation time, Rabi oscillations were observed. In this experiment the amplitude of the pumping pulse rather than duration was varied, which affected the Rabi frequency and allowed the observation of oscillation of the level population for fixed duration of the pumping pulse.

The Grenoble group³⁴ has observed coherent oscillations in a multi-level quantum system, formed by a current-biased dc SQUID. These oscillations have been induced by applying resonant microwave pulses of flux. Quantum measurement is performed by a nanosecond flux pulse that projects the final state onto one of two different voltage states of the dc SQUID, which can be read out. The number of quantum states involved in the coherent oscillations increases with increasing microwave power. The dependence of the oscillation frequency on microwave power deviates strongly from the linear regime expected for a two-level system and can be very well explained by a theoretical model taking into account the anharmonicity of the multi-level system.

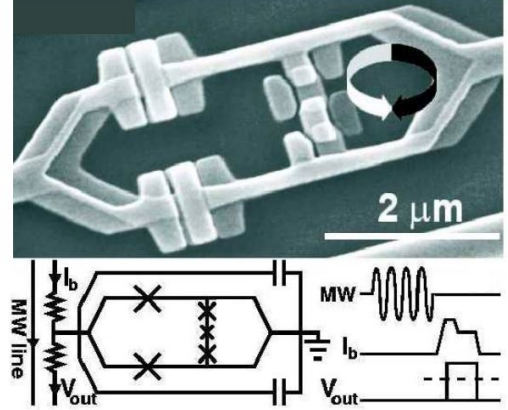


FIG. 44: Upper panel: Scanning electron micrograph of a small-loop flux-qubit with three Josephson junctions of critical current $\sim 0.5\text{ mA}$, and an attached large-loop SQUID with two big Josephson junctions of critical current $\sim 2.2\text{ mA}$. Arrows indicate the two directions of the persistent current in the qubit. Lower panels: Schematic of the on-chip circuit; crosses represent the Josephson junctions. The SQUID is shunted by two capacitors to reduce the SQUID plasma frequency and biased through a small resistor to avoid parasitic resonances in the leads. Symmetry of the circuit is introduced to suppress excitation of the SQUID from the qubit-control pulses. The MW line provides microwave current bursts inducing oscillating magnetic fields in the qubit loop. The current line provides the measuring pulse I_b and the voltage line allows the readout of the switching pulse V_{out} . Adapted from Chiorescu *et al.*²⁴

D. Flux qubits

1. Delft 3-junction persistent current qubit with dc-pulse (DCP) readout

The original design of the 3-junction qubit (Fig. 1 was published by Mooij *et al.* in 1999⁶, and the first spectroscopic measurements by van der Wal *et al.* in 2000⁷ (and simultaneously by Friedman *et al.*⁸ for a single-junction rf-SQUID). Recently the Delft group has also investigated designs where the 3-junction qubit is sharing a loop with the measurement SQUID to increase the coupling strength²⁴, as shown in Fig. 44.

To observe and study Rabi oscillations, the qubit was biased at the degeneracy point and the qubit $|0\rangle \rightarrow |1\rangle$ transition excited by a pulse of 5.71 GHz microwave radiation of variable length, followed by a bias-current (I_b) readout pulse applied to the SQUID (Fig. 44, lower left panel). The first (high) part of the readout pulse (about 10 ns) has two functions: It displaces the qubit away from the degeneracy point so that the qubit eigenstates carry finite current, and it tilts the SQUID potential so that the SQUID can escape to the voltage state if the qubit is in its upper state. The purpose of the long lower plateau of the the readout pulse is to prevent the SQUID from

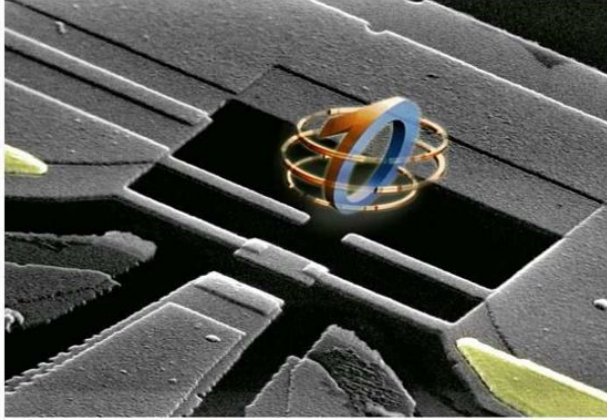


FIG. 45: AFM picture of the charge-phase qubit ("quantronium") corresponding to the circuit scheme in Fig. 25. The working point is controlled by two external "knobs", a voltage gate controlling the induced charge (n_g) on the SCT island, and a current gate controlling the total phase across the SCT via the external flux (ϕ_e) threading the loop. The large readout JJ is seen in the left part of the figure. *Courtesy of D. Esteve, CEA-Saclay.*

returning ("retrapping") to the zero-voltage state. With these operation and readout techniques, Rabi (driven) oscillations, Ramsey (free) oscillations and spin-echos of the qubit were observed²⁴, giving a Ramsey free oscillation dephasing time of 20 ns and spin echo dephasing time of 30 ns.

As mentioned above, relaxation times around 80 μ s have been measured with ACP readout¹⁶⁸, demonstrating that the properties of readout devices are critically important for observing intrinsic qubit decoherence times. Recent further improvements have resulted in Ramsey decoherence times $T_{2,Ramsey}$ of 200 ns, Rabi (driven) decoherence times $T_{2,Rabi}$ of 5 μ s, and relaxation times T_1 of more than 100 μ s.

E. Charge-phase qubit

1. General considerations

As described in Section VII, the charge-phase qubit circuit consists of a single-Cooper-pair transistor (SCT) in a superconducting loop. The Hamiltonian for the SCT part of this circuit is given by

$$\hat{H}_{SCT} = -\frac{1}{2} [\epsilon(n_g) \sigma_z + \Delta(\phi_e) \sigma_x] \quad (11.1)$$

where the charging and tunneling parameters are themselves functions of external control parameters, gate charge n_g and loop flux ϕ_e , $\epsilon(n_g) = E_C(1 - 2n_g)$ and

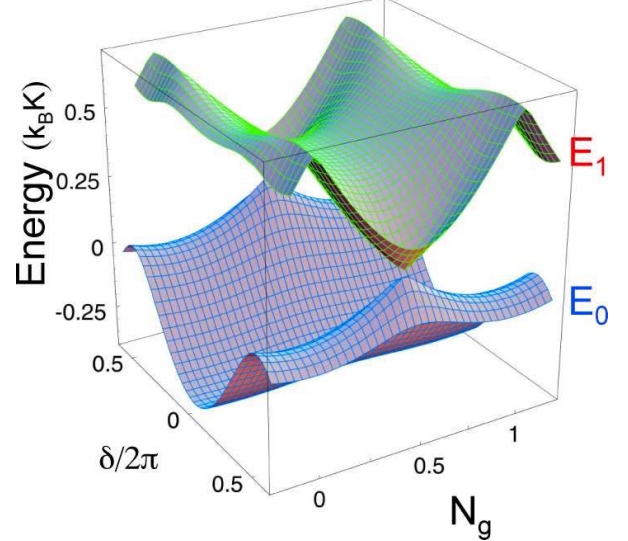


FIG. 46: Charge-phase qubit energy surface. ($N_g = n_g$; $\delta/2\pi = \phi_e$.) *Courtesy of D. Esteve, CEA-Saclay.*

$\Delta(\phi_e) = 2E_J \cos(\phi_e/2)$. The qubit energy levels

$$E_{1,2} = \mp \frac{1}{2} \sqrt{\epsilon(n_g)^2 + \Delta(\phi_e)^2} \quad (11.2)$$

then form a 2-dimensional landscape as functions of the gate charge $n_g(V)$ and phase $\phi_e(\Phi)$, which are functions of the gate voltage $V = C_g 2e n_g$ and gate magnetic flux $\Phi = (\hbar/2e)\phi_e$. The energy level surfaces are therefore functions of two parameters, gate voltage and flux, giving us two independent knobs for controlling the working point of the (charge-phase) qubit. Expanding the energy in Taylor series around some bias working point (V_b, Φ_b) , one obtains

$$\begin{aligned} \delta E(V, \Phi) &= E(V, \Phi) - E(V_b, \Phi_b) \\ &= \frac{\delta E}{\delta V} \delta V + \frac{\delta E}{\delta \Phi} \delta \Phi + \frac{1}{2} \frac{\delta^2 E}{\delta V^2} \delta V^2 + \frac{1}{2} \frac{\delta^2 E}{\delta \Phi^2} \delta \Phi^2 \end{aligned} \quad (11.3)$$

The derivatives are response functions for charge, current, capacitance and inductance (omitting the cross term) ($i = 1, 2$),

$$\delta E_i(V, \Phi) = Q_i \delta V + I_i \delta \Phi + C_i \delta V^2 + L_i \delta \Phi^2 \quad (11.4)$$

or, equivalently,

$$\delta E_i(n_g, \phi_e) = \tilde{Q}_i \delta n_g + \tilde{I}_i \delta \phi_e + \tilde{C}_i \delta n_g^2 + \tilde{L}_i \delta \phi_e^2 \quad (11.5)$$

On the energy level surfaces (Fig. 46), the special point $(n_g, \phi_e) = (0.5, 0)$ is an extreme point with zero first derivative. This means that the energies of the $|0\rangle$ and $|1\rangle$ states will be invariant to first order to small variations of charge and phase, which will minimize the qubit sensitivity to fluctuations of the working point caused by noise.

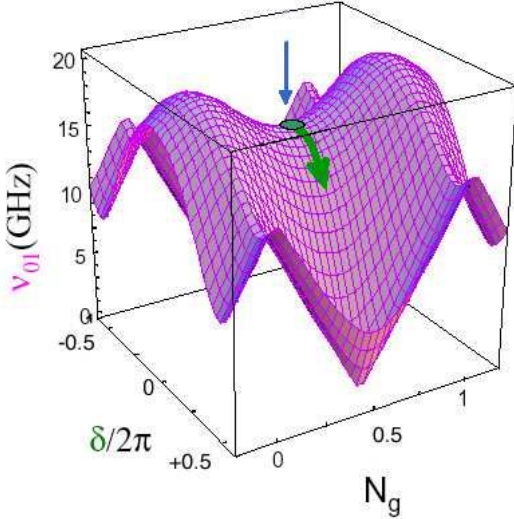


FIG. 47: The charge-phase qubit frequency surface. ($N_g = n_g$; $\delta/2\pi = \phi_e$) Courtesy of D. Esteve, CEA-Saclay.

The point $(n_g, \phi_e) = (0.5, 0)$ is often referred to as the "degeneracy" point because the charging energy is zero, $\epsilon(n_g) = E_C(1 - 2n_g) = 0$. The level splitting at this point is determined by the Josephson tunneling interaction E_J , and is a function of the external bias ϕ_e $\Delta(\phi_e) = 2E_J \cos(\phi_e/2)$.

Figure 47 shows the frequency surface $\nu_{01} = \Delta E/h$, $\Delta E = E_2 - E_1$. During operation, the qubit is preferably parked at the degeneracy point $(n_g, \phi_e) = (0.5, 0)$ where $Q = I = 0$, in order to minimize the decohering influence of noise. In order to induce a qubit response, for gate operation or readout, one must therefore either (i) move the bias point away from point $(0.5, 0)$ to have finite first-order response with $Q \neq 0$ or $I \neq 0$, or (ii) stay at $(0.5, 0)$ and apply a perturbing ac-field that makes the second-order response significant.

2. The CEA-Saclay "quantronium" charge-phase qubit

The "quantronium" charge-phase circuit is given by Fig. 45 adding a large readout Josephson junction in the loop (cf. Fig. 25). The minimum linewidth (Fig. 39) corresponds to a Q-value of 20000 and a decoherence time $T_2 = 0.5 \mu\text{s}$. With the measured relaxation time $T_1 = 1.8 \mu\text{s}$ (Fig. 40), the dephasing time can be estimated to $T_\phi = 0.8 \mu\text{s}$.

A set of results for Rabi oscillations of the Saclay quantronium qubit is shown in Fig. 41. The decoherence time represents decoherence under driving conditions. Another, more fundamental, measure of decoherence is the free precession dephasing time T_2 when the qubit is left to itself. This is measured in the Ramsey two-pulse experiment, as already described above in Fig. 42 showing the CEA-Saclay data^{21,22}, giving $T_2 = 0.5 \mu\text{s}$.

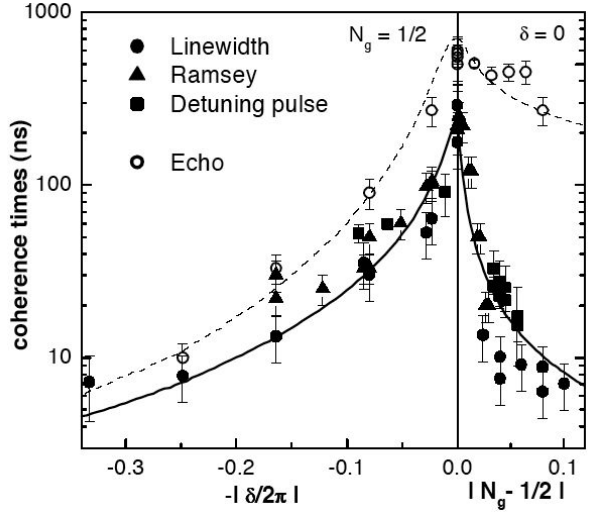


FIG. 48: Free-evolution decoherence times for the quantronium charge-phase SCT qubit.¹⁷⁰ ($N_g = n_g$; $\delta/2\pi = \phi_e$) Full and dashed curves represent results of theoretical modeling. Courtesy of D. Esteve, CEA-Saclay.

The spin-echo results in Ref.²² gave a lifetime as long as $T_2 = 1\mu\text{s}$.

In a recent systematic experimental and theoretical investigation of a specific charge-phase device, investigating the effects of relaxation and dephasing on Rabi oscillation, Ramsey fringes and spin-echos¹⁷⁰, one obtains the following picture of different coherence times for the quantronium charge-phase qubit:

Fluctuations of charge δn_g and flux $\delta\phi_e$ will shift energy levels and make the qubit transition energy $\sqrt{\epsilon(n_g + \delta n_g)^2 + \Delta(\phi_e + \delta\phi_e)^2}$ fluctuate. However, the charge degeneracy point is a saddle point, which means that at that working point the qubit transition frequency is insensitive to low-frequency noise to first order, allowing long coherence times. As can be seen in Fig. 48, the coherence is sharply peaked around the "magic" degeneracy point. The spin-echo experiment indicates the presence of slow charge fluctuations from perturbing impurity two-level systems (TLS) (1/f noise) and that long coherence time can be recovered by spin-echo techniques until the decoherence becomes too rapid at significant distances from the magic point along the charge axis. In contrast, in the experiments with this device the decoherence due to phase fluctuations could not be significantly compensated for by spin-echo techniques, indicating that the phase noise (current and flux noise) in this device is high-frequency noise.

XII. EXPERIMENTS WITH QUBITS COUPLED TO QUANTUM OSCILLATORS

A. General discussion

The present development of quantum information processing with Josephson Junctions (JJ-QIP) goes in the direction of coupling qubits with quantum oscillators, for operation, readout and memory. In Section VIII we discussed the SCT, i.e. a single Cooper-pair transistor in a superconducting loop⁷¹, providing one typical form of the Hamiltonian for a qubit-oscillator coupled system. We also showed with perturbation theory how the Hamiltonian gave rise to qubit-dependent deformed oscillator potential and shifted oscillator frequency. In VIII, in addition we discussed the SCT charge-coupled to an LC-oscillator, which is also representative for a flux qubit coupled to a SQUID oscillator, and which describes a charge qubit in a microwave cavity.

To connect to the language of quantum optics and cavity QED and the current work on solid-state applications, we now explicitly introduce quantization of the oscillator. Quantizing the oscillator, $\tilde{\phi} \sim (a^+ + a)$, a representative form of the qubit-oscillator Hamiltonian reads:

$$\hat{H} = \hat{H}_q + \hat{H}_{int} + \hat{H}_{osc} \quad (12.1)$$

$$\hat{H}_q = -\frac{1}{2}E \sigma_z \quad (12.2)$$

$$\hat{H}_{int} = g \sigma_x (a^+ + a) \quad (12.3)$$

$$\hat{H}_{osc} = \hbar\omega (a^+ a + \frac{1}{2}) \quad (12.4)$$

Introducing the step operators $\sigma_{\pm} = \sigma_x \pm i \sigma_y$, the interaction term can be written as

$$\hat{H}_{int} = g (\sigma_+ a + \sigma_- a^+) + g (\sigma_+ a^+ + \sigma_- a) \quad (12.5)$$

The first term

$$\hat{H}_{int} = g (\sigma_+ a + \sigma_- a^+) \quad (12.6)$$

represents the resonant (co-rotating) part of the interaction, while the second term represents the non-resonant counter-rotating part. In the rotating-wave approximation (RWA) one only keeps the first term, which gives the Jaynes-Cummings model^{171,172,173,174}. Diagonalizing the Jaynes-Cummings Hamiltonian to second order by a unitary transformation gives

$$H = -\frac{1}{2}(E + \frac{g^2}{\delta}) \sigma_z + (\hbar\omega + \frac{g^2}{\delta} \sigma_z) a^+ a \quad (12.7)$$

where $\delta = E - \hbar\omega$ is the so called detuning. The result illustrates what we have already discussed in detail, namely that (i) the qubit transition energy E is shifted (renormalized) by the coupling to the oscillator, and (ii) the oscillator energy $\hbar\omega$ is shifted by the qubit in different directions depending on the state of the qubit, which allows discriminating the two qubit states.

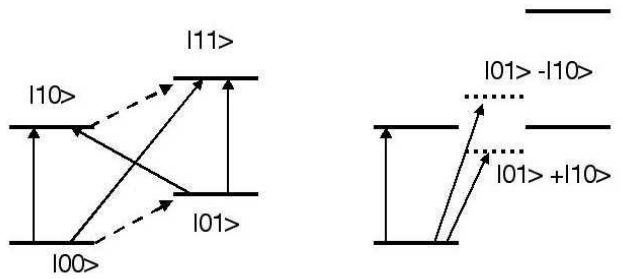


FIG. 49: Qubit-oscillator level structure. The notation for the states is: $|qubit; oscillator\rangle = |0/1; n = 0, 1, ..\rangle$; (a) $E \approx 2\hbar\omega$: very large "detuning", weak coupling. (b) $E \approx \hbar\omega$: resonance, strong coupling and hybridization, level ("vacuum Rabi") splitting.

Figure 49 shows the basic level structure of the qubit-oscillator system in the cases of (a) weak and (b) strong coupling.

What is weak or strong coupling is determined by the strength of the level hybridization, which in the end depends on qubit-oscillator detuning and level degeneracies. The perturbative Hamiltonian in Eq. (12.7) is valid for large detuning ($g \ll \delta_{qr}$) and allows us to approach the case of strong coupling between the qubit and the oscillator. Close to resonance the degenerate states have to be treated non-perturbatively.

Figure 49(a) corresponds to the weak-coupling (non-resonant) case where the levels of the two subsystems are only weakly perturbed by the coupling, adding red and blue sideband transitions $|01\rangle \rightarrow |10\rangle$ and $|00\rangle \rightarrow |11\rangle$ to the main zero-photon transition $|00\rangle \rightarrow |10\rangle$.

Figure 49(b) corresponds to the resonant strong-coupling case when the $|01\rangle$ and $|10\rangle$ states are degenerate, in which case the qubit-oscillator coupling produces two "bonding-antibonding" states in the usual way, and the main line becomes split into two lines ("vacuum Rabi splitting"). Of major importance are the linewidths of the qubit and the oscillator relative to the splittings caused by the interaction. To discriminate between the two qubit states, the oscillator shift must be larger than the average level width.

Since the qubit and the oscillator form a coherent multi-level system, as described before (Section XB 3), the time evolution can be written as $c_1(t)|00\rangle + c_2(t)|01\rangle + c_3(t)|10\rangle + c_4(t)|11\rangle$, which in general does not reduce to a product of qubit and oscillator states, and therefore represents (time-dependent) entanglement. This provides opportunities for implementing quantum gate operation involving qubits and oscillators.

Generation and control of entangled states can be achieved by using microwave pulses to induce Rabi oscillation between specific transitions of the coupled qubit-oscillator system, and the result can be studied by spectroscopy on suitable transitions or by time-resolved detection of suitable Rabi oscillations.

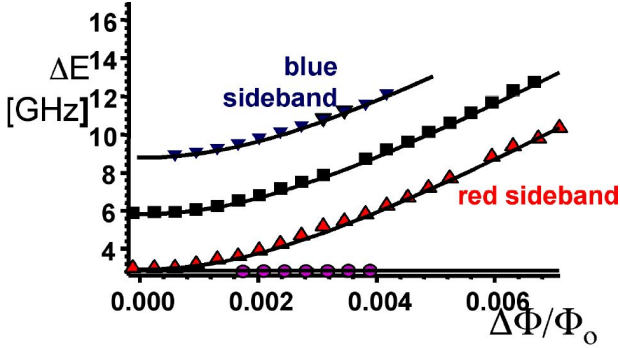


FIG. 50: Resonant frequencies indicated by peaks in the SQUID switching probability when a long (300 ns) microwave pulse excites (saturates) the system before the readout pulse. Data are represented as a function of the external flux Φ_{ext} through the qubit area away from the qubit symmetry point. The blue $|00\rangle \rightarrow |11\rangle$ and red $|01\rangle \rightarrow |10\rangle$ sidebands are shown by down- and up-triangles, respectively; continuous lines are obtained by adding 2.96 GHz and -2.90 GHz, respectively, to the central continuous line (numerical fit). These values are close to the oscillator resonance frequency ν_p at 2.91 GHz (solid circles). *Courtesy of J.E. Mooij, TU Delft.*

B. Delft persistent current flux qubit coupled to a quantum oscillator

The Delft experiment²⁵ demonstrates entanglement between a superconducting flux qubit and a SQUID quantum oscillator. The SQUID provides the measurement system for detecting the quantum states (threshold switching detector, Fig. 44). It is also presents an effective inductance that, in parallel with an external shunt capacitance, acts as a low-frequency harmonic oscillator; the qubit and oscillator frequencies are approximately $h\nu_q = h\nu_{01} \approx 6$ GHz and $h\nu_r \approx 3$ GHz, corresponding to Fig. 49(a).

In the Delft experiment²⁵, performing spectroscopy on the coupled qubit-oscillator multi-level system reveals the variation of the main and sideband transitions with flux bias Φ_{ext} , as shown in Fig. 50. The presence of visible sideband transitions demonstrates the qubit-oscillator interaction and (weak) level hybridization.

Short microwave pulses can now be used to induce Rabi oscillations between the various qubit-oscillator transitions. In the Delft experiment²⁵, microwave pulses with frequency $\nu_q = \nu_{01} \approx \Delta/h \approx 5.9$ GHz (qubit symmetry point) were first used to induce Rabi oscillations with ~ 25 ns decay time at the main qubit transition $|00\rangle \rightarrow |10\rangle$ (and $|01\rangle \rightarrow |11\rangle$) for different values of the microwave power. The Rabi frequency as function of the amplitude of the microwave voltage demonstrated qubit-oscillator hybridization (avoided crossings) at the oscillator ν_p (ν_r) and Larmor Δ/h (!) frequencies.

The dynamics of the coupled qubit-oscillator system can be studied by inducing microwave-driven Rabi oscillation between the blue $|00\rangle \rightarrow |11\rangle$ and red $|01\rangle \rightarrow |10\rangle$ sidebands. In particular one can study the conditional

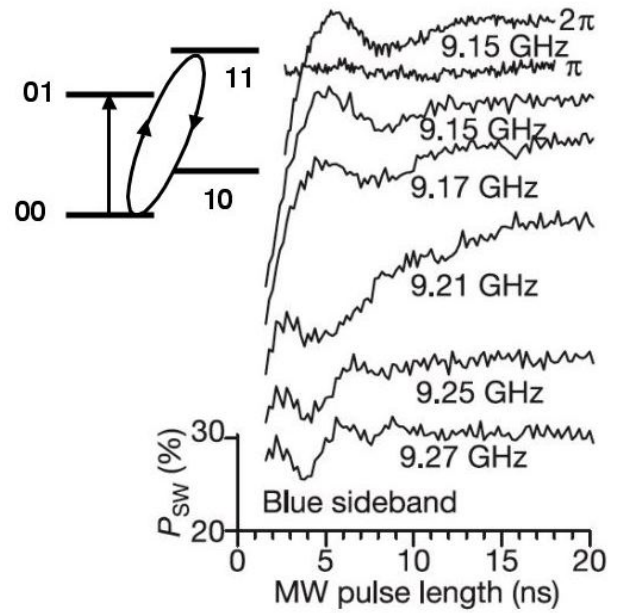


FIG. 51: Generation and control of entangled states via π and 2π Rabi pulses on the qubit transition $|00\rangle \rightarrow |10\rangle$, followed by Rabi driving of blue sideband transitions $|00\rangle \rightarrow$. A π pulse excites the system from $|00\rangle$ to $|10\rangle$, which suppresses the blue sideband transitions $|00\rangle \rightarrow |11\rangle$ (second curve from the top). On the other hand, with a 2π pulse the system returns to $|00\rangle$, which allows Rabi oscillation on the blue sideband. *Adapted from Chiorescu et al.²⁵*

dynamics in microwave multi-pulse experiments: by coherently (de)populating selected levels via proper timing of Rabi oscillations induced by a first pulse, a second pulse can induce Rabi oscillations on another transition connected to the levels controlled by the first pulse. Alternatively, such Rabi oscillations can instead be blocked by the first excitation.

This is shown experimentally in Fig. ??: by preparing the initial state with initial π and 2π pulses, the sideband Rabi oscillations could be turned off and on again. The corresponding Rabi oscillations are shown in the left part of Fig. ??(b), demonstrating rapid decay due to the strong damping of the SQUID oscillator (lifetime ~ 3 ns; $Q=100-150$).

In the previous example, the control pulse (first pulse) was applied to the main $|00\rangle \rightarrow |10\rangle$ transition, controlling the populations of the "0" and "1" levels. In the next example, microwave control pulse is applied to the $|00\rangle \rightarrow |01\rangle$ transition, inducing Rabi oscillations which populate the first excited state of oscillator. A second microwave pulse (in principle, with different frequency) can then induce Rabi oscillations on the $|01\rangle \rightarrow |10\rangle$ transition (red-sideband). The experimental result²⁵ is shown Fig. 53. Clearly, for sufficiently long qubit and oscillator lifetimes, one can prepare entangled Bell states, $\frac{1}{2}(|00\rangle \pm |01\rangle)$ and $\frac{1}{2}(|01\rangle \pm |10\rangle)$ by applying $\pi/2$ microwave pulses to the $|00\rangle \rightarrow |11\rangle$ and $|01\rangle \rightarrow |10\rangle$ tran-

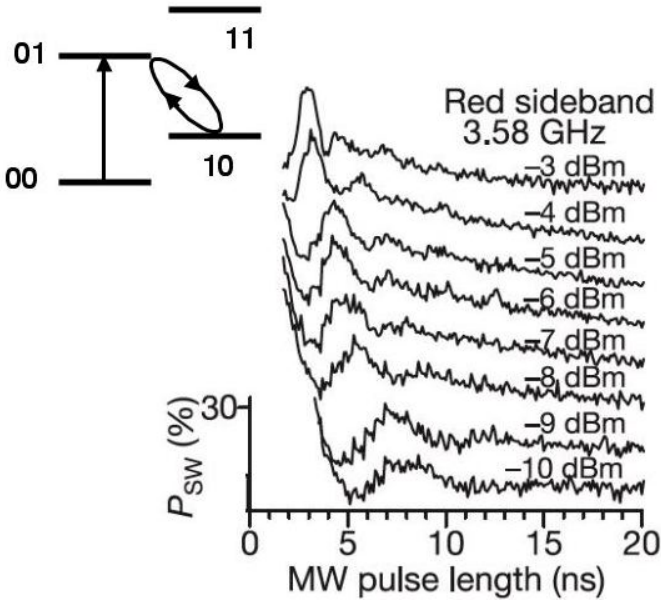


FIG. 52: Generation and control of entangled states via π and 2π Rabi pulses on the qubit transition $|00\rangle \rightarrow |10\rangle$, followed by Rabi driving of red sideband transitions $|10\rangle \rightarrow |01\rangle$. A π pulse excites the system from $|00\rangle$ to $|10\rangle$, which In the right panel, a π pulse excites the system from $|00\rangle$ to $|10\rangle$, which populates the $|10\rangle$ state and allows Rabi oscillation on the red sideband transitions $|01\rangle \rightarrow |10\rangle$. *Adapted from Chiorescu et al.*²⁵

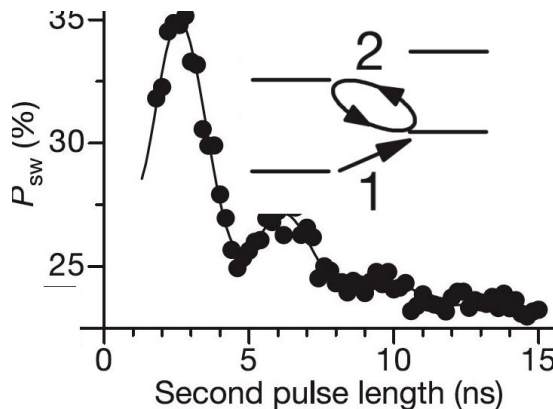


FIG. 53: Generation and control of entangled states and study of decay and lifetimes. Here a Rabi π pulse on the oscillator transition $|00\rangle \rightarrow |01\rangle$ populates the state $|01\rangle$, which then allows Rabi oscillation on the red sideband transition $|01\rangle \rightarrow |10\rangle$. The decay of both the Rabi oscillation and the average probability gives evidence for short oscillator life time (~ 3 ns; Q=100-150). *Adapted from Chiorescu et al.*²⁵

sitions.

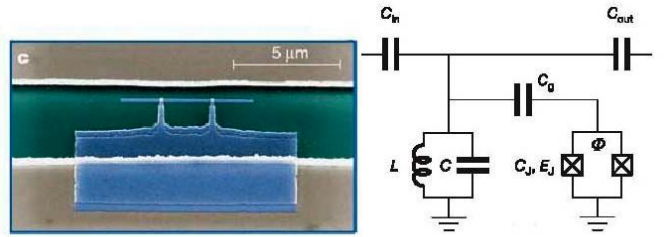


FIG. 54: Yale SCB charge-phase qubit coupled to an oscillator in the form of a superconducting microwave stripline resonator. *Adapted from Wallraff et al.*¹⁵¹

C. Yale charge-phase qubit coupled to a strip-line resonator

In the Yale experiments^{151,152} a coherent qubit-quantum oscillator system is realized in the form of a Cooper pair box capacitively coupled to a superconducting stripline resonator (Fig. 54) forming one section of a microwave transmission line. The stripline resonator, a finite length (24 mm) of planar wave guide, is a solid-state analogue of the cavity electromagnetic resonator used in quantum optics to study strong atom-photon interaction and entanglement. In the Yale experiments, the qubit is placed in the transverse field in the gap between the resonator strip lines, i.e. inside the microwave cavity. The E_C and E_J parameters are such that the SCT is effectively in the charge-phase region, and it is operated by controlling both the charge and phase (flux) ports.

The large effective electric dipole moment d of Cooper pair box and the large vacuum electric field E_0 in the transmission line cavity lead to a large vacuum Rabi frequency $\nu_{Rabi} = 2dE_0/h$, which allows reaching the strong coupling limit of cavity QED in the circuit.

In the Yale experiment, spectroscopic measurements are performed by driving the qubit with resonant microwave pulses and simultaneously detecting the frequency and intensity-dependent amplitude and phase of probe pulses of microwave radiation sent through a transmission line coupled to the stripline resonator via input/out capacitors (Fig. 54). The oscillator frequency is fixed at $\hbar\nu_r \approx 6$ GHz. The qubit level separation, on the other hand, is tunable over a wide frequency range around 6 GHz in two independent ways: (i) by varying the magnetic flux ϕ_e through the loop, forming the phase (flux) gate VD, or (ii) by varying the charge n_g via the voltage gate, primarily around the charge degeneracy point, $n_g=1/2$, to minimize the effect of charge fluctuations.

The flux bias is used to tune the qubit transition frequency at $n_g=1/2$ to values larger or smaller than the resonator frequency. The tuning the qubit frequency with the charge gate will provide two distinct cases: the qubit always detuned from the oscillator, and the qubit being degenerate with the resonator at certain values of n_g .

A central result¹⁵¹ is the evidence for the qut oscillator hybridization and splitting of the degenerate $|01\rangle$ and $|10\rangle$ states, $\nu_{01} \rightarrow \nu_{\pm}$, as illustrated in Fig. 49 (right). This splitting is often called "vacuum Rabi splitting" because the oscillator is in its ground (vacuum) state.

The $|01\rangle$, $|10\rangle$ level splitting is observed through microwave excitation of the $0 \rightarrow 1$ resonance transition and observing the splitting of the resonance line as the qubit and the oscillator are tuned into resonance (by tuning the qubit frequency to zero qubit-oscillator detuning: $\delta = \nu_q - \nu_r = 0$).

Another central result¹⁵² is the evidence for a long qubit dephasing time of $T_2 > 200$ ns under optimal conditions: qubit parked at the charge degeneracy point and weak driving field (low photon occupation number in the resonator cavity). In the experiment¹⁵¹ the qut oscillator detuning is large, the qubit resonance transition $\nu_q = \nu_{01}$ is scanned by microwave radiation, and the dispersive shift of the resonator frequency ν_r seen by a microwave probe beam is used to determine the occupation of the qubit levels. Scanning the qubit $|00\rangle \rightarrow |10\rangle$ resonance line profile allowed to determine the lineshape and linewidth as a function of microwave power, giving the best value of $T_2 > 200$ ns. Moreover, observation of the position of the resonance as a function of microwave power allowed the determination of the ac-Stark shift, i.e. the Rabi frequency as a function of the photon occupation (electric field) of the cavity. The measurement induces an ac-Stark shift of 0.6 MHz per photon in the qubit level separation. Fluctuations in the photon number (shot noise) induce level fluctuations in the qubit leading to dephasing which is the characteristic back-action of the measurement. A cross-over from Lorentzian to Gaussian resonance line shape with increasing measurement power is observed and explained by dependence of the resonance linewidth on the cavity occupation number, exceeding the linewidth due to intrinsic decoherence at high rf-power.

D. Comparison of the Delft and Yale approaches

In comparison, the Delft experiment²⁵ corresponds to the case of very large detuning ($\nu_q = 6$ GHz, $\nu_r = 3$ GHz; $\delta = \nu_q - \nu_r \sim \nu_r$; Fig. 49 (left)), so that one will observe a main resonance line $|00\rangle \rightarrow |10\rangle$ and two sidebands, $|00\rangle \rightarrow |11\rangle$ (blue) and $|01\rangle \rightarrow |10\rangle$ (red). Decreasing the detuning δ , the blue and red sidebands will move away to higher resp. lower frequencies, and one will arrive at the case of zero detuning and qubit-oscillator degeneracy. If the qubit-oscillator coupling is larger than the average linewidth, one will then observe a splitting of the main line (Fig. 49 (right)).

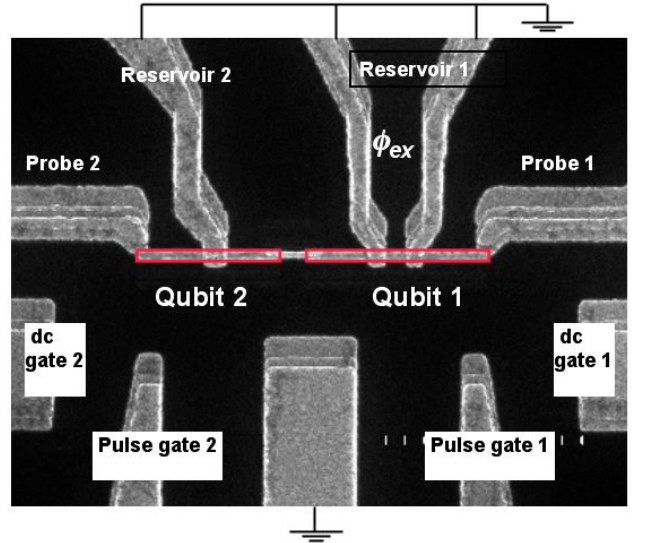


FIG. 55: The NEC 2-qubit system: two capacitively coupled charge qubits. The left qubit is a single Cooper pair box (SCB) and the right qubit is an SCT with flux-tunable Josephson energy. *Courtesy of J.S. Tsai, NEC, Tsukuba, Japan.*

XIII. EXPERIMENTAL MANIPULATION OF COUPLED TWO-QUBIT SYSTEMS

A. Capacitively coupled charge qubits

An AFM picture of the NEC SCB 2-qubit system³⁶ is shown in Fig. 55 and the corresponding circuit JJ circuit in Fig. 28 (note that in the NEC circuit the left SCT is replaced by a simple SCB).

Two coupled qubits constitute a 4-level system. The Hamiltonian for the NEC system of two capacitively coupled charge qubits (SCBs) was analyzed in the Appendix. The four energy eigenvalues $E_{1,2,3,4}(n_{g1}, n_{g2})$ are plotted in Fig. 56 as a functions of the gate charges. At each point in the parameter space, an arbitrary two-qubit state can be written as a superposition of the four two-qubit energy eigenstates.

As described in Sections IV and X, the general procedure for operating with dc-pulses is to initialize the system to its ground state $|00\rangle$ at the chosen starting point (n_{g10}, n_{g20}) and then suddenly change the Hamiltonian at time $t = 0$ to the gate bias (n_{g1}, n_{g2}) . If the change is strictly sudden, then the state at (n_{g1}, n_{g2}) at time $t = 0$ is $|\psi(t=0)\rangle = |00\rangle$, which can be expanded in the energy basis of the Hamiltonian,

$$|\psi(0)\rangle = |00\rangle = c_1|E_1\rangle + c_2|E_2\rangle + c_3|E_3\rangle + c_4|E_4\rangle \quad (13.1)$$

This stationary state then develops in time governed by the constant Hamiltonian as

$$|\psi(t)\rangle = c_1 e^{-iE_1 t} |E_1\rangle + c_2 e^{-iE_2 t} |E_2\rangle +$$

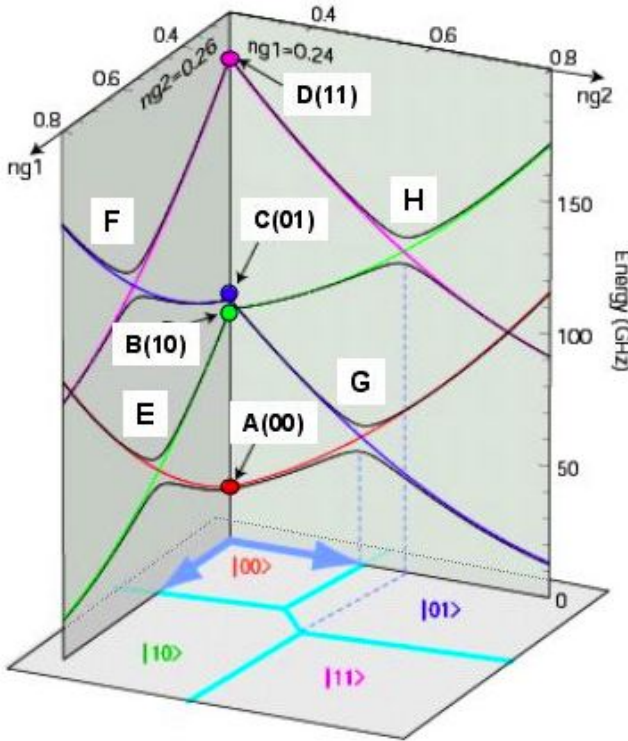


FIG. 56: The NEC 2-qubit system: Energy-level structure as a function of the gate charges n_{g1} and n_{g2} , independently controlled by the gate voltages V_{g1} and V_{g2} . *Courtesy of J.S. Tsai, NEC, Tsukuba, Japan.*

$$+c_3e^{-iE_3t}|E_3\rangle +c_4e^{-iE_4t}|E_4\rangle \quad (13.2)$$

If one re-expands this state in the charge basis of the starting point A (Fig. 56), then one obtains a system with periodic coefficients $a_i(t)$,

$$|\psi(t)\rangle = a_1(t)|00\rangle + a_2(t)|01\rangle + a_3(t)|10\rangle + a_4(t)|11\rangle \quad (13.3)$$

developing in time through all of the charge states.

To perform a two-qubit conditional gate operation, one performs a series of pulses moving the system around in parameter space. Specifically, the NEC scheme is to apply sequential dc-pulses to the charge pulse gates of each of the two qubits in Fig. 55. Two cases have been studied so far:

(1) $V_{g1}(t) = V_{g2}(t)$: This is the case with common control dc-pulses for studied by Pashkin et al.³⁵. Since $\epsilon_1(t) = \epsilon_2(t)$, the plane of operation is at 45 degrees to the axes in Fig. 56. As a result, Pashkin et al.³⁵ observed interference effects and beating oscillations between the two qubits, as described by Eq. (10.43).

(2) $V_{g1}(t) = 0; V_{g2}(t), V_{g1}(t); V_{g2}(t) = 0$: This is the case with separate sequential dc pulses on separate gates recently studied by Yamamoto et al.³⁶. The scheme is illustrated in Fig. 56: Starting at point A, first the system is pulsed in the n_{g1} direction, putting the system in a superposition of the states at points A and B; then the system is pulsed in the n_{g2} direction, allowing condi-

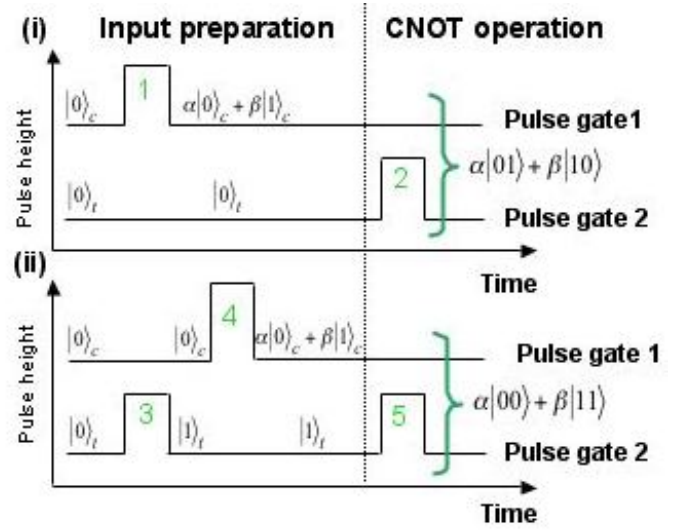


FIG. 57: The NEC 2-qubit system: pulse sequences for a CNOT gate (actually, the gate is a *NOT* – *CNOT* gate). *Courtesy of J.S. Tsai, NEC, Tsukuba, Japan.*

tional gate operation due to the different time evolution of the states departing from A or B.

Specifically, an entangling gate of controlled-NOT (CNOT) type was demonstrated by Yamamoto et al.³⁶ using the pulse sequences shown in Fig. 57: First one applies a dc-pulse to gate 1 of the control qubit, moving out (down left) left from $|00\rangle$ (point A in Fig. 56) in the n_{g1} direction to the single-qubit degeneracy point (point E), staying for a certain time, and then moving back (turning off the pulse), putting the system in a superposition $\alpha|00\rangle + \beta|10\rangle$ (points A and B). Next one applies a dc-pulse to gate 2 of the target qubit, moving out (right) in the n_{g2} direction and back. The pulse is designed to reach the first degeneracy point (point G), allowing the state to develop into a superposition of 00 (point A) and 01 (point C) if the control state was 00. If instead the control state was 10 (point B), the dc-pulse on gate 2 will not reach the two-qubit degeneracy point (point H) and the development will be roughly adiabatic, taking the state back to 10 (point B), never reaching 11 (point D).

With timing such ($\pi/2$ -pulse) that $00 \rightarrow 01$ ($A \rightarrow G \rightarrow C$), the control gate leads to $00+10$, and the target gate only modifies the first component ($00 \rightarrow 01$), resulting in $01+10$, i.e. one of the Bell states. This is shown in the top panel of Fig. 57.

If instead one first applies a $\pi/2$ -pulse in the n_{g2} direction to the target qubit, inducing $00 \rightarrow 01$ (C), and then applies a $\pi/2$ -pulse in the n_{g1} direction to this state, reaching $01+11$, and then again applies a $\pi/2$ -pulse to the target qubit 2, resulting $00+11$, one obtains the other Bell state. This is shown in the bottom panel of Fig. 57.

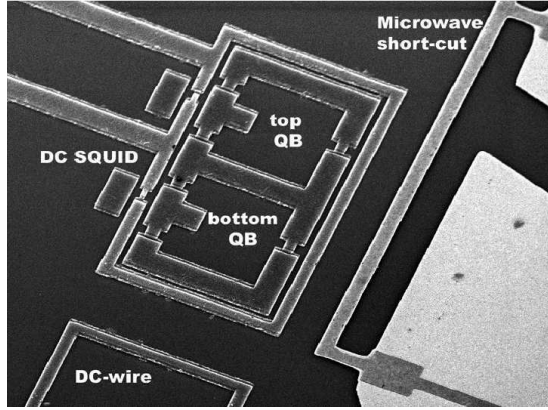


FIG. 58: Scanning microscope image of two inductively coupled qubits surrounded by a DC-SQUID. *Courtesy of J. Majer, TU Delft.*

B. Inductively coupled flux qubits

Figure 58 shows a circuit with two inductively coupled flux qubits forming a four-level quantum system, excited by a single microwave line and surrounded by a single measurement SQUID^{37,38}. With this circuit Majer et al.^{37,38} have spectroscopically mapped large portions of the level structure and determined the device parameters entering in the Hamiltonian matrix Eq. (10.10), finding good agreement with the design parameters. Majer et al. found clear manifestations of qubit-qubit interaction and hybridization in the level structure as a function of bias flux. Presently, ter Haar et al.¹⁷⁵ are investigating a more strongly coupled system with a JJ in the common leg (cf. Fig. 32), inducing Rabi oscillations and performing conditional spectroscopy along the lines described in Section XII in connection with the coupled qubit-oscillator system.

A similar device with two flux qubits inside a coupling/measurement SQUID has recently been investigated by et al.^{176,177}, so far demonstrating Rabi oscillation of individual qubits. Finally, Izmalkov et al.³⁹ have spectroscopically demonstrated effects of qubit-qubit interaction and hybridization for two inductively coupled flux qubits inside a low-frequency tank circuit.

C. Two capacitively coupled JJ qubits

Capacitive coupling of two JJ qubits (Section IX E, Fig. 30) has recently been investigated by several groups^{40,178}, showing indirect⁴⁰ and direct¹⁷⁸ evidence for qubit entanglement. Figure 59 shows the circuit used by McDermott et al.¹⁷⁸. The potential-well and level structure of each JJ qubit under operation and measurement conditions are shown in Fig. 60.

The 2-qubit circuit behaves as two dipole-coupled pseudo-2-level systems, illustrated in Fig. 49. With "identical" qubits, the $|01\rangle$ and $|10\rangle$ states are degenerate and

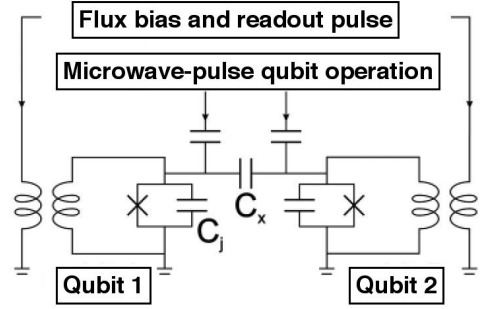


FIG. 59: Circuit scheme for two capacitively coupled current (flux) biased JJ qubits with rf and dc control/readout lines. *Adapted from McDermott et al.¹⁷⁸*

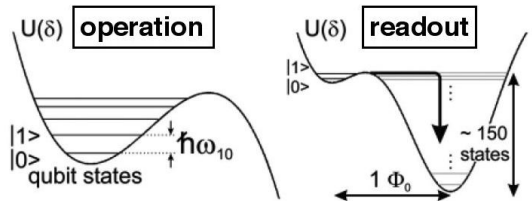


FIG. 60: Potential energies and quantized energy levels the Josephson phase qubit: left, during qubit operation; right, during state measurement, in which case the qubit well is much shallower and state $|1\rangle$ rapidly tunnels to the right hand well. *Adapted from McDermott et al.¹⁷⁸*

become hybridized and split by the interaction. A microwave π -pulse tuned to the $|0\rangle \rightarrow |1\rangle$ transition of one of the isolated qubits will "suddenly" induce a $|00\rangle \rightarrow |10\rangle$ transition, populating the $|E_+\rangle = |10\rangle + |01\rangle$ and $|E_-\rangle = |10\rangle - |01\rangle$ states with equal weights. This will leave the system oscillating between the two qubits, between the $|10\rangle$ and $|01\rangle$ states, $|\psi(t)\rangle = |E_+\rangle + e^{-i\delta Et}|E_-\rangle = \cos(\delta Et/2)|10\rangle + \sin(\delta Et/2)|01\rangle$ where $\delta E = E_- - E_+$. This means that the two-qubit system oscillates between non-entangled and entangled states. With one ideal detector for each qubit we can measure the state of each qubit with any prescribed time delay between measurements. With simultaneous measurements we can determine all the probabilities $p_{ij} = |\langle ij|\psi(t)\rangle|^2$, ideally giving $p_{10} = \frac{1}{2}(1 + \cos(\delta Et))$, $p_{01} = \frac{1}{2}(1 - \cos(\delta Et))$, and $p_{00} = p_{11} = 0$ in the absence of relaxation, decoherence and perturbations caused by the detectors.

Figure 61 shows the actual experimental results of Ref.¹⁷⁸ for the probabilities $p_{ij}(t)$: The p_{10} and p_{01} probabilities oscillate out-of-phase, as expected. In addition, the average probabilities and oscillation amplitudes all decay with time. The results are compatible¹⁷⁸ with the finite rise time of the initial π -pulse (5 ns), the single-qubit readout fidelity (70 percent) and the single-qubit relaxation time T_1 (25 ns), and the limited two-qubit readout fidelity, as used in the numerical simulations. Of particular interest is that for simultaneous (within 2 ns)

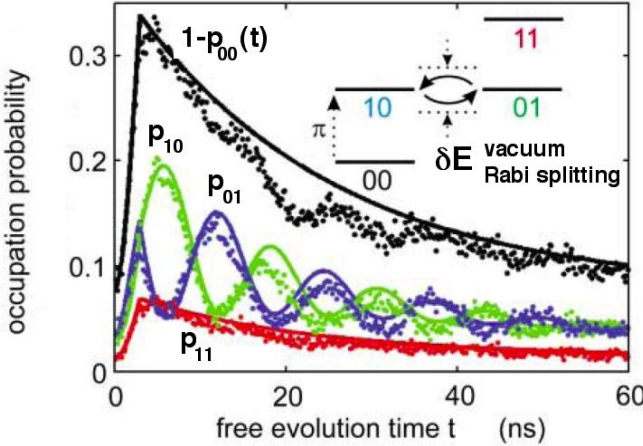


FIG. 61: Interaction of the coupled qubits in the time domain. The qubits are tuned into resonance and the system is suddenly prepared in state (10) by a microwave π -pulse applied to qubit 1. Simultaneous single-shot measurement of each of the qubits 1 and 2 reads out the probabilities $p_{00}, p_{10}, p_{01}, p_{11}$ for finding the 1+2 system in states 00, 10, 01, and 11, respectively. The full lines represent results of numerical simulations. *Adapted from McDermott *et al.*¹⁷⁸*

readout of the qubits, the experiments show that readout of one qubit only leads to small perturbation of the other qubit¹⁷⁸, which is promising for multi-qubit applications.

XIV. QUANTUM STATE ENGINEERING WITH MULTI-QUBIT JJ SYSTEMS

Due to the recent experimental progress, protocols and algorithms for multi-qubit JJ systems can soon begin to be implemented in order to test the performance of JJ qubit and readout circuits and to study the full dynamics of the quantum systems. The general principles are well known (see e.g.^{49,50}) and have very recently been successfully applied in several other systems to achieve interesting and significant results in well-controlled quantum systems: ion-trap technology has been used to entangle 4 qubits¹⁸⁰, implement 2-qubit gates and test Bell's inequalities^{181,184}, perform the Deutsch-Josza algorithm¹⁸², achieve teleportation (within the system)^{185,186,187}, and perform error correction¹⁸⁸; quantum optics has recently demonstrated long-distance teleportation¹⁹⁰ as well as 4-photon entanglement^{190,191}. There are presently a considerable theoretical literature on how to implement these and similar protocols and algorithms in JJ circuits. Below we will describe a few examples to illustrate what may need to be done experimentally.

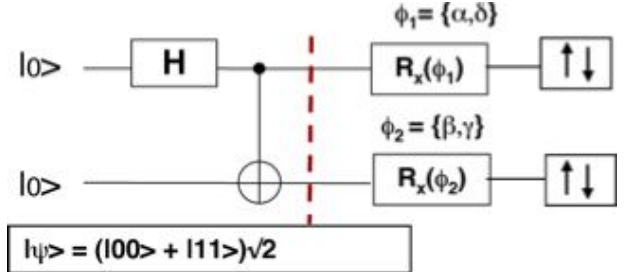


FIG. 62: EPR anticorrelation in the singlet state

A. Bell measurements

The first essential step is to study the quantum dynamics of a two-qubit circuit and to perform a test of Bell's inequalities by creating entangled two-qubit Bell states (Section III, Ref.⁴⁹) and performing simultaneous projective measurements on the two qubits, similarly to the ion trap experiments^{181,184}. Clearly the experiment will be a test of the quantum properties of the circuit and the measurement process rather than a test of a Bell inequality.

The general principle is to (a) entangle the two qubits, (b) measure the projection along different detector axes ("polarization directions"), (c) perform four independent measurements, and finally (d) analyze the correlations. If the detector axes are fixed, as is the case for the JJ readout (measuring charge *or* flux), one can instead rotate each of the qubits.

Figure 62 shows the quantum network for creating a Bell state $|\psi\rangle$, perform single qubit rotations $R_x(\phi_1)$, $R_x(\phi_2)$, and finally perform a projective measurement on each of the qubits along the same common fixed quantization axis. For each setting of the angles, (ϕ_1, ϕ_2) , one then performs a series of measurements obtaining the probabilities $P_{ij} = |\langle ij|\psi\rangle|^2 = \langle\psi|i j\rangle\langle i j|\psi\rangle$. These can be combined into the results for finding the two qubits in the same state, $P_{\text{same}} = P_{00} + P_{11}$, or in different states, $P_{\text{diff}} = P_{01} + P_{10}$, and finally into the difference $q(\phi_1, \phi_2) = P_{\text{same}} - P_{\text{diff}}$. This quantity $q(\phi_1, \phi_2)$ is evaluated in four experiments for two independent settings of the two angles, $\phi_1 = (\alpha, \delta)$, $\phi_2 = (\beta, \gamma)$, constructing the function

$$B(\alpha, \delta; \beta, \gamma) = |q(\alpha, \beta) + q(\delta, \beta)| + |q(\alpha, \gamma) - q(\delta, \gamma)| \quad (14.1)$$

The Clauser-Horne-Shimony-Holt (CSCH) condition¹⁹² for violation of classical physics is then $B > 2$ (maximum value $2\sqrt{2}$).

The application to JJ charge-phase qubits has been discussed by Refs.^{193,194}. Experimentally, a first step in this direction has been taken by Martinis *et al.*¹⁷⁸ who directly detected the anticorrelation in the oscillating superposition of Bell states $|\psi(t)\rangle = \cos(\delta Et/2)|10\rangle + \sin(\delta Et/2)|01\rangle$.

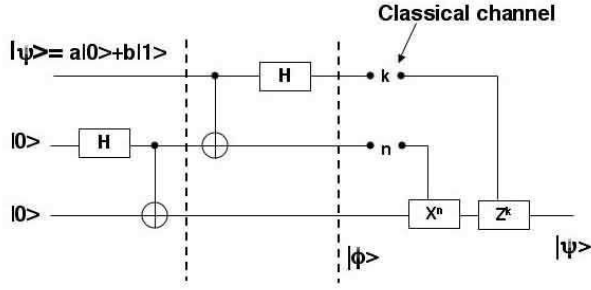


FIG. 63: Teleportation in a 3-qubit system. The unknown qubit (1) to be teleported is $|\psi\rangle = a|0\rangle + b|1\rangle$. The result of the measurement is sent by Alice via classical channels to Bob who performs the appropriate unitary transformations to restore the original single-qubit state. As a result of the teleportation, a specific but unknown state has been transferred from one qubit to another.

B. Teleportation

In the simplest form of teleportation an unknown single-qubit quantum state is transferred from one part of the system to another, i.e. from one qubit to another, as illustrated in Fig. 63. In Fig. 63, the initial state is given by

$$(a|0\rangle + b|1\rangle)(|00\rangle) \quad (14.2)$$

Next, applying CNOT and Hadamard gates entangles qubits 2 and 3 into a Bell state,

$$(a|0\rangle + b|1\rangle)(1/\sqrt{2})(|00\rangle + |11\rangle) \quad (14.3)$$

which is the resource needed for teleportation (in quantum optics this corresponds to the entangled photon pair shared between Alice and Bob). One member of the Bell pair (qubit 2) is now "sent" to Alice and entangled with the unknown qubit to be teleported, creating a 3-qubit entangled state,

$$\begin{aligned} &|00\rangle(a|0\rangle + b|1\rangle) \\ &+ |01\rangle(b|0\rangle + a|1\rangle) \\ &+ |10\rangle(a|0\rangle - b|1\rangle) \\ &+ |11\rangle(-b|0\rangle + a|1\rangle) \end{aligned} \quad (14.4)$$

At this point, qubit 3 is sent to Bob, meaning that a 3-qubit entangled state is shared between Alice and Bob. Moreover, at this point, in each component of this 3-qubit entangled state in Eq. (14.4), the two upper qubits are in eigenstates. This means that a projective measurement of the these two qubits by Alice will collapse the total state to one of the four components. If the result of Alice's measurement is $|ij\rangle$, the first two qubits are in the state $|ij\rangle$ and the 3-qubit state is known, given by the corresponding component in the previous equation. Any of these 3-qubit products can be transformed by a

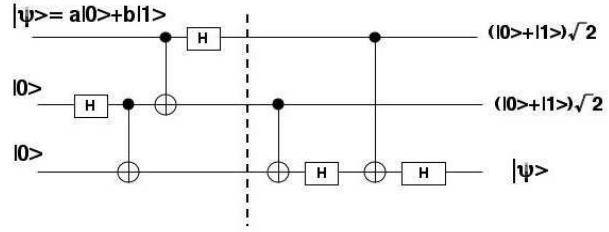


FIG. 64: Teleportation in a 3-qubit system without measurement and classical transmission. The unknown qubit (1) to be transferred is again $|\psi\rangle = a|0\rangle + b|1\rangle$. The state of qubits 1 and 2 are now used to control CNOT gates to restore the original single-qubit state on qubit 3. As a result of the teleportation, a specific but unknown state has been transferred from qubit 1 to qubit 3, leaving qubits 1 and 2 in superposition states.

unitary transformation back to the original state:

$$I(a|0\rangle + b|1\rangle) = |\psi\rangle \quad (14.5)$$

$$\sigma_x(b|0\rangle + a|1\rangle) = |\psi\rangle \quad (14.6)$$

$$\sigma_z(a|0\rangle - b|1\rangle) = |\psi\rangle \quad (14.7)$$

$$\sigma_z\sigma_x(-b|0\rangle + a|1\rangle) = |\psi\rangle \quad (14.8)$$

corresponding to resp. no change, bit flip, phase flip and bit-plus-phase flip of the original unknown state $|\psi\rangle$. Alice's measurement causes *instantaneous* collapse, after which Alice by classical means (e.g. e-mail!) can tell Bob which unitary transformation to apply to recover the original single-qubit state.

An alternative approach, without measurement and classical transmission, is shown in Fig. 64. In this case, the final 3-qubit state is still a disentangled product state with the correct state $|\psi\rangle = a|0\rangle + b|1\rangle$ on qubit 3,

$$\frac{1}{\sqrt{2}}(|0\rangle + |1\rangle)\frac{1}{\sqrt{2}}(|0\rangle + |1\rangle)(a|0\rangle + b|1\rangle) \quad (14.9)$$

while qubits 1 and 2 are now in superposition states. If desired, these states can be rotated back to $|00\rangle$ by single qubit gates.

The teleportation protocol has been implemented in ion trap experiments^{186,187} (and of course in quantum optics¹⁸⁹). A proposal for a setup for implementing a teleportation scheme in JJ circuitry is shown in Fig. 65, describing a 3-qubit chain of charge-phase qubits coupled by current-biased large JJ oscillators, in principle allowing controllable nearest-neighbour qubit couplings^{158,159}: In the absence of bias currents, to first order the qubits are non-interacting and isolated from each other. The basic two-qubit gates are achieved by switching on the bias-current-controlled qubit-qubit interaction for a given time. CNOT gates can be achieved in combination with single-qubit Hadamard and phase gates^{158,159,160}. By applying the sequence of gates shown in Fig. 64 (or an equivalent sequence), the unknown state will be physically moved from the left end to the right end of the chain.

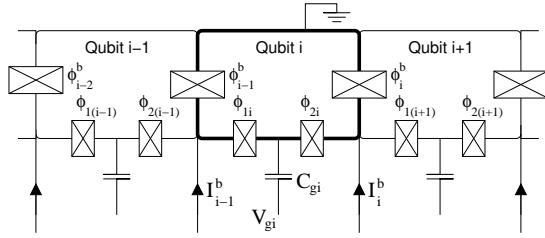


FIG. 65: Network of loop-shaped SCT charge qubits, coupled by large Josephson junctions. The interaction of the qubits (i) and ($i + 1$) is controlled by the current bias I_{bi} . Individual qubits are controlled by voltage gates, V_{gi} . Single-qubit readout is performed by applying an ac current pulse to a particular JJ readout junction (not shown), or using an RF-SET capacitively coupled to the island [27].

Moreover, by applying coupling pulses simultaneously to several qubits, one can in principle create multi-qubit entangled states in fewer operations than with sequential two-qubit gates^{195,196} as well as perform operations in parallel on different parts of the system.

Extending the system to a five-qubit chain one can in a similar way transfer an entangled two-qubit state from the left to the right end of the chain.

C. Qubit buses and entanglement transfer

With entangled "flying qubits" like photons, quantum correlations can be shared in a spatially highly extended states. However, with solid-state circuitry the issue becomes how to transfer entanglement among spatially fixed qubits.

The standard answer is to apply entangling two-qubit gates between distant qubits. The qubit-qubit interaction can be direct, e.g. dipole-dipole-type interaction between distant qubits, or mediated by excitations in the system. The transfer can be mediated via virtual or real excitations in a passive polarizable medium, a "system bus", or via a protocol for coupling qubits and bus oscillators.

A classic example of protocol-controlled oscillator-mediated coupling is the Cirac-Zoller gate¹⁹⁷ between two ions sequentially entangled via exchange coupling with the lowest vibrational mode of the ions in the trap. Another example is the Molmer-Sorensen gate^{198,199,200} which creates qubit-qubit interaction via virtual excitation of ion-trap modes. Similar concepts for controlling entanglement have recently been theoretically investigated in applications to JJ-qubit-oscillator circuits^{164,201,202,203,204,205,206,207,208}

An different approach is to allow the bus ("spin-chain") states to develop in time governed by the fixed bus Hamiltonian and to tailor the interactions and the initial conditions such that useful dynamics and information transfer is achieved^{209,210,211,212}. Also these concepts have

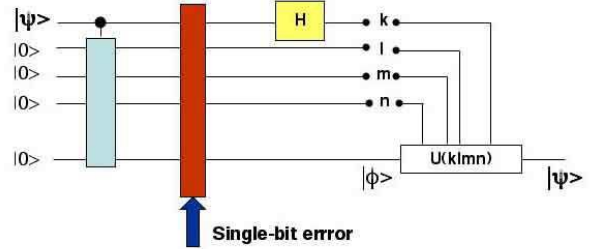


FIG. 66: Teleportation with error correction in a 5-qubit system without measurement.

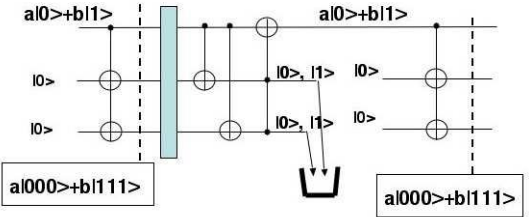


FIG. 67: Coding, decoding and correcting a bit flip error in a 3-qubit logic qubit. The first gate on the left represents two sequential CNOT gates. The last gate before the garbage can is a control-control-NOT (Toffoli) gate.

been applied to JJ-circuits in a number of recent theoretical studies^{213,214,215,216,217,218,219}.

D. Qubit encoding and quantum error correction

Quantum error correction (QEC) (see e.g. Refs. 49,220,221,222,223,224,225,226) will most certainly be necessary for successful operation of solid state quantum information devices in order to fight decoherence. The algorithmic approach to QEC follows the principles of classical error correction, by encoding bits to create redundancy, and by devising procedures for identifying and correcting the errors based on specific models for the errors.

The quantum circuit in Fig. 66 illustrates QEC in terms of five-qubit teleportation with bit errors, illustrating restoration of the state including error correction by measurement-controlled unitary transformation.

The quantum circuit in Fig. 67 demonstrates some essential steps of QEC in the case of one logical qubit encoded in three physical qubits: The first step is to encode the physical qubit in logical qubit basis states $|000\rangle$ and $|111\rangle$ by applying two CNOT gates to create a 3-qubit entangled state:

$$(a|0\rangle + b|1\rangle)|00\rangle \rightarrow (a|000\rangle + b|111\rangle) \quad (14.10)$$

Next, there may occur a bit-flip error in one of the qubits:

$$a|000\rangle + b|111\rangle \quad (\text{no bit flip}) \quad (14.11)$$

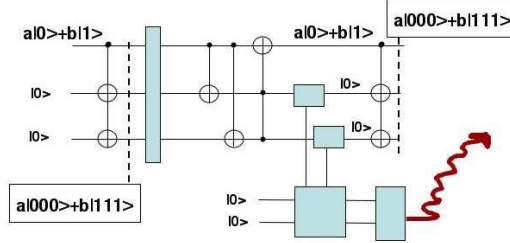


FIG. 68: Coding, decoding and correcting a bit flip error in 3-qubit logic qubit.

$$a|100\rangle + b|011\rangle \text{ (bit flip in qubit 1)} \quad (14.12)$$

$$a|010\rangle + b|101\rangle \text{ (bit flip in qubit 2)} \quad (14.13)$$

$$a|001\rangle + b|110\rangle \text{ (bit flip in qubit 3)} \quad (14.14)$$

The next step applies a number of disentangling CNOT gates to check for the type of error. For the four possible states above we obtain:

$$a|000\rangle + b|111\rangle \rightarrow (a|0\rangle + b|1\rangle) |00\rangle \quad (14.15)$$

$$a|100\rangle + b|011\rangle \rightarrow (a|1\rangle + b|0\rangle) |11\rangle \quad (14.16)$$

$$a|000\rangle + b|111\rangle \rightarrow (a|0\rangle + b|1\rangle) |10\rangle \quad (14.17)$$

$$a|000\rangle + b|111\rangle \rightarrow (a|0\rangle + b|1\rangle) |01\rangle \quad (14.18)$$

At this stage, qubits 2 and 3 have become independent eigenstates, just as in teleportation. The corresponding eigenvalues are called *syndrome*, and indicate which corrective operations should be implemented. Remarkably, in two of the above bit-flipped cases, with error syndromes ((01) and (10), qubit 1 is now correct, the error residing in qubits 2 or 3 in the workspace ("ancillas"). The only case where a transformation is needed is when the error syndrom is (11), which corresponds to a bit flip in qubit 1, to be corrected with a CCNOT (control-control-NOT, or Toffoli, gate), controlled by the truth table of an AND gate. In Fig. 67 we have used a compact single-gate notation for CCNOT, while in reality it must be implemented through a sequence of eight two-qubit gates⁴⁹ (there is no direct three-qubit interaction in the Hamiltonian). At this stage, the 3-qubit state is completely disentangled into a product state.

The final step consists in re-encoding the physical qubit 1 to the logical qubit $a|000\rangle + b|111\rangle$. However, although the physical qubit 1 is always correct at this stage, the workspace is not. This can be handled in a number of ways. Figure 67 dumps the "hot" qubits in the garbage can (i.e. leaves them, or forces them, to relax), and re-encodes with fresh qubits from a larger workspace. Alternatively, Fig. 68 describes a variation where the old qubits 2 and 3 are re-initialized by entanglement with a measurement device which then dissipates the heat from the bitflip and the error correction procedure.

In both of these cases, as described, we need a total workspace with five qubits. In principle, however, one can do with three qubits if we can rapidly re-initialize

qubits 2 and 3 without inducing new errors. Recently an error correcting procedure with cooling of the system without measurement has been proposed²²⁷.

Phase flips (sign changes), e.g. $a|0\rangle + b|1\rangle \rightarrow a|0\rangle - b|1\rangle$ can be handled by similar 3-qubit encoding, decoding and correction. Combining these two approaches gives the 9-qubit Shor code²²⁰ for correcting also combined bit and phase flips, e.g. $a|0\rangle + b|1\rangle \rightarrow a|1\rangle - b|0\rangle$. The minimum code to achieve the same thing is a 5-qubit code²²¹ and there are more efficient codes with 7 qubits^{223,224,225}.

A related approach to fighting decoherence is to encode the quantum information in noiseless subsystems, so called Decoherence Free Subspaces (DFS)^{124,125,228,229}

A different approach is the so called "bang-bang" dynamic correction method^{230,231,232,233,234,235}, basically corresponding to very frequent application of the spin-echo technique. This is related to the quantum Zeno effect (see e.g. Ref.²³⁶, describing situations where the quantum system via very strong interaction with the environment is forced into a subspace from where it cannot decay.

In this Section we have restricted the discussion to a few different protocols for quantum state engineering, representing basic steps in algorithms for solving specific computational problems. For a discussion of quantum algorithms and computational complexity we refer to the books by Nielsen and Chuang⁴⁹ and Gruska⁵⁰, and to the original papers. We would however like to mention a few papers discussing how to implement a few well-known algorithms in JJ circuitry. The basics of quantum gates in JJ-circuits can be found in e.g. Refs.^{42,237,238}. The Deutsch-Josza (DJ) and related algorithms have been discussed by Siewert and Fazio²³⁸ describing a 3-qubit DJ implementation with three charge-phase qubits connected in a ring via phase-coupling JJs with variable Josephson coupling energy (SQUIDS), and by Schuch and Siewert analyzing a 4-qubit implementation²³⁹. For the Grover search algorithm there seems to be nothing published on the implementation in JJ circuitry. Concerning Shor's factorization algorithm there is a recent paper by Vartiainen et al.²⁴². There is also recent work on optimization of two-qubit gates²⁴³, and relations between error correction and entanglement²⁰⁸.

Finally there are a number of papers connecting JJ-circuits with geometric phases and holonomic quantum computing^{246,247,248,249} and on adiabatic computation²⁵² and Cooper pair pumps^{250,251}. For a recent paper discussing the universality of adiabatic quantum computing, see Aharonov et al.²⁵³.

XV. CONCLUSION AND PERSPECTIVES

Within 5 years, engineered JJ quantum systems with 5-10 qubits will most likely begin seriously to test the scalability of solid state QI processors.

For this to happen, a few decisive initial steps and breakthroughs are needed and expected: The first essen-

tial step is to develop JJ-hardware with long coherence time to study the quantum dynamics of a two-qubit circuit and to perform a "test" of Bell's inequalities (or rather the JJ-ciruity) by creating entangled two-qubit Bell states and performing simultaneous projective measurements on the two qubits.

A first breakthrough would be to perform a significant number of single- and two-qubit gates on a 3-qubit cluster to entangle three qubits. Combined with simultaneous projective readout of individual qubits, not disturbing unmeasured qubits, this would form a basis for the first solid-state experiments with teleportation, quantum error correction (QEC), and elementary quantum algorithms. This will provide a platform for scaling up the system to 10 qubits.

This may not look very impressive but nevertheless would be an achievement far beyond expectations only a decade back. The NMR successes, e.g. running Shor-type algorithms using a molecule with 7 qubits⁷⁶, are based on technologies developed during 50 years using natural systems with naturally long coherence times. Similarly, semiconductor technologies have developed for 50 years to reach today's scale and performance of classical computers. It is therefore to be expected that QI technologies will need several decades to develop truly significant potential. Moreover, in the same way as for the classical technologies, QI technologies will most probably develop slowly step by step, "qubit by qubit", which in itself will be an exponential development.

Moreover, in future scalable information processors, different physical realizations and technologies might be combined into hybrid systems to achieve fast processing in one system and long coherence and long-time information storage in another system. In this way, solid state technologies might be combined with ion trap physics to build large microtrap systems²⁵⁴, which in turn might be coupled to superconducting Josephson junctions processors via microwave transmission lines²⁵⁵.

Acknowledgments

This work has been supported by European Commission through the IST-SQUBIT and SQUBIT-2 projects, by the Swedish Research Council, the Swedish Foundation for Strategic Research and the Royal Academy of Sciences.

GLOSSARY

Adiabatic evolution - Development of a quantum system without transitions among the quantum levels.

Algorithm - Finite sequence of logical operations, which produces a solution for a given problem.

Level crossing - Degeneracy of quantum levels appearing at a certain value of a controlling system parameter (e.g. gate voltage, bias flux, etc.).

Anticrossing - Lifting of degeneracy (level crossing) of quantum levels during variation of the system parameters when an interaction is switched on

Average measurement - Measurement of an expectation value of a dynamic variable in a certain state

Bloch sphere - Geometrical representation of the manifold of quantum states of a two-level system as points on the unit sphere.

Bloch vector - Normalized state vector of a two-level system represented by a radial unit vector of the Bloch sphere.

Charging energy - Electrostatic energy of a capacitor charged with a single electron (e) (or a single Cooper pair (2e)).

Charge qubit - Superconducting qubit based on a single Cooper pair box (SCB), whose computational basis consists of the two charge states of the superconducting island.

Charge-phase qubit - Superconducting qubit based on a single Cooper pair box (SCB) whose charging energy is of the order of the Josephson energy of tunnel junctions

CNOT gate - Controlled-NOT gate: two-qubit gate which changes or does not change the state of a target qubit depending on the state of a controlling qubit.

Cooper pair - Bound state of two electrons (2e), the elementary charge carrier in superconducting equilibrium state.

Coulomb blockade - Suppression of current through a tunnel junction or small metallic island due to large charging energy associated with a passage of a single electron.

CPHASE gate - Controlled-phase gate: two-qubit gate which changes or does not change the phase of a target qubit depending on the state of a controlling qubit.

Decoherence - Evolution of a quantum system, interacting with its environment; cannot be described with a unitary operator; consists of decay of phase coherence (dephasing) and/or changing of level population (relaxation).

Density matrix - Characteristics of a quantum system, which contains full statistical information about the state of the system.

Dephasing - Decay of phase coherence of a superposition state, represented by decreasing off-diagonal elements of the density matrix.

Entanglement - Specific non-local coupling of quantum systems when the wave function of whole system cannot be presented as a product of partial wave functions

Flux qubit - Superconducting qubit based on a SQUID, whose computational basis consists of the two states of the SQUID having opposite directions of the induced flux.

Hadamard gate - Transformation of computational basis states of a single qubit to equally weighted superpositions of the basis states (cat states).

Holonomic quantum computation - Using the geometric phases when a quantum system is taken around a closed circuit in the space of control parameters.

Gate operation - Controlled transformation of the state of one or several qubits; a basic element of an algorithm.

Josephson effect - Non-dissipative current flow between two superconductors separated by a non-superconducting material (insulator, normal metal, etc.).

Josephson junction - Junction of two superconductors, which exhibits the Josephson effect.

Josephson critical current - Maximal value of the Josephson current maintained by a particular junction.

Josephson energy - Inductive energy of a Josephson junction proportional to the critical Josephson current.

π pulse - High frequency control pulse with a specific duration applied to a qubit, producing inversion of the qubit level populations (π rotation; qubit flip)

$\pi/2$ pulse - High frequency control pulse with a specific duration applied to a qubit, typically tipping the Bloch vector from a pole to the equator, or from the equator to a pole, on the Bloch sphere.

Phase gate - Single qubit gate, transforms a superposition of two quantum states into another superposition with different relative phase of the states

Precession - Dynamic evolution of a two-level system in a superposition state, i.e. linear combination of energy eigenstates.

QND measurement - Quantum Non-Demolition Measurement: measurement of a state of a quantum system, which does not destroy the quantum state and makes possible repeated measurements of the same state.

QPC - Quantum Point Contact: a constriction in a conductor with ballistic transport through a small number of conduction channels.

Qubit - Quantum two-level system; basic element of a quantum processor.

PCQ - Persistent Current Qubit: synonymous with flux qubit.

Rabi oscillation - Dynamics of two-level system under

resonant driving perturbation, consists of periodic oscillation of the level populations with the frequency proportional to the amplitude of the perturbation.

Readout - Measurement of a qubit state.

Relaxation - Change of population of the energy eigenstates resulting in approaching the equilibrium population.

SCB - Single Cooper pair Box: superconducting analog of SEB, where it is energetically favorable to have only paired electrons on the island.

SCT - Single Cooper pair Transistor: a superconducting device containing a small island whose charging energy is controlled by an electrostatic gate electrode to increase or decrease current flowing through the island from one large electrode (source) to another (drain).

SEB - Single Electron Box: small metallic island connected to a large electrode via resistive tunnel junction, whose charging energy hence amount of trapped electrons is controlled by an electrostatic gate.

SET - Single Electron Transistor: a device containing a small island whose charging energy is controlled by an electrostatic gate electrode to increase or decrease current flowing through the island from one large electrode (source) to another (drain).

rf-SET - SET driven by an rf signal, is used as an ultra sensitive electrometer by monitoring a linear response function of the SET, which is sensitive to the electrostatic gate potential.

SQUID - Superconducting Quantum Interferometer Device: a device consisting of a one or more Josephson junctions included in a superconducting loop.

dc-SQUID - SQUID containing two Josephson junctions.

rf-SQUID - SQUID containing one Josephson junction.

Single-shot measurement - A measurement which gives an "up/down" answer in one single detection event.

¹ Y. Nakamura, Yu. Pashkin and J.S. Tsai: "Coherent control of macroscopic quantum states in a single-Cooper-pair box", *Nature* **398**, 786 (1999).

² A.O. Caldeira and A. Leggett: "Influence of dissipation on quantum tunneling in macroscopic systems", *Phys. Rev. Lett.* **46**, 211 (1981).

³ A.J. Leggett et al.: "Dynamics of the dissipative two-state system", *Rev. Mod. Phys.* **59**, 1 (1987).

⁴ M.H. Devoret, J.M. Martinis and J. Clarke: "Measurements of macroscopic quantum tunneling out of the zero-voltage state of a current-biased Josephson junction", *Phys. Rev. Lett.* **55**, 1908 (1985).

⁵ J. Clarke, A.N. Cleland, M.H. Devoret, D. Esteve and J.M. Martinis: "Quantum mechanics of a macroscopic variable: the phase difference of a Josephson junction", *Science* **239**, 992 (1988).

⁶ J.E. Mooij, T.P. Orlando, L. Levitov, Lin Tian, C.H. van der Wal, and S. Lloyd: "Josephson persistent current qubit", *Science* **285**, 1036 (1999).

⁷ C.H. van der Wal, A.C.J. ter Haar, F. Wilhelm, R.N.

Schouten, C.J.P.M. Harmans, T.P. Orlando, S. Lloyd J.E. and Mooij: "Quantum superposition of macroscopic persistent-current states", *Science* **290**, 773 (2000).

⁸ J.R. Friedman, V. Patel, W. Chen, S.K. Tolpygo and J.E. Lukens: "Detection of a Schrödinger's cat state in an rf-SQUID", *Nature* **406**, 43 (2000).

⁹ K.K. Likharev: "Dynamics of Josephson junctions and circuits", Gordon and Breach (1986).

¹⁰ K.K. Likharev, Y. Naveh and D. Averin: "Physics of high-*jc* Josephson junctions and prospects of their RSFQ VLSI applications", *IEEE Trans. on Appl. Supercond.* **11**, 1056 (2001).

¹¹ K. Gaj, E.G. Friedman and M.J. Feldman: "Timing of multi-gigahertz rapid single flux quantum digital circuits", *J. VLSI Signal Processing* **16**, 247 (1997).

¹² K.K. Likharev and A. Zorin: "Theory of Bloch-wave oscillations in small Josephson junctions", *J. Low. Temp. Phys.* **59** 347 (1985).

¹³ V. Bouchiat, P. Joyez, H. Pothier, C. Urbina, D. Esteve, and M.H. Devoret: "Quantum coherence with a single

Cooper pair", Phys. Scripta **T76**, 165 (1998).

¹⁴ A. Shnirman, G. Schön, Z. Hermon: "Quantum manipulation of small Josephson junctions", Phys. Rev. Lett. **79**, 2371 (1997).

¹⁵ G. Wendin: "Scalable solid state qubits: challenging decoherence and read-out", Phil. Trans. R. Soc. Lond. A **361**, 1323 (2003).

¹⁶ G. Wendin: "Superconducting quantum computing", Physics World, May 2003.

¹⁷ M.H. Devoret and J.M. Martinis: "Implementing qubits with superconducting circuits", Quantum Information Processing **3** (2004), in press.

¹⁸ M.H. Devoret, A. Wallraff, and J.M. Martinis: "Superconducting qubits: A short review", (2004); cond-mat/0411174.

¹⁹ D. Esteve and D. Vion: "Solid state quantum bit circuits", Les Houches Summer School-Session LXXXI on Nanoscopic Quantum Physics, (2004).

²⁰ G. Burkard: "Theory of solid state quantum information processing", prepared for Handbook of Theoretical and Computational Nanotechnology (2004); cond-mat/0409626.

²¹ D. Vion, A. Cottet, A. Aassime, P. Joyez, H. Pothier, C. Urbina, D. Esteve and M.H. Devoret: "Manipulating the quantum state of an electrical circuit", Science **296**, 886 (2002).

²² D. Vion, A. Aassime, A. Cottet, P. Joyez, H. Pothier, C. Urbina, D. Esteve and M.H. Devoret: "Rabi oscillations, Ramsey fringes and spin echoes in an electrical circuit", Fortschritte der Physik **51**, 462 (2003).

²³ E. Collin, G. Ithier, A. Aassime, P. Joyez, D. Vion and D. Esteve: "NMR-like control of a quantum bit superconducting circuit", Phys. Rev. Lett. **93**, 157005 (2004).

²⁴ I. Chiorescu, Y. Nakamura, C.J.P.M. Harmans, J.E. Mooij: "Coherent Quantum Dynamics of a Superconducting Flux Qubit", Science **299**, 1869 (2003).

²⁵ I. Chiorescu, P. Bertet, K. Semba, Y. Nakamura, C.J.P.M. Harmans and J.E. Mooij: "Coherent dynamics of a flux qubit coupled to a harmonic oscillator", Nature **431**, 159 (2004).

²⁶ P. Bertet, I Chiorescu, C. J. P. M. Harmans, J. E. Mooij and K. Semba: "Detection of a persistent-current qubit by resonant activation", Phys. Rev. B, **70**, 100501(R) (2004).

²⁷ E. Il'ichev, N. Oukhanski, A. Izmalkov, Th. Wagner, M. Grajcar, H.-G. Meyer, A.Yu. Smirnov, Alec Maassen van den Brink, M.H.S. Amin and A.M. Zagoskin: "Continuous monitoring of Rabi oscillations in a Josephson flux qubit", Phys. Rev. Lett. **91**, 097906 (2003).

²⁸ T. Duty, D. Gunnarsson, K. Bladh and P. Delsing: "Coherent dynamics of a charge qubit", Phys. Rev. B **69**, 1405023(R) (2004).

²⁹ Y. Yu, S. Han, X. Chu, S.-I. Chu and Z. Wang: "Coherent temporal oscillations of macroscopic quantum states in a Josephson junction", Science **296**, 889 (2002).

³⁰ J. Martinis, S. Nam, J. Aumentado, and C. Urbina: "Rabi oscillations in a large Josephson-junction qubit", Phys. Rev. Lett. **89**, 117901 (2002).

³¹ J. M. Martinis, S. Nam, J. Aumentado, K. M. Lang, and C. Urbina, Phys. Rev. B **67**, 094510 (2003).

³² R. W. Simmonds, K. M. Lang, D. A. Hite, D. P. Pappas, and John M. Martinis: "Decoherence in Josephson qubits from junction resonances", Phys. Rev. Lett. **93**, 077003 (2004).

³³ K. B. Cooper, M. Steffen, R. McDermott, R. W. Simmonds, S. Oh, D. A. Hite, D. P. Pappas, and John M. Martinis: "Observation of quantum oscillations between a Josephson phase qubit and a microscopic resonator using fast readout", Phys. Rev. Lett. **93**, 180401 (2004).

³⁴ J. Claudon, F. Balestro, F.W.J. Hekking and O. Buisson: "Coherent oscillations in a superconducting multi-level system", Phys. Rev. Lett. **93**, 187003 (2004).

³⁵ Yu.A. Pashkin, T. Yamamoto, O. Astafiev, Y. Nakamura, D.V. Averin and J.S. Tsai: "Quantum Oscillations in Two Coupled Charge Qubits", Nature **421**, 823 (2003).

³⁶ T. Yamamoto, Yu. Pashkin, O. Astafiev, Y. Nakamura and J.S. Tsai: "Demonstration of conditional gate operation using superconducting charge qubits", Nature **425**, 941 (2003)

³⁷ J.B. Majer, Superconducting Quantum Circuits, PhD thesis, TU Delft, The Netherlands, 2002.

³⁸ J.B. Majer, J.B., Paauw, A. ter Haar C.J.P.M. Harmans, C.J.P.M. and J.E. Mooij: "Spectroscopy on two coupled flux qubits", Phys. Rev. Lett. **94**, 090501 (2005).

³⁹ A. Izmalkov, M. Grajcar, E. Il'ichev, Th. Wagner, H.-G. Meyer, A.Yu. Smirnov, M.H.S. Amin, Alec Maassen van den Brink and A.M. Zagoskin: "Experimental evidence for entangled states in a system of two coupled flux qubits", Phys. Rev. Lett. **93**, 037003 (2004); Phys. Rev. Lett. **93**, 049902 (E) (2004).

⁴⁰ A.J. Berkley, H. Xu, R.C. Ramos, M.A. Gubrud, F.W. Strach, P.R. Johnson, J.R. Anderson, A.J. Dagt, C.J. Lobb and F.C. Wellstood: "Entangled macroscopic quantum states in two superconducting qubits", Science **368**, 284 (2003).

⁴¹ Yu. Makhlin, G. Schön, A. Shnirman: "Josephson junction qubits with controlled couplings", Nature **398**, 305 (1999).

⁴² Yu. Makhlin, G. Schön, and A. Shnirman: "Quantum state engineering with Josephson-junction devices", Rev. Mod. Phys. **73**, 357 (2001).

⁴³ R. Landauer: "Irreversibility and Heat Generation in the Computing Process", IBM Journal of Research and Development **5**, 183 (1961).

⁴⁴ E. Fredkin and T. Toffoli, "Conservative Logic Int. J. Theor. Phys. **21**, 219 (1982).

⁴⁵ K.K. Likharev: "Classical and quantum limitations on energy consumption in computation", Int. J. Theor. Phys. **21**, 311 (1982).

⁴⁶ K.K. Likharev, S.V. Rylov and V.K. Semenov: "Reversible conveyer computation in Array of paramagnetic qantrons", IEEE Transactions on Magnetics **21**, 947 (1985).

⁴⁷ C. Bennett: "Notes on the history of reversible computation", IBM Journal of Research and Development **32**, 16 (1988).

⁴⁸ Feynman, R.P. 1996, in *Feynman Lectures on Computation*, (ed. A.J.G. Hey and R.W. Allen), Reading, Massachusetts, USA: Perseus Books).

⁴⁹ M.A. Nielsen and I.L. Chuang: "Quantum Computation and Quantum Information, Cambridge", UK: Cambridge University Press, 2000.

⁵⁰ J. Gruska: "Quantum computing", McGraw-Hill, 1999.

⁵¹ N. Gershenfeld: "Signal entropy and the thermodynamics of computation", IBM Systems Journal **35**, 577 (1996).

⁵² M.P. Frank: "Physical limits of computing", Computing in Science and Engineering **4**, 16 (2002).

⁵³ M.P. Frank: "Nanocomputers - Theoretical Models", in *Encyclopedia of Nanoscience and Nanotechnology*, H.S. Malva, ed., American Scientific Publishers, 2003.

⁵⁴ V.K. Semenov, G. Danilov and D.V. Averin: "Reversible Josephson-Junction Circuits with SQUID Based Cells", Si-

mons Conference on Quantum and Reversible Computation, Stony Brook, May 28-31, 2003.

⁵⁵ R.G. Clark, R. Brenner, T.M. Buehler, V. Chan, N.J. Curson, A.S. Dzurak, E. Gauja, H.-S. Goan, A.D. Greene-tree, T. Hallam, A.R. Hamilton, L.C.L. Hollenberg, D.N. Jamieson, J.C. MacCallum, G.J. Milburn, J.L. O'Brien, L. Oberbeck, C.I. Pakes, S. Prawer, D.J. Reilly, F.J. Ruess, S.R. Schofield, M.Y. Simmons, F.E. Stanley, R.P. Starrett, C. Wellard, and C. Yang: "Progress in silicon-based quantum computing", *Phil. Trans. R. Soc. Lond. A* **361**, 1451 (2003).

⁵⁶ S.R. Schofield, N.J. Curson, M.Y. Simmons, F.J. Ruess, T. Hallam, L. Oberbeck, and R.G. Clark: "Atomically precise placement of single dopants in Si", *Phys. Rev. Lett.* **91**, 136104 (2003).

⁵⁷ M.N. Leuenberger, D. Loss, M. Poggio and D.D. Awschalom: "Quantum information processing with large nuclear spins in GaAs semiconductors", *Phys. Rev. Lett.* **89**, 207601 (2002).

⁵⁸ W. Hahnert, C. Meyer, A. Weidinger, D. Suter and J. Twamley: "Architectures for a spin quantum computer based on endohedral fullerenes", *phys. stat. sol. (b)* **233**, 453 (2003).

⁵⁹ D. Loss and D.P. DiVincenzo: "Quantum computation with quantum dots", *Phys. Rev. A* **57**, 120 (1998).

⁶⁰ A. Zrenner, E. Beham, S. Stufler, F. findeis, M. Bichler and G. Abstreiter: "Coherent properties of a two-level system based on a quantum-dot photodiode", *Nature* **418**, 612 (2002).

⁶¹ H. Kamada and H. Gotoh: "Quantum computation with quantum dot excitons", *Semicond. Sci. Technol.* **19**, S392 (2004).

⁶² X. Li, Y. Wu, D. Steel, D. Gammon, T.H. Stievater, D.S. Katzer, D. Park, C. Piermarocchi and L.J. Sham: "Coherent optical control of the quantum state of a single quantum dot", *Science* **301**, 809 (2003).

⁶³ T. Hyashi, T. Fujisawa, H.D. Cheong, Y.H. Jeong and Y. Hirayama: "Coherent manipulation of electronic states in a double quantum dot", *Phys. Rev. Lett.* **91**, 196802 (2003).

⁶⁴ W.G. van der Wiel, S. De Franceschi, J.M. Elzerman, T. Fujisawa, S. Tarucha, and L.P. Kouwenhoven: "Electron transport through double quantum dots", *Rev. Mod. Phys.* **75**, 1 (2003).

⁶⁵ J.M. Elzerman, R. Hanson, L.H. Willems van Beveren, B. Witkamp, J.S. Greidanus, R.N. Schouten, S. De Franceschi, S. Tarucha, L.M.K. Vandersypen and L.P. Kouwenhoven: "Semiconductore few-electron quantum dots as spin qubits", in *Quantum Dots: A Doorway to Nanoscale Physics*, Lecture Notes in Physics Vol. 667, ed. W.D. Heiss, (2005).

⁶⁶ R. Hanson, B. Witkamp, L.M.K. Vandersypen, L.H. Willems van Beveren, J.M. Elzerman, L.P. Kouwenhoven: "Zeeman energy and spin relaxation in a one-electron quantum dot", *Phys. Rev. Lett.* **91**, 196802 (2003).

⁶⁷ J. M. Elzerman, R. Hanson, L. H. Willems van Beveren, B. Witkamp, L. M. K. Vandersypen and L. P. Kouwenhoven: "Single-shot read-out of an individual electron spin in a quantum dot", *Nature* **430**, 431 (2004).

⁶⁸ P.M. Platzman and M.L. Dykman: "Quantum computing with electrons floating on liquid helium", *Science* **284**, 1967 (1999).

⁶⁹ A. Aassime, G. Johansson, G. Wendin, R. J. Schoelkopf and P. Delsing: "Radio-frequency single-electron transistor as readout device for qubits: Charge sensitivity and back-action", *Phys. Rev. Lett.* **86**, 3376 (2001).

⁷⁰ A. Cottet, D. Vion, P. Joyez, A. Aassime, D. Esteve, and M.H. Devoret: "Implementation of a combined charge-phase quantum bit in a superconducting circuit", *Physica C* **367**, 197 (2002).

⁷¹ A. Zorin: "Cooper pair qubit and electrometer in one device", *Physica C* **368**, 284 (2002).

⁷² D.P. DiVincenzo: "The physical implementation of quantum computation", *Fortschritte der Physik* **48**, 771 (2000).

⁷³ D.M. Greenberger, M.A. Horne and A. Zeilinger: "Multi-particle interferometry and the superposition principle", *Physics Today*, August (1993), p. 2229.

⁷⁴ L.M.K. Vandersypen, M. Steffen, M. Sherwood, C.S. Yannoni, G. Breyta and I.L. Chuang: "Implementation of a three-quantum-bit search algorithm", *Appl. Phys. Lett.* **76**, 646 (2000).

⁷⁵ L.M.K. Vandersypen, M. Steffen, G. Breyta, C.S. Yannoni, R. Cleve, and I.L. Chuang: "Experimental realization of an order-finding algorithm with an NMR quantum computer", *Phys. Rev. Lett.* **85**, 5452 (2000).

⁷⁶ L.M.K. Vandersypen, M. Steffen, G. Breyta, C.S. Yannoni, M.H. Sherwood and I.L. Chuang: "Experimental realization of Shor's quantum factoring algorithm using nuclear magnetic resonance", *Nature* **414**, 883 (2001).

⁷⁷ L. Tian, S. Lloyd and T.P. Orlando: "Projective measurement scheme for solid-state qubits", *Phys. Rev. B* **67**, 220505(R) (2003).

⁷⁸ T.P. Orlando, L. Tian, D.S. Crankshaw, S. Lloyd, C.H. van der Wal, J.E. Mooij, and F.K. Wilhelm: "Engineering the quantum measurement process for the persistent current qubit", *Physica C* **368**, 294 (2002).

⁷⁹ F.K. Wilhelm: "An asymptotical von-Neumann measurement strategy for solid-state quantum bits", *Phys. Rev.* **68**, 060503(R) (2003).

⁸⁰ P. Grangier, J.A. Levenson and J.-P. Poizat: "Quantum non-demolition measurements in optics", *Nature* **396**, 537 (1998).

⁸¹ L.D. Landau and E.M. Lifshitz, *Quantum mechanics: non-relativistic theory* (Oxford, Pergamon) 1977.

⁸² U. Weiss: "Quantum dissipative systems", 2nd ed., (Singapore, World Scientific) 1999.

⁸³ C.P. Slichter, *Principles of Magnetic Resonance* (Springer-Verlag, New York, 1990).

⁸⁴ K. Blum, *Density matrix: theory and applications* (New York, Plenum) 1996.

⁸⁵ B.D. Josephson: "Possible new effects in superconductive tunneling", *Phys. Lett.* **1**, 251 (1962).

⁸⁶ Yu. Makhlin, G. Schön, and A. Shnirman: "Statistics and noise in a quantum measurement process", *Phys. Rev. Lett.* **85**, 4578 (2000).

⁸⁷ G. Falci, E. Paladino and R. Fazio: "Decoherence in Josephson qubits", in *Quantum Phenomena of Mesoscopic Systems*, B. Altshuler and V. Tognetti (eds.), IOS Press Amsterdam, 2004; Proc. of the International School of Physics "Enrico Fermi", Course CLI, Varenna (Italy) July 2002. cond-mat/0312550

⁸⁸ E. Paladino, L. Faoro, G. Falci, Rosario Fazio: "Decoherence and 1/f noise in Josephson qubits", *Phys. Rev. Lett.* **88**, 228304 (2002).

⁸⁹ E. Paladino, L. Faoro and G. Falci, "Decoherence due to discrete noise in Josephson qubits", *Adv. Sol. State Phys.* **43**, 747 (2003).

⁹⁰ Yu. Makhlin and A. Shnirman: "Dephasing of qubits by transverse low-frequency noise", *JETP Lett.* **78**, 497 (2003).

⁹¹ Yu. Makhlin, and A. Shnirman: "Dephasing of solid-state qubits at optimal points", *Phys. Rev. Lett.* **92**, 178301 (2004).

⁹² A. Shnirman, D. Mozyrsky, and I. Martin: "Output noise of a measuring device at arbitrary voltage and temperature", *Europhys. Lett.* **67**, 840 (2004).

⁹³ G. Falci, A. D'Arrigo, A. Mastellone and E. Paladino: "Initial decoherence in solid state qubits", *cond-mat/0409422*.

⁹⁴ F.K. Wilhelm, G. Schön, and G.T. Zimanyi, "Superconducting single-charge transistor in a tunable dissipative environment", *Phys. Rev. Lett.* **87**, 136802 (2001).

⁹⁵ F.K. Wilhelm, M.J. Storcz, C.H. van der Wal, C.J.P.M. Harmans, and J.E. Mooij: "Decoherence of flux qubits coupled to electronic circuits", *Adv. Sol. St. Phys.* **43**, 763 (2003).

⁹⁶ M.C. Goorden and F.K. Wilhelm: "Theoretical analysis of continuously driven Josephson qubits", *Phys. Rev. B* **68**, 012508 (2003).

⁹⁷ C.H. van der Wal, F.K. Wilhelm, C.J.P.M. Harmans, J.E. Mooij: "Engineering decoherence in Josephson persistent-current qubits", *European Physics Journal B* **31**, 111 (2003).

⁹⁸ K. W. Lehnert, B. A. Turek, K. Bladh, L. F. Spietz, D. Gunnarsson, P. Delsing, and R. J. Schoelkopf: "Quantum charge fluctuations and the polarizability of the single electron box", *Phys. Rev. Lett.* **91**, 106801 (2003).

⁹⁹ K. W. Lehnert, K. Bladh, L. F. Spietz, D. Gunnarsson, D. I. Schuster, P. Delsing and R. J. Schoelkopf: "Measurement of the excited-state lifetime of a microelectronic circuit", *Phys. Rev. Lett.* **90**, 027002 (2003).

¹⁰⁰ L. Roschier, P. Hakonen, K. Bladh, P. Delsing, K. Lehnert, L. Spietz, and R. Schoelkopf: "Noise performance of the RF-SET", *J. Appl. Phys.* **95**, 1274 (2004).

¹⁰¹ G. Burkard, D.P. DiVincenzo, P. Bertet, I. Chiorescu, and J. E. Mooij: "Asymmetry and decoherence in a double-layer persistent-current qubit", *Phys. Rev. B* **71**, 134504 (2005).

¹⁰² P. Bertet, I. Chiorescu, G. Burkard, K. Semba, C.J.P.M. Harmans, D.P. DiVincenzo, and J. E. Mooij: "Relaxation and dephasing in a flux qubit", (2004); *cond-mat/0412485*

¹⁰³ P. Bertet, I. Chiorescu, C.J.P.M. Harmans and J. E. Mooij: "Dephasing of a flux qubit coupled to a harmonic oscillator", (2005); *cond-mat/0507290*.

¹⁰⁴ D.V. Averin and R. Fazio: "Active suppression of dephasing in Josephson-junction qubits", *JETP Lett.* **78**, 1162 (2003).

¹⁰⁵ A. Zazunov, V.S. Shumeiko, G. Wendin and E.N. Bratus: "Dynamics and phonon-induced decoherence of Andreev level qubits", *Phys. Rev. B* **71**, 214505 (2005).

¹⁰⁶ M. Governale, M. Grifoni, and G. Schön: "Decoherence and dephasing in coupled Josephson-junction qubits", *Chem. Phys.* **268**, 273 (2001).

¹⁰⁷ M.J. Storcz und F.K. Wilhelm: "Decoherence and gate performance of coupled solid state qubits", *Phys. Rev. A* **67**, 042319 (2003).

¹⁰⁸ K. Rabenstein, V.A. Sverdlov and D.V. Averin: "Qubit decoherence by Gaussian low-frequency noise", *ZhETF Lett.* **79**, 783 (2004); *cond-mat/0401519*.

¹⁰⁹ K. Rabenstein and D.V. Averin: "Decoherence in two coupled qubits", *Turk. J. Phys.* **27**, 1 (2003); *cond-mat/0310193*.

¹¹⁰ L.B. Ioffe, V.B. Geshkenbein, Ch. Helm and G. Batter: "Decoherence in superconducting quantum bits by phonon radiation", *Phys. Rev. Lett.* **93**, 057001 (2004).

¹¹¹ P.G. deGennes, *Superconductivity of Metals and Alloys* (New York, W.A. Benjamin) 1966.

¹¹² M. Tinkham, *Introduction to superconductivity* (New York, McGraw Hill) 1996.

¹¹³ A. Barone and G. Paterno, *Physics and applications of the Josephson effect* (New York, Wiley) 1982.

¹¹⁴ M.A. Kastner: "The single-electron transistor", *Rev. Mod. Phys.* **64**, 849 (1992).

¹¹⁵ I. Giaever and H.R. Zeller: "Tunneling, zero-bias anomalies, and small superconductors", *Phys. Rev. Lett.* **20**, 1504 (1968).

¹ I.O. Kulik and R.I. Shekhter: "Kinetic phenomena and charge discreteness effects in granulated media", *Sov. Phys. JETP* **41**, 308 (1975).

¹¹⁶ P. Lafarge, P. Joyez, D. Esteve, C. Urbina, and M. H. Devoret: "Measurement of the even-odd free-energy difference of an isolated superconductor", *Phys. Rev. Lett.* **70**, 994 (1993).

¹¹⁷ P. Lafarge, P. Joyez, D. Esteve, C. Urbina, and M. H. Devoret: "Two-electron quantization of the charge on a superconductor", *Nature* **365**, 422 (1993).

¹¹⁸ *Single Charge Tunneling*, Ed. H. Grabert and M.H. Devoret, NATO ASI Series (Plenum Press, New York) 1992.

¹¹⁹ Y. Nakamura Y., Yu.A. Pashkin and J.S. Tsai: "Rabi Oscillations in a Josephson-Junction Charge Two-Level System", *Phys. Rev. Lett.* **87**, 246601 (2002).

¹²⁰ Nakamura Y., Pashkin Yu. A., and Tsai J. S.: "Charge Echo in a Cooper-Pair Box", *Phys. Rev. Lett.* **88**, 047901 (2002).

¹²¹ Mahn-Soo Choi, R. Fazio, J. Siewert, and C. Bruder: "Coherent oscillations in a Cooper-pair box", *Europhys. Lett.* **53**, 251 (2001).

¹²² A.J. Leggett and A. Garg: "Quantum mechanics versus macroscopic realism: Is the flux there when nobody looks?", *Phys. Rev. Lett.* **54**, 857 (1985).

¹²³ J.M. Martinis, M.H. Devoret, and J. Clarke: "Experimental tests for the quantum behavior of a macroscopic degree of freedom: The phase difference across a Josephson junction", *Phys. Rev. B* **35**, 4682 (1987).

¹²⁴ L.B. Ioffe, M.V. Feigel'man, A. Ioselevich, D. Ivanov, M. Troyer and G. Blatter: "Topologically protected quantum bits using Josephson junction arrays", *Nature*, **415**, 503 (2002).

¹²⁵ M.V. Feigel'man, L.B. Ioffe, V.B. Geshkenbein, P. Dayal, and G. Blatter: "Superconducting tetrahedral Quantum bits", *Phys. Rev. Lett.* **92**, 098301 (2004).

¹²⁶ A. Zazunov, V.S. Shumeiko, E. Bratus, J. Lantz, and G. Wendin: "Andreev level qubit", *Phys. Rev. Lett.* **90**, 0870031 (2003).

¹²⁷ A. Furusaki and M. Tsukada: "Unified theory of clean Josephson junctions", *Physica B* **165-166**, 967 (1990).

¹²⁸ V.S. Shumeiko, G. Wendin, and E.N. Bratus': "Resonance excitation of superconducting bound states in a tunnel junction by an electromagnetic field: nonlinear response of the Josephson current", *Phys. Rev. B* **48**, 13129 (1993).

¹²⁹ V.S. Shumeiko, E.N. Bratus', and G. Wendin: "Dynamics of Andreev level qubits, in: *Electronic correlations: from meso- to nano-physics*", Proceedings of XXXIII Moriond Conference, ed. T. Martin, G. Montambaux, J.T. Thanh Van, EDP Sciences, 2001.

¹³⁰ J. Lantz, V.S. Shumeiko, E.N. Bratus', and G. Wendin, "Flux qubit with a quantum point contact", *Physica C*, **368**, 315 (2002).

¹³¹ Yu-Xi Liu, L.F. Wei and F. Nori: "Quantum tomography for solid state qubits", *Europhys. Lett.* **67**, 874 (2004).

¹³² D.V Averin: "Continuous weak measurement of the macroscopic quantum coherent oscillations", *Fortschritte der Physik* **48**, 1055 (2000).

¹³³ M.H. Devoret and R.J. Schoelkopf: "Amplifying quantum signals with the single-electron transistor", *Nature* **406**, 1039 (2000).

¹³⁴ R.J. Schoelkopf, P. Wahlgren, A.A. Kozhevnikov, P. Delsing and D.E. Prober: "The radio-frequency single-electron transistor (rf-SET): A fast and ultra-sensititve electrometer", *Science* **280**, 1238 (1998).

¹³⁵ A. Aassime, D. Gunnarsson, K. Bladh, R.S. Schoelkopf, and P. Delsing: "Radio frequency single electron transistor towards the quantum limit", *Appl. Phys. Lett.* **79**, 4031 (2001).

¹³⁶ O. Astafiev, Yu. A. Pashkin, T. Yamamoto, Y. Nakamura, and J. S. Tsai: "Single-shot measurement of the Josephson charge qubit", *Phys. Rev. B* **69**, 180507(R) (2004).

¹³⁷ G. Johansson, A. Käck, and G. Wendin: "Full frequency back-action spectrum of a single electron transistor during qubit read-out", *Phys. Rev. Lett.* **88**, 046802 (2002).

¹³⁸ A. Käck, G. Johansson and G. Wendin: "Full frequency voltage-noise spectral density of a single electron transistor", *Phys. Rev. B* **67**, 035301 (2003).

¹³⁹ A.N. Korotkov and D.V. Averin: "Continuous weak measurement of quantum coherent oscillations", *Phys. Rev. B* **64**, 165310 (2001).

¹⁴⁰ D.V. Averin: "Quantum nondemolition measurements of a qubit", *Phys. Rev. Lett.* **88**, 207901 (2002).

¹⁴¹ H.-S. Goan, G.J. Milburn, H.M. Wiseman and H.B. Sun: "Continuous quantum measurement of two coupled quantum dots using a point contact: A quantum trajectory approach", *Phys. Rev. B* **63**, 125326 (2001).

¹⁴² H.-S. Goan and G. J. Milburn: "Dynamcis of a mesoscopic qubit under continuous quantum measurement", *Phys. Rev. B* **64**, 235307 (2001).

¹⁴³ A.L. Shelankov and J. Rammer: "Charge transfer counting statistics revisited", *Europhysics Letters* **63**, 485 (2003).

¹⁴⁴ J. Rammer, A.L. Shelankov, J. Wabnig: "Quantum measurement in the charge representation", *Phys. Rev. B* **70**, 115327 (2004).

¹⁴⁵ F.W.J. Hekking, O. Buisson, F. Balestro and M.G. Vergniory: "Cooper pair box coupled to a current-biased Josephson junction", in: *Electronic correlations: from meso- to nano-physics*, Proceedings of XXXIII Moriond Conference, ed. T. Martin, G. Montamboux, J.T. Thanh Van, EDP Sciences, 2001, p.515.

¹⁴⁶ F. Marquardt and C. Bruder: "Superposition of two mesoscopically distinct quantum states: Coupling a Cooper-pair box to a large superconducting island", *Phys. Rev. B* **63**, 054514 (2001).

¹⁴⁷ S.M. Girvin, Ren-Shou Huang, Alexandre Blais, Andreas Wallraff and R. J. Schoelkopf: "Prospects of strong cavity quantum electrodynamics with superconducting circuits", Proceedings of Les Houches Summer School, Session LXXIX, Quantum Entanglement and Information Processing (2003); cond-mat/0310670

¹⁴⁸ A. Blais, R.-S. Huang, A. Wallraff, S. M. Girvin R. J. Schoelkopf: "Cavity quantum electrodynamics for superconducting electrical circuits: an architecture for quantum computation", *Phys. Rev. A* **69**, 062320 (2004).

¹⁴⁹ I. Rau, G. Johansson, and A. Shnirman: "Cavity QED in superconducting circuits: susceptibility at elevated temperatures", *Phys. Rev. B* **70**, 054521 (2004).

¹⁵⁰ L. Roschier, M. Sillanpää and P. Hakonen: "Quantum capacitive phasse detector", *Phys. Rev. B* **71**, 024530 (2005).

¹⁵¹ A. Wallraff, D. Schuster, A. Blais, L. Frunzo, R.-S. Huang, J. Majer, S. Kumar, S.M. Girvin and R. J. Schoelkopf: "Cavity quantum electrodynamics: Coherent coupling of a single photon to a Cooper pair box", *Nature* **431**, 165 (2004).

¹⁵² D.I. Schuster, A. Wallraff, A. Blais, L. Frunzio, R.-S. Huang, J. Majer, S.M. Girvin and R.J. Schoelkopf: "AC-Stark Shift and Dephasing of a Superconducting Qubit Strongly Coupled to a Cavity Field", *Phys. Rev. Lett.* **94**, 123602 (2005).

¹⁵³ A. Wallraff, D. Schuster, A. Blais, L. Frunzo, J. Majer, S.M. Girvin and R. J. Schoelkopf: "Approaching unit visibility for control of a superconducting qubit with dispersive readout", (2005); cond-mat/0502645.

¹⁵⁴ J. Siewert, R. Fazio, G. M. Palma and E. Sciacca: "Aspects of qubit dynamics in the presence of leakage", *Low. Temp. Phys.* **118**, 795 (2000).

¹⁵⁵ J.Q. You, J.S. Tsai, J.S., F. Nori: "Scalabale quantum computing with Josephson charge qubits", *Phys. Rev. Lett.* **89**, 197902 (2002).

¹⁵⁶ J.Q. You, J.S. Tsai, F. Nori: "Controllable manipulation and entanglement of macroscopic quantum states in coupled charge qubits", *Phys. Rev. B* **68**, 024510 (2003).

¹⁵⁷ Y.D. Wang, P. Zhang, D.L. Zhou and C.P. Sun: "Fast entanglement of two charge-phase qubits through non-adiabatic coupling to a large junction", *Ohys. Rev. B* **70**, 224515 (2004).

¹⁵⁸ J. Lantz, M. Wallquist, V.S. Shumeiko and G. Wendin: "Josephson junction qubit network with current-controlled interaction", *Phys. Rev. B* **70** 140507(R) (2004).

¹⁵⁹ M. Wallquist, J. Lantz, V.S. Shumeiko and G. Wendin: "Current-controlled coupling of superconducting charge qubits", in *Quantum Computation: solid state systems*, eds. P. Delsing, C. Granata, Y. Pashkin, B. Ruggiero and P. Silvestrini, Kluwer Academic Plenum Publishers, December 2005, in press.

¹⁶⁰ M. Wallquist, J. Lantz, V.S. Shumeiko and G. Wendin: "Superconducting qubit network with controllable nearest-neighbor coupling", *New J. Phys.* (2005), in press.

¹⁶¹ L.F. Wei, Yu-Xi Liu and F. Nori: "Coupling Josephson qubits via a current-biased information bus", *Europhys. Lett.* **67**, 1004 (2004).

¹⁶² C. Rigetti, A. Blais and M. Devoret: "Protocol for universal gates in optimally biased superconducting qubits", *Phys. Rev. Lett.* **94**, 240502 (2005).

¹⁶³ M.J. Storcz und F.K. Wilhelm: "Design of realistic switches for coupling superconducting solid-state qubits", *Appl. Phys. Lett.* **83**, 2389 (2003).

¹⁶⁴ A. Blais, A. Maassen van den Brink and A.M. Zagoskin: "Tunable coupling of superconducting qubits", *Phys. Rev. Lett.* **90**, 127901 (2003).

¹⁶⁵ D.V. Averin, C. Bruder: "Variable electrostatic transformer: controllable coupling of two charge qubits", *Phys. Rev. Lett.* **91**, 057003 (2003).

¹⁶⁶ F.W. Strauch, P.R. Johnson, A.J. Dragt, C. J. Lobb, J. R. Anderson, and F. C. Wellstood: "Quantum logic gates for coupled superconducting phase qubits", *Phys. Rev. Lett.* **91**, 167005 (2003).

¹⁶⁷ C. Cosmelli, M.G. Castellano, F. Chiarello, R. Leon, G. Torrioli, and P. Carelli: "Controllable flux coupling for integration of flux qubits", cond-mat/0403690

¹⁶⁸ A. Lupascu, C. J. M. Verwijs, R. N. Schouten, C. J. P. M. Harmans, J. E. Mooij: "Nondestructive readout for a

superconducting flux qubit", Phys. Rev. Lett. **93**, 177006 (2004).

¹⁶⁹ I. Siddiqi, R. Vijay, F. Pierre, C.M. Wilson, L. Frunzio, M. Metcalfe, C. Rigetti, R.J. Schoelkopf, M.H. Devoret, D. Vion and D. Esteve: "Direct Observation of Dynamical Switching between Two Driven Oscillation States of a Josephson Junction", Phys. Rev. Lett. **93**, 207002 (2004).

¹⁷⁰ G. Ithier, E. Collin, P. Joyez, P. Meeson, D. Vion, D. Esteve, F. Chiarello, A. Shnirman, Y. Makhlin and G. Schön: "Decoherence in a quantum bit superconducting circuit", preprint (Dec. 2004).

¹⁷¹ E.T. Jaynes and F.W. Cummings: "Comparison of quantum and semiclassical radiation theories with application to the beam maser", Proc. IEEE **51**, 89 (1963).

¹⁷² S. Stenholm, Phys. Rep. **C6**, 1 (1973).

¹⁷³ B.W. Shore and P.L. Knight: "The Jaynes-Cummings model", J. Mod. Opt. **40**, 1195 (1993).

¹⁷⁴ C. Gerry and P.L. Knight, Introductory Quantum Optics, Cambridge University Press, 2004.

¹⁷⁵ A. ter Haar: "Single and coupled Josephson junction qubits", PhD thesis, Delft University (2005).

¹⁷⁶ B.L.T. Plourde, J. Zhang, K.B. Whaley, F.K. Wilhelm, T.L. Robertson, T. Hime, S. Linzen, P.A. Reichardt C.-E. Wu and J. Clarke: "Entangling flux qubits with a bipolar dynamic inductance", Phys. Rev. B **70**, 140501(R) (2004).

¹⁷⁷ B.L.T. Plourde, T.L. Robertson, P.A. Reichardt, T. Hime, S. Linzen, C.-E. Wu and J. Clarke: "Flux qubits and read-out device with two independent flux lines", Phys. Rev. B (R), (2005), in press; cond-mat/0501679.

¹⁷⁸ R. McDermott, R.W. Simmonds, M. Steffen, K.B. Cooper, K. Cicak, K. Osborn, S. Oh, D.P. Pappas and J.M. Martinis: "Simultaneous state measurement of coupled Josephson phase qubits", Science **307**, 1299 (2005).

¹⁷⁹ O. Buisson, F. Balestro, J. P. Pekola, and F. W. J. Hekking, "One-shot quantum measurement using a hysteretic dc SQUID", Phys. Rev. Lett. **90**, 238304 (2003).

¹⁸⁰ C. Sackett, D. Kielpinski, Q. Turchette, V. Meyer, M. Rowe, C. Langer, C. Myatt, B. King, W. Itano, D. Wineland, and C. Monroe: "Experimental Entanglement of Four Particles", Nature **404**, 256 (2000).

¹⁸¹ F. Schmidt-Kaler, H. Häffner, M. Riebe, S. Gulde, G.P.T. Lancaster, T. Deuschle, C. Becher, C.F. Roos, J. Eschner and R. Blatt: "Realization of the Cirac-Zoller controlled-NOT quantum gate", Nature **422**, 408 (2003).

¹⁸² S. Gulde, M. Riebe, G.P.T. Lancaster, C. Becher, J. Eschner, H. Häffner, F. Schmidt-Kaler, I. L. Chuan and R. Blatt: "Implementation of the Deutsch-Jozsa algorithm on an ion-trap quantum computer", Nature **421**, 48 (2003).

¹⁸³ D. Leibfried, B. DeMarco, V. Meyer, D. Lucas M. Barrett, J. Britton, W. M. Itano, B. Jelenkovic, C. Lange, T. Rosenband and D. J. Wineland: "Experimental demonstration of a robust, high-fidelity geometric two ion-qubit phase gate", Nature **422**, 412 (2003).

¹⁸⁴ C.F. Roos, G.P.T. Lancaster, M. Riebe, H. Häffner, W. Hänsel, S. Gulde, C. Becher, J. Eschner, F. Schmidt-Kaler and R. Blatt: "Bell states of atoms with ultralong lifetimes and their tomographic state analysis", Phys. Rev. Lett. **92**, 220402 (2004).

¹⁸⁵ C.F. Roos, M. Riebe, H. Häffner, W. Hänsel, J. Benhelm, G.P.T. Lancaster, C. Becher, F. Schmidt-Kaler and R. Blatt: "Control and measurement of three-qubit entangled states", Science **304**, 1478 (2004).

¹⁸⁶ M. Riebe, H. Häffner, C.F. Roos, W. Hänsel, J. Benhelm, G.P.T. Lancaster, T.W. Körber, C. Becher, F. Schmidt-Kaler, D.F.V. James and R. Blatt: "Deterministic quantum teleportation with atoms", Nature **429**, 734 (2004).

¹⁸⁷ M.D. Barrett, J. Chiaverini, T. Schaetz, J. Britton, W.M. Itano, J. D. Jost, E. Knill, C. Langer, D. Leibfried, R. Ozeri and D.J. Wineland: "Deterministic quantum teleportation of atomic qubits", Nature **429**, 737 (2004).

¹⁸⁸ J. Chiaverini, D. Leibfried, T. Schaetz, M.D. Barrett, R.B. Blakstad, J. Britton, W.M. Itano, J. D. Jost, E. Knill, C. Langer, R. Ozeri and D.J. Wineland: "Deterministic quantum teleportation of atomic qubits", Nature **432**, 602 (2004).

¹⁸⁹ R. Ursin, T. Jennewein, M. Aspelmeyer, R. Kaltenbaeck, M. Lindenthal, P. Walther and A. Zeilinger: "Quantum teleportation across the Danube", Nature **430**, 849 (2004).

¹⁹⁰ P. Walther, J.-W. Pan, M. Aspelmeyer, R. Ursin, S. Gasparoni and A. Zeilinger: "De Broglie wavelength of a non-local four-photon state", Nature **429**, 158 (2004).

¹⁹¹ M. Bourennane, M. Eibl, Ch. Kurtsiefer, S. Gaertner, H. Weinfurter, O. Gühne, P. Hyllus, D. Bru, M. Lewenstein and A. Sanpera: "Experimental detection of multipartite entanglement using Witness Operators", Phys. Rev. Lett. **92** 087902 (2004).

¹⁹² J.F. Clauser, M.A. Horne, A. Shimony and R.A. Holt: "Proposed experiment to test local hidden-variable theories", Phys. Rev. Lett. **23**, 880 (1969).

¹⁹³ G.P. He, S.L. Zhu, Z.D. Wang, H.Z. Li: "Testing Bell's inequality and measuring the entanglement using superconducting nanocircuits", Phys. Rev. A **68**, 012315 (2003).

¹⁹⁴ L.F. Wei, Yu-Xi Liu and Franco Nori: "Testing Bell's inequality in a capacitively coupled Josephson circuit", (2004); quant-ph/0408089.

¹⁹⁵ A.O. Niskanen, J.J. Vartiainen and M. M. Salomaa: "Optimal multiqubit operation for Josephson charge qubits", Phys. Rev. Lett. **67**, 012319 (2003).

¹⁹⁶ J.J. Vartiainen, A.O. Niskanen, M. Nakahara and M. M. Salomaa: "Acceleration of quantum algorithms using three-qubit gates", Int. J. Quant. Information **2**, 1 (2004).

¹⁹⁷ I. Cirac and P. Zoller: "Quantum computation with cold trapped ions", Phys. Rev. Lett. **74**, 4091 (1995).

¹⁹⁸ K. Molmer and A. Sorensen: "Multiparticle entanglement of hot trapped ions", Phys. Rev. Lett. **82**, 1835 (1999).

¹⁹⁹ A. Sorensen and K. Molmer: "Quantum computation with ions in thermal motion", Phys. Rev. Lett. **82**, 1971 (1999).

²⁰⁰ A. Sorensen and K. Molmer: "Entanglement and quantum computation with ions in thermal motion", Phys. Rev. A **62**, 022311 (2000).

²⁰¹ F. Plastina, R. Fazio, G.M. Palma: "Macroscopic entanglement in Josephson nanocircuits", Phys. Rev. B **64**, 113306 (2001).

²⁰² F. Plastina, R. Fazio, and G.M. Palma: "Entanglement Detection in Josephson nanocircuits", J. Mod. Optics **49**, 1389 (2002).

²⁰³ F. Plastina and G. Falci: "Communicating Josephson qubits", Physical Review B **67**, 224514 (2003).

²⁰⁴ M. Paternostro, W. Son, M. S. Kim, G. Falci, G. M. Palma: "Dynamical entanglement-transfer for quantum information networks", Phys. Rev. A **70**, 022320 (2004).

²⁰⁵ M. Paternostro, G. Falci, M.S. Kim and G.M. Palma: "Entanglement between two superconducting qubits via interaction with non-classical radiation", Phys. Rev. B **69**, 214502 (2004).

²⁰⁶ S.L. Zhu, Z.D. Wang, K. Yang: "Quantum-information processing using Josephson junctions coupled through cav-

ities", Phys. Rev. A **68**, 034303 (2003).

²⁰⁷ J.Q. You and F. Nori: "Quantum information processing with superconducting qubits in a microwave field", Phys. Rev. B **68**, 064509 (2003).

²⁰⁸ G. De Chiara, R. Fazio, C. Macchiavello, G. M. Palma: "Entanglement production by quantum error correction in the presence of correlated environment", Europhys. Lett. **67**, 714 (2004).

²⁰⁹ S. Bose: "Quantum communication through an unmodulated spin chain", Phys. Rev. Lett. **91** 207901 (2003).

²¹⁰ M. Christandl, N. Datta, A. Ekert and A.J. Landahl: "Perfect state transfer in quantum spin networks", Phys. Rev. Lett. **92**, 187902 (2004).

²¹¹ M. Christandl, N. Datta, T. Dorlas, A. Ekert, A. Kay and A.J. Landahl: "Perfect transfer of arbitrary states in quantum spin networks", (2004); quant-ph/0411020.

²¹² C. Albanese, M. Christandl, N. Datta and A. Ekert: "Mirror inversion of quantum states in linear registers", Phys. Rev. Lett. **93**, 230502 (2004).

²¹³ G. De Chiara, R. Fazio, C. Macchiavello, S. Montangero, G. M. Palma: "Quantum cloning in spin networks", Phys. Rev. A **70**, 062308 (2004).

²¹⁴ G. De Chiara, R. Fazio, C. Macchiavello, S. Montangero, G.M. Palma: "Quantum cloning without external control", (2004); quant-ph/0410211.

²¹⁵ A. Romito, R. Fazio and C. Bruder: "Solid-State Quantum Communication With Josephson Arrays", Phys. Rev. B **71**, 100501(R) (2005)..

²¹⁶ S. Montangero, G. Benenti and R. Fazio: "Dynamics of entanglement in quantum computers with imperfections", Phys. Rev. Lett. **91**, 187901 (2003).

²¹⁷ S. Montangero, A. Romito, G. Benenti and R. Fazio: "Chaotic dynamics in superconducting nanocircuits", (2004); cond-mat/0407274.

²¹⁸ P. Facchi, S. Montangero, R. Fazio and S. Pascazio: "Dynamical imperfections in quantum computers", Phys. Rev. A, in press; quant-ph/0407098.

²¹⁹ M. Paternostro, G.M. Palma, M.S. Kim and G. Falci: "Quantum state transfer in imperfect artificial spin networks", Phys. Rev. A **71**, 042311 (2005); quant-ph/0407058.

²²⁰ P.W. Shor: "Scheme for reducing decoherence in quantum computer memory", Phys. Rev. A **52**, R2493 (1995).

²²¹ E. Knill, R. Laflamme, R. Martinez and C. Negrevergne: "Implementation of the five qubit correction benchmark", Phys. Rev. Lett. **86**, 5811 (2001).

²²² A.M. Steane: "Active stabilisation, quantum computation, and quantum state synthesis", Phys. Rev. Lett. **77**, 793 (1996).

²²³ A.M. Steane: "Active stabilisation, quantum computation, and quantum state synthesis", Phys. Rev. Lett. **78**, 2252 (1997).

²²⁴ A.M. Steane: "Quantum computing and error correction", in *Decoherence and its implications in quantum computation and information transfer*, Gonis and Tuchi (eds.), pp.282-298 (IOS Press, Amsterdam, 2001); quant-ph/0304016.

²²⁵ A.M. Steane: "Overhead and noise threshold of fault-tolerant error correction", Phys. Rev. A **68**, 042322 (2003).

²²⁶ A.M. Steane: "Information science: Quantum errors corrected", Nature **432**, 560 (2004).

²²⁷ M. Sarovar and G.J. Milburn: "Continuous quantum error correction by cooling", (2005); quant-ph/0501038.

²²⁸ E. Celeghini, L. Faoro, and M. Rasetti: "Dynamical algebra of single and coupled Josephson Junctions", Phys. Rev. B **62**, 3054 (2000).

²²⁹ D.A. Lidar and K.B. Whaley: "Decoherence-free subspaces and subsystems", in "Irreversible Quantum Dynamics", F. Benatti and R. Floreanini (Eds.), pp. 83-120 (Springer Lecture Notes in Physics vol. 622, Berlin, 2003).

²³⁰ L. Viola, E. Knill and S. Lloyd: "Dynamical decoupling of open quantum systems", Phys. Rev. Lett. **82**, 2417 (1999).

²³¹ L. Faoro and L. Viola, "Dynamical suppression of 1/f noise processes in qubit systems", Phys. Rev. Lett. **92**, 117905 (2004).

²³² A. Shnirman and Yu. Makhlin: "Quantum Zeno effect in the Cooper-pair transport through a double-island Josephson system", JETP Lett. **78**, 447 (2003).

²³³ G. Falci, A. D'Arrigo, A. Mastellone and E. Paladino, "Dynamical suppression of telegraph and 1/f noise due to quantum bistable fluctuator", Phys. Rev. A **70**, R40101 (2004).

²³⁴ P. Facchi, D.A. Lidar, and S. Pascazio: "Unification of dynamical decoupling and the quantum Zeno effect", Phys. Rev. A **69**, 032314 (2004).

²³⁵ P. Facchi, S. Tasaki, S. Pascazio, H. Nakazato, A. Tokuse, and D.A. Lidar: "Control of decoherence: Analysis and comparison of three different strategies", Phys. Rev. A **71**, 022302 (2005).

²³⁶ R. Alicki: "A unified picture of decoherence control", (2005); quant-ph/0501109.

²³⁷ Yu. Makhlin, G. Schön, and A. Shnirman: "Josephson junction quantum logic gates", Computer Physics Communications (Elsevier) **127**, 156 (2000).

²³⁸ J. Siewert and R. Fazio: "Quantum algorithms for Josephson networks", Phys. Rev. Lett. **87**, 257905 (2001).

²³⁹ N. Schuch, J. Siewert: "Implementation of the four-bit Deutsch-Jozsa algorithm with Josephson charge qubits", physica status solidi (b) **233** (3), 482 (2002).

²⁴⁰ J. Siewert and R. Fazio: "Implementation of the Deutsch-Jozsa algorithm with Josephson charge qubits", J. Mod. Optics **49**, 1245 (2002)

²⁴¹ N. Schuch and J. Siewert: "Programmable networks for quantum algorithms", Phys. Rev. Lett. **91**, 027902 (2003).

²⁴² J.J. Vartiainen, A.O. Niskanen, M. Nakahara and M.M. Salomaa: "Implementing Shor's algorithm on Josephson charge qubits", Phys. Rev. A **70**, 012319 (2004).

²⁴³ J. Zhang, J. Vala, S. Sastry and K.B. Whaley: "Minimum construction of two-qubit operations", Phys. Rev. Lett. **93**, 020502 (2004).

²⁴⁴ A.O. Niskanen, M. Nakahara and M. M. Salomaa: "Realization of arbitrary gates in holonomic quantum computation", Phys. Rev. A **90**, 197901 (2003).

²⁴⁵ J. Siewert, L. Faoro, R. Fazio: "Holonomic quantum computation with Josephson networks", phys. stat. sol. **233**, 490 (2002)

²⁴⁶ G. Falci, R. Fazio and G.M, Palma: "Quantum gates and Berry phases in Josephson nanostructures", Fortschritte der Physik **51**, 442 (2003).

²⁴⁷ L. Faoro, J. Siewert and R. Fazio: "Non-Abelian phases, pumping, and quantum computation with Josephson junctions", Phys. Rev. Lett. **90**, 028301 (2003)

²⁴⁸ G. Falci, R. Fazio, G.M. Palma, J. Siewert and V. Vedral: "Detection of geometric phases in superconducting nanocircuits", Nature **407**, 355 (2000).

²⁴⁹ M. Cholascinski: "Quantum holonomies with Josephson-junction devices", Phys. Rev. A **69**, 134516 (2004).

²⁵⁰ Yu. Makhlin and A. Mirlin: "Counting statistics for ar-

bitrary cycles in quantum pumps" Phys. Rev. Lett. **87**, 276803 (2001).

²⁵¹ M. Aunola and J. J. Toppuri: "Connecting Berry's phase and the pumped charge in a Cooper pair pump", Phys. Rev. B **68**, 020502 (2003).

²⁵² D.V. Averin: "Adiabatic quantum computation with Cooper pairs", Solid State Commun. **105**, 659 (1998).

²⁵³ D. Aharonov, W. van Dam, J. Kempe, Z. Landau, S. Lloyd, O. Regev: "Adiabatic quantum computation is equivalent to standard quantum computation", Proc. 45th FOCS (2004), p. 42-51; quant-ph/0405098.

²⁵⁴ A.M. Steane: "How to build a 300 bit, 1 Gop quantum computer", quant-ph/0412165 (2004).

²⁵⁵ L. Tian, P. Rabl, R. Blatt, and P. Zoller: "Interfacing quantum-optical and solid-state qubits", Phys. Rev. Lett. **92**, 247902 (2004).